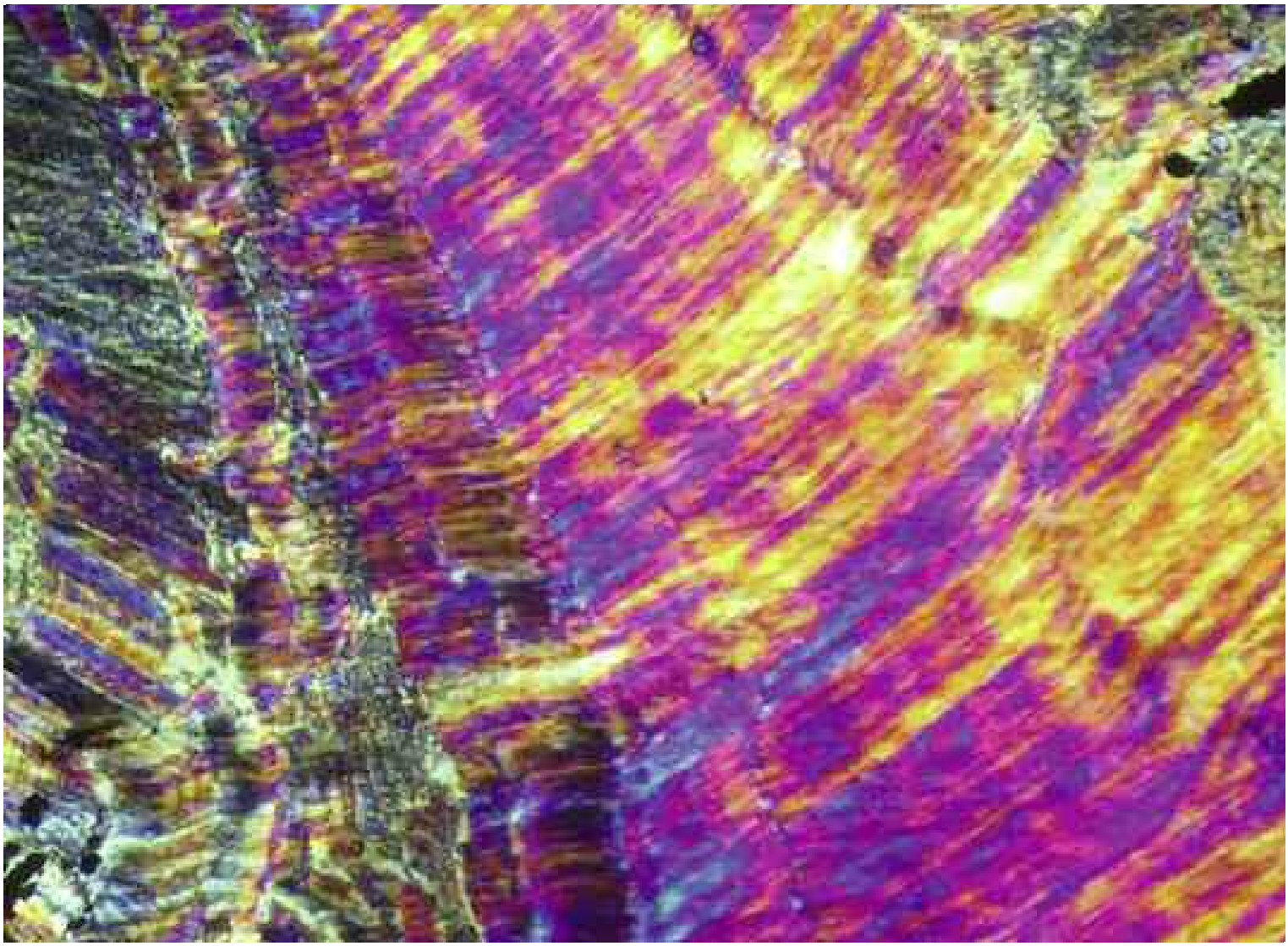

2016 ANNUAL REPORT

HP-HT laboratory

EXPERIMENTAL VOLCANOLOGY AND GEOPHYSICS

laboratory

NEW TECHNOLOGIES

Department of Seismology and Tectonophysics
Istituto Nazionale di Geofisica e Vulcanologia

Via di Vigna Murata 605 | 00143 Roma - Italia | Tel +39-0651860437 | Fax +39-0651860507
www.ingv.it

About the cover
Antigorite Vein, from the Monte Fico shear zone (Elba Island, Italy). Crossed Nichols, view width 5 mm.
Credits: T. Tesei

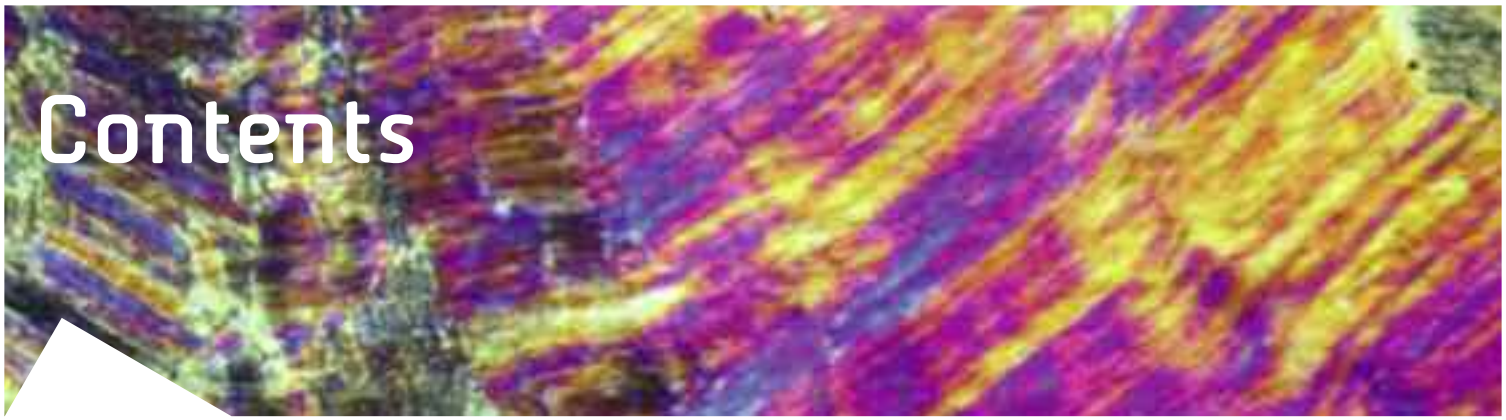

Contents

HP-HT Laboratory of Experimental Volcanology and Geophysics
LNT Laboratory of New Technologies

2016 Annual Report

1| ABSTRACT

This report summarizes the facilities, activities, collaborations, scientific and technological products of the High Pressure High Temperature Laboratory of Experimental Volcanology and Geophysics (HPHT Lab) and of the Laboratory of New Technologies (LNTS) updated to the year 2016. The two laboratories are part of the three main Structures of INGV: Earthquake, Volcano and Environment. Research activities were framed within 14 national and international research projects and involved 33 proposals. In collaboration with Italian and foreigner universities, the laboratories hosted 11 Master students and 11 PhD students, together with 13 visiting scientists.

Scientific production for 2016 amounts to 29 publications and 1 patent.

In 2016 the **HPHT Lab** continued its activities under several research projects, most notably the three EU-funded projects: 1) ERC Consolidator Grant NOFEAR (New Outlook on seismic faults: From EARthquake nucleation to arrest), 2) ERC Starting Grant Project GLASS (InteGrated Laboratories to investigate the mechanics of ASeismic vs. Seismic faulting), and 3) ITN VERTIGO (Volcanic ash: fiEld, expeRimenTal and numerIcal investiGations of prOcesses during its lifecycle). Instrumental upgrades involved several equipments. The Multianvil 840 tons press has been equipped with a new assembly design, expanding the experimental pressure range from 2.5 to 26 GPa. The QuickPress piston cylinder has been equipped with a new 1/2" pressure plate and furnace assemblies to expand the experimental pressure range from 1 to 2.5 GPa. The SHIVA rotary shear apparatus has been implemented by the acquisition of two new modules, one for the study of the friction properties of pore fluid pressurized powders, the other for the measurement of the elastic properties of the sample. The BRAVA tri-axial system has been furnished with new, smaller-volume pressure intensifier system specifically designed to enhance the accuracy of fluid pressure and sample volume measurements. Finally, a new, state-of-the-art system for the acquisition and monitoring of acoustic emission has been acquired, to locate, track and follow dynamic rupture and other associated events during experiments at SHIVA, BRAVA and other laboratory facilities.

The 'Slug Burster' shock tube apparatus of the analog laboratory has been modified to host powders and pyroclasts together with liquids. In this new configuration, termed 'Jet Burster', the setup has been used to perform experiments on the effect of pressure, source depth and vent geometry on the ejection dynamics of pyroclasts. Finally, the field-based BACIO campaign at Stromboli volcano has successfully seen the deployment of the largest array of high-speed cameras

ever used to record explosive volcanic activity, including 4 high-speed cameras, one thermal camera, and three ultra-high definition cameras, together with two drones and three microphone arrays. This joint deployment will allow unprecedented, multidisciplinary insights into the volcano dynamics.

During the 2016, the **LNTS** has conducted many activities, in particular within the Olimpo project, the GLASS project and the NOFEAR project. The LNTS has started also a new project, in collaboration with the University "La Sapienza" of Rome, related to the design of a micro ACS (Attitude Control System) for stratospheric payloads to use for night flights in polar areas.

The activity of designing and building automatic devices, avio-trasportable on board of drones, for the LUSILAB project is still in progress. New payloads (sampler mud, new gas sampler and contact thermometer), with sensors and remotely controlled devices, have been designed and prototyped. Furthermore, a mud sampler for capturing fluid mud in the depth of a crater, suitable for the crater of LUSI, has been designed and it is under construction at the mechanical workshop.

The LNTS has participated to two arctic missions (Svalbard Islands) for the official test (performed together with the ASI inspection) where the attitude of the OLIMPO gondola was tested. During the test of the attitude control system some devices, like sun sensors and sun tracker developed at the LNTS, were validated and approved for the next launch of the telescope of OLIMPO. The LNTS has participated at the first launch of a small experimental subsystem (sensors and telemetry) containing a new micro ACS version.

Moreover, the LNTS supplies assistance to the Roma1 UF2 for maintaining the geochemical stations designed by LNTS. It has collaborated with the Etna Observatory (INGV Catania) for the electronic development and mechanical design of some parts of instruments implemented for continuous analyzing of the gaseous emissions from craters during the activity of the Etna volcano.

2| PERSONNEL

HPHT Laboratory

Piergiorgio Scarlato | Senior Researcher

Carmela (Lilli) Freda | Senior Researcher

Gianfilippo De Astis | Researcher

Elisabetta Del Bello | Contract Researcher

Pierdomenico Del Gaudio | Researcher

Damien Gaudin | Contract Researcher (now at LMU Germany)

Valeria Misiti | Technologist

Matteo Masotta | Researcher (now at University of Pisa)

Silvio Mollo | Researcher (now at Sapienza University of Rome)

Manuela Nazzari | Researcher

Tullio Ricci | Researcher

Elena Spagnuolo | Researcher

Jacopo Taddeucci | Researcher

Telemaco Tesei | Contract Researcher

Pierre Yves Tournigand | Contract Researcher

Laboratory of New Technologies

Giovanni Romeo | Technical Director

Giuseppe Di Stefano | Senior Technologist

Alessandro Iarocci | Engineer Technologist

Massimo Mari | Technician

Francesco Pongetti | Engineer Technician

Giuseppe Spinelli | Engineer Technologist

Mario Tozzi | Technician

Giuseppe Urbini | Engineer Technologist

Associated researchers

Cristiano Collettini I Sapienza Università di Roma, Italy **I Associated Professor**

Giancarlo Della Ventura I Università di Roma Tre **I Professor of Mineralogy**

Giulio Di Toro I University of Manchester, UK **I Chair of Geology**

Mario Gaeta I Sapienza Università di Roma, Italy **I Researcher**

Gianluca Iezzi I Università di Chieti, Italy **I Researcher**

Brent T. Poe I Università di Chieti, Italy **I Professor of Mineralogy**

Marco M. Scuderi I Sapienza Università di Roma, Italy **I Marie Curie Fellow**

Vincenzo Stagno I Sapienza Università di Roma, Italy **I Researcher**

Valentin R. Troll I Uppsala University, Sweden **I Chair of Petrology**

3I INSTRUMENTS and FACILITIES

HPHT Laboratory

- Multiple press 840 ton I Voggenreiter
- Piston cylinder - 3/4" and 1" pressure plates I Voggenreiter
- Multianvil - Walker type 6/8 I Voggenreiter
- Quick Press - Piston Cylinder 3/4" and 1" pressure plates I Depth of the Earth
- Bi-Tri-Axial Press (BRAVA) I RMP - INGV
- Low to High Velocity Apparatus (SHIVA) I RMP - INGV
- Electron microprobe equipped with 5 WDS and 1 EDS I JEOL JXA-8200
- Field Emission Scanning Electron Microscope equipped with EDS and BSE detectors I JEOL JSM-6500F
- Auto Carbon coater I JEOL JEC-530
- Fine coater I JEOL JFC-2300HR
- High and low temperature furnaces I Lenton
- Impedance analyser I Solartron SI1260
- Digital oscilloscope I Tektronix DPO4032
- Wave generator I Agilent 33250A
- H-Frame presses 10 ton I Enerpac
- Uniaxial testing machine with double load cell (15 and 250 kN) and LVDT controller I Tecnotest
- Precision balance I Sartorius
- Optical and stereo microscopes I Leica DMRXP and Euromex
- Ultra-high velocity, intensified, gated digital camera I Cordin 204-2
- High speed digital camcorder I Optronis and NAC 512 SC
- Stereomicroscopes I Leica MZ 9.5
- Semiautomatic polisher I Buehler Minimet 1000
- Power Supply I Agilent 6575A
- Helium Picnometer I AccuPyc II 1340
- Permeameter with double intensifier I Rock Physics
- Reometer MCR 301 Physica I Anton Paar
- Vertical Furnace RHTV 120-300/18 I Nabertherm
- High Temperature Furnace LHT 04/18 I Nabertherm

- Cecchi data acquisition system | Applied Seismology
- Rock drilling, cutting, and grinding equipment for samples preparation
- Thermal High speed camera | FLIR SC 645
- Welder PUK U3 | Lampert
- Laser line generator | Edmund optics
- Precision test sieves | Endecotts
- Laser MGL-III, 532nm 200mW, PSU-III-LED/Unit | Changchun New Industries
- Multi-Wavelenght Analyser PSA with Particle sizing according to ISO 13317 | LuMiReader®
- 2 Polarized Free-field Microphones 40AN 1/2", Low Frequency (0.5Hz - 20kHz) | G.R.A.S.
- Vacuometro Pirani PVG-500
- Petrographic microscope ECLIPSE E-50i POL | Nikon
- Drying oven UF 75 | Memmert
- 4K digital camcordes | Sony
- High speed digital camcorder | NAC Memrecam-HX6

Acquired in 2016

- High speed digital camcorder | NAC Memrecam-HX3
- Acoustic Emission System Triggered and continuous recording | Istaca Consulting Ltd
- Elastic properties prototype modulus built in the rotary apparatus, adaptable for stand-alone applications

Laboratory of New Technologies

- Analog Oscilloscope | HP
- Analog Oscilloscope | Iwatsu SS5710
- Analog Oscilloscope | Tektronix TDS220
- Analog Oscilloscope | Tektronix
- Acoustic Emission System Triggered and continuous recording | Istaca Consulting Ltd
- Elastic properties prototype modulus built in the rotary apparatus, adaptable for stand-alone applications.
- Oscilloscope | HP54201
- Oscilloscope | HP54602b
- Power supply | Elind HL series
- Power supply | Elind 6TD20

- Power supply | DC DF1731SB
- Signal generator | HP8656A
- Function generator | HP3325A
- Multimeter | HP3478A
- Milling machine for printed circuit boards | T-Tech
- Logic state analyzer | HP16500A
- Superheterodyne spectrum analyzer | Tektronix
- Soldering-reworking station | JBC advanced AM6500
- Oscilloscope | FLUKE 199C
- Oscilloscope | Tektronix DPO4000
- Oscilloscope | Tektronix MSO4034
- Calibrator | FLUKE 5700 (series II)
- Function generator | HP33120
- Function generator | AGILENT 33250 A
- PXI Industrial computer with I/O boards | National Instruments
- Universal counter | HP53131A
- Waveform generator | Agilent 33210 A
- Oscilloscope W wave surfer | LeCroy 44MXs-A

Machine shop

- Lathe | Grazioli Fortuna
- Small lathe | Ceriani
- Small milling machine | Schaublin
- Cutting machine | Ercoletta
- Bending machine | Ercoletta
- Drill press | Serrmac
- Small drill press | Webo
- Bandsaw | Femi
- Grinder | Femi
- Extractor hood | Filcar
- Inverter welding machine | Tecnica

- TIG welding machine I Cebora
- Miter saw
- Numerically controlled milling machine

4| LABORATORY ACTIVITIES

Experimental laboratory

Super press | Multi Anvil

6 experiments have been conducted in the frame of 2 projects. One devoted to calibration of the apparatus and the second ones on Olivine experiments.

Quick press | Piston cylinder

The 1 inch pressure plate has been used for 30 experiments in the frame of 5 projects and different calibration.

Furnaces

10 experiments have been performed in the frame of the following project:

- Experimental study on radon emissions from phonolite lavas exposed to sub-volcanic temperatures up to 1000 °C.

Slow to High Velocity rotary shear Apparatus (SHIVA)

The sixth year of activity of SHIVA has been mainly dedicated at the investigation of frictional properties of cohesive and non-cohesive gouges, clay mixtures and fault products derived from deep drilling projects (e.g. CRISP IODP, JFAST IODP, Wenchuan fault). We use vacuum, room humidity conditions and we work in the presence of various types of fluids. We investigated the nucleation, propagation and arrest of earthquakes resulting from crustal deformation conditions (pressure, temperature, presence of fluids, stress perturbations, etc.). We studied the physico-chemical processes related to the deformation (i.e. acoustic emission, gases, radon emanation) which are considered precursory to rupture nucleation. We focused on fluid-rock interaction by varying fluid viscosity and fluid mixture to contribute to the increasing knowledge about triggered seismicity, induced seismicity and carbon storage. We specifically designed experiments to provide inputs for the modelling of earthquakes occurring along great subduction margins to create and strengthen the binomial between rock mechanics and seismology. With similar purposes we designed a prototypal device to monitor Vp/Vs and seismic attenuation Q during an experimentally simulated seismic cycle. All the implementation addressed to these studies are motivated and funded bythe ERC "NOFEAR" project (P.I. Giulio Di Toro).

To achieve these goals, we performed 161 experiments during year 2016.

Some of these experiments were performed in collaboration with juniors scientists such as Stefano Aretusini (PhD student, University of Manchester, UK), Luca Smeraglia (PhD student, "Sapienza" University, Roma, IT), Matteo Demurtas (PhD, Padova University, IT) and guests as Francois Passalegue (Postdoc, University of Manchester, UK),

Nicola Tisato (University of Texas at Austin, US), Li Wei Kuo (University of Taipei, TW), Paola Vannucchi (University College London, UK) and Marie Violay (Postdoc, ETH, Zurich, Swiss).

Bi-Tri-Axial Press (BRAVA)

During the 2016 we performed more than 140 experiments testing most of the capabilities of the apparatus. The experimental work has been focused on consolidating the research lines developed during the year before and on developing new research topics and/or experimental facilities. In the following we summarize the main research themes:

1) Characterization of the frictional properties of carbonate-bearing faults during experiments at high strain and slow sliding velocities.

2) Frictional properties and gouge development on large (20x20 cm) experimental faults. Roughness characterization of large experimental faults using laser profilometers.

3) Weakness of serpentine minerals revealed by friction experiments under room and hydrothermal conditions .

4) The role of anisotropy in fault mechanics tested via cylindrical samples of sandstone with a pre-imposed saw-cut filled with powdered weak marl.

5) The spectrum of fault slip behaviour and precursory velocity changes along experimental faults.

6) The role of fluid pressure in induced and triggered seismicity. a) Evolution of the rate and state friction parameters and permeability under different levels of fluid pressure. b) Slip behaviour of carbonate and shale-rich faults subjected to fluid pressure stimulations.

Finally, we have used BRAVA for teaching rock-physics at Master students of the Petrophysics course at La Sapienza University of Rome and for outreach with high-school students.

Analog laboratory

Rheometer

55 rheological experiments have been conducted on natural suspensions composed by different proportion of: water-mud-sand-clay-marble powder. Furthemore 10 calibration tests and 6 rheological experiments on Lusi mud volcano products were performed.

FAMoUS (Fast Multiparametric Setup) TOOLBOX

Connection and synchronization for the recently acquired NAC Memrecam HX-3 high-speed camera was provided. The Third BAcIO (Broadband Acquisition and Imaging Operation) multidisciplinary experiment was carried out at Stromboli (May 2016), in order to study the behavior of basaltic explosive eruptions.

Microanalitical laboratory

FE-SEM and EMP performed 136 days of analysis in the frame of the following 33 research proposals. Analysed samples included natural rocks, minerals, experimental products.

Proposals

Analysis of the pyroclastic deposits of the December 29th 2013 eruption of Chaparrastique volcano (San Miguel, El Salvador)
E. Del Bello I INGV Roma 1

Cannonballs: a peculiar feature of basaltic monogenic volcanoes?
A. Di Piazza I INGV Roma 1

Characterisation of anthropogenic pollutants in natural snow deposit, magnetic contribution and geochemical determination
L. Alfonsi I INGV Roma 2

Characterisation of the mud emissions occurred after M 6.5 earthquake in Central Italy
T. Ricci and V. Misiti I INGV Roma 1

Crystal-chemical variations induced by variable cooling rate in sub-alkaline silicate liquids
G. Iezzi and V. Misiti I Università di Chieti- INGV Roma 1

Crystallization path of basaltic magmas as a function of decompression and cooling rate
S. Mollo I Sapienza University of Rome

Dynamic crystallisation in magmas
M. Nazzari I INGV Roma 1

EC Collaborative Project ASTARTE "Assessment, STrategy And Risk Reduction for Tsunamis in Europe"
P.M. De Martini I INGV Roma 1

Experimental fault rocks at the microscale
T. Tesei I INGV Roma 1

Experimental viscosity measurements of carbonatitic melts at pressures and temperatures representative for the Earth's upper mantle
V. Stopponi (Bachelor thesis) and V. Stagno I Sapienza University of Rome

Frictional processes of clay-rich gouges in megathrust and landslide decollement environments
G. Di Toro I Università di Padova

Geochemical characterization of ultramafic xenoliths in North Hartland lamprophyre dikes (New Hampshire-USA)
P.P. Giacomoni I Università di Ferrara

Generating phonolites from fractionation of trachyandesite and melting of peridotite
M. Brenna I University of Otago (New Zealand)

Igneous rocks as source and sink of abiotic hydrocarbons and CO_2
G. Etiope I INGV Roma 2

Imaging of the volcanic glass samples exposed to gases (SO_2, HCl) in an gas-ash reactor
I. Tomasek I University of Durham

Noble gases in fluid inclusions (FI) of olivine and pyroxene crystals from active volcanoes along subduction zones
A.L. Rizzo I INGV Palermo

Olivine-carbonate melt interaction at 1-3 GPa and 1300-1500 °C
V. Stagno I Sapienza University of Rome

Oxygen fugacity, pressure and temperature conditions at which elemental carbon turns into CO_2-bearing melts within eclogite and peridotite assemblages
V. Stagno I Sapienza University of Rome

Paleoenvironmental reconstruction (FIRB Abruzzo)
A. Smedile I INGV Roma 1

Physical-chemical constraints of the magmatic feeding system of the 2014-2015 explosive eruptive activity at Mt. Etna
P.P. Giacomoni I Università di Ferrara

Rheological properties of debris- and mud- flows
P. Del Gaudio I INGV Roma 1

Studies on the formation of rhyolites from Ramadas Volcanic Center (Altiplano-Puna, Argentina) through microprobe analyses and experiments of melting at variable pressure
G. De Astis I INGV Roma 1

Study of the characteristic behaviour of active/exhumed faults vs large scale gravitative movements sliding planes in central Italy
M. Moro I INGV Roma 1

Solidification of a rhyolitic magma beneath the Krafla caldera
M. Masotta I now at University of Pisa

Textural characterization of natural and experimental samples of mugearitic mega-crystic lavas from Mt Etna volcano
A. Di Piazza I INGV Roma 1

Textural and micro-chemical features of fault rocks from Central Apennines
G. Iezzi I Università di Chieti

The causes and consequences of large scale ash aggregation
S. Mueller I Ludwig-Maximilians-Universität München

The Earth's deep volatile cycle over geological time as function of mantle redox state, pressure and temperature
M. Caruso I Sapienza University of Rome

The role of crystal mushes in the differentiation processes of calcalkaline magmas: field relationships, petrography, geochemistry and experimental modelling
V. Tecchiato I Sapienza University of Rome

TOTAL France. Pore pressure changes and stability/leakage in an active fault zone
C. Collettini I Sapienza University of Rome

Unrest at Turrialba volcano (Costa Rica)
A. Di Piazza I INGV Roma 1

Viscosity of crystallised silicate melt
V. Misiti and F. Vetere I INGV Roma 1, Università di Perugia

Volcanology of the acid magmatism in the Parana Province, Brazil
S.P. De Cristofaro I Università degli Studi di Torino

5| RESEARCH PROJECTS

1. École polytechnique fédérale de Lausanne | Frictional properties of Opalinus clay | **P.I. Violay M.**
2. European Research Project - ERC Consolidator Grant Project | NOFEAR: New Outlook on seismic faults: From EARthquake nucleation to arrest | **P.I. Di Toro G.**
3. European Research project | EPOS 'European Plate Observing System' Implementation Phase, WP 16 Multi-scale Laboratories | **P.I. Cocco M.**
4. European Research project - ERC Starting Grant Project LUSILAB | Lusi: a unique natural laboratory for multidisciplinary studies of focused fluid flow in sedimentary basins | **P.I. Mazzini A.**
5. European Research Project | MED-SUV (Mediterranean Super Volcanoes): Long-term monitoring experiment in geologically active regions of Europe prone to natural hazards: the Supersite concept | **P.I. Puglisi G.**
6. European Research Project | VERTIGO 'Volcanic ash: fiEld, expeRimenTal and numerIcal investiGations of prOcesses during its lifecycle', an EU International Training Network | **P.I. Kueppers U.**
7. European Research Infrastructures Transnational Access EUROPLANET 2020 | Agreement n.: 654208 (15-EPN-003). Approved proposal grant n. 10341: 'High-Speed Imaging Of Gas-Particle And Particle-Particle Interactions In Lab-Sized Volcanic Jets/plumes' | **P.I. Taddeucci J., Del Bello E.**
8. International Continental Scientific Drilling Program - ICDP | Krafla Magma Drilling Project **| P.I. Eichelberger J.**
9. Italian Civil Protection, INGV 2016 Agreement | B2, Objective 4 - 'Centro di Pericolosità Vulcanica' **| P.I. Macedonio G., Calvari S.**
10. Marie Curie Individual Fellow FEAT (n° 656676) | The role of Fluid pressure in EArthquake Triggering **| P.I. Scuderi M.M.**
11. MIUR – Programma Nazionale di Ricerche in Antartide | "Voli di pallone invernali a lunga durata da regioni polari" | **P.I. Piacentini F.**
12. National Science Foundation project | Strombolian and Hawaiian Explosions: New Insights From Synchronizing Videos and Exsolved Volatiles | **P.I. Houghton B.**
13. Sapienza Progetti Ateneo | The role of fluid pressure in carbonate-fault frictional stability and earthquake triggering **| P.I. Collettini C.**
14. Sapienza Progetti di Ateneo | The role of fluid pressure in the mechanics of slow earthquakes: insights from rock deformation experiments **| P.I. Collettini C.**

6| PARTNER LABORATORIES

1. **Institute of Geochemistry and Petrology** | ETH Zurich | **Switzerland**
2. **Dipartimento di Scienze Biologiche, Geologiche e Ambientali** | Università di Catania | **Italy**
3. **Dipartimento di Fisica e Scienze della Terra** | Università di Ferrara | **Italy**
4. **Institute of Fluid Dynamics and Technical Acoustics (ISTA)** | Technische Universität | **Berlin**
5. **Petro - Volcanology Research Group (PVRG) Department of Physics and Geology** | University of Perugia | **Italy**
6. **Planetary Environmental Facilities** | Aarhus University | **Denmark**

7| PARTNER INSTITUTIONS

1. Institute of Geochemistry and Petrology | Swiss Federal Institute of Technology in Zurich (ETHZ) | Switzerland
2. Dipartimento Geotecnologie | Università di Chieti | Italy
3. Dipartimento di Scienze della Terra | Sapienza University of Rome | Italy
4. Dipartimento di Scienze Geologiche | Università degli Studi Roma Tre | Italy
5. Istituto di Geoscienze e Georisorse | CNR | Italy
6. Dipartimento di Fisica e Scienze della Terra | Università degli Studi di Ferrara | Italy
7. Dipartimento di Scienze Biologiche, Geologiche e Ambientali | Università di Catania | Italy
8. Department of Geology and Geophysics, SOEST | University of Hawaii | USA
9. Department of Physics and Astronomy | Aarhus University | Denmark
10. HVO Hawaiian volcano observatory | USGS | USA
11. Ludwig Maximillians Universitat Munchen | Munich | Germany
12. School of Earth and Environmental Sciences | Manchester | England

8.1 PETROLOGY, MINERALOGY, VOLCANOLOGY

Multi-parametric investigation of Mt. Etna 2014 eruption: evidences for interconnected dynamics at multiple vents

L. Spina, J. Taddeucci, A. Cannata, M. Sciotto, E. Del Bello, P. Scarlato, U. Kueppers, D. Andronico, E. Privitera,T. Ricci, J.J. Pena-Fernandez, J. Sesterhenn, D.B. Dingwell

On 5th July 2014, a new eruptive fissure (hereafter EF; Fig. 1) opened on the eastern flank of Mt. Etna volcano, at the base of North East Crater (NEC). The activity was characterised by Strombolian explosions from two neighbouring vents and the effusion of lava feeding a lava flow that reached the base of the Valle del Bove. This activity allowed for the growth of two few tens of meters high cones (Fig. 1). On 16th July, in the framework of the MED-SUV project, we performed a multi-parametric investigation of this explosive activity at the two vents (here defined crater N and crater S, distance = ca. 40 meters) by means of a dense instrumental network. The setup, deployed at ca. 300 m from EF, comprised 2 broadband seismometers, 3 microphones as well as high speed video and thermal cameras. The analysis of thermal images allowed for a comparison of the activity at each eruptive vent. Indeed, for each crater, we derived a series of thermal transients, marking the arrival of the incandescent gas/pyroclasts at the crater rim. Successively, we applied a percentile-based method to detect individual explosions. Hence, we were able to define the eruptive history and style at each crater. Additionally, the inter-arrival time of explosive events was evaluated

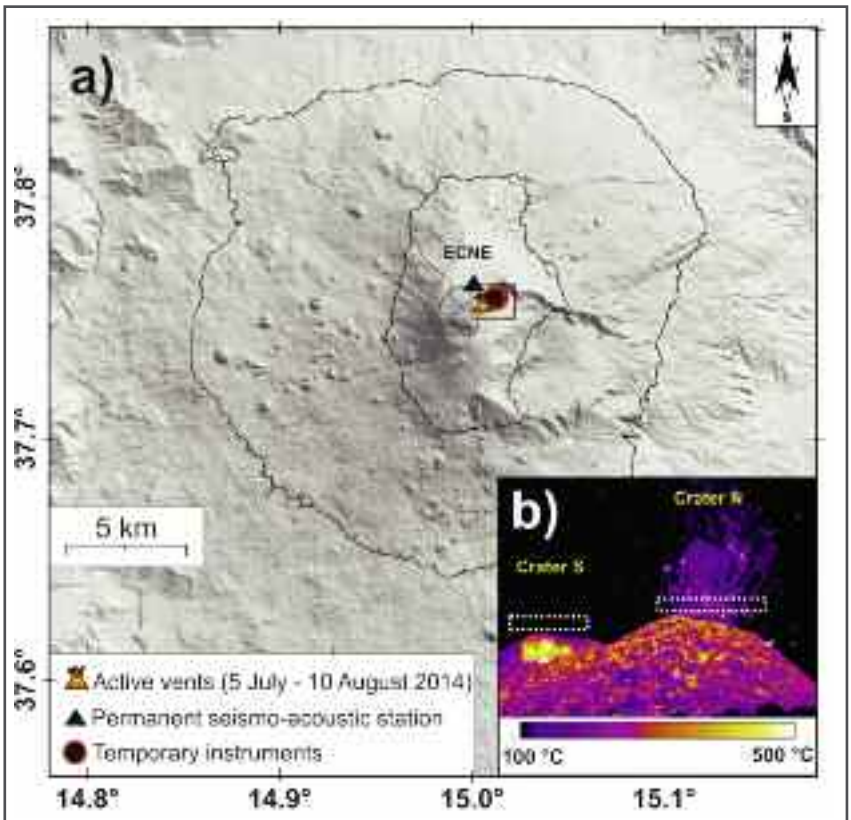

Fig. 1 | **a)** Digital elevation model of Mt. Etna, showing the position of the active vents, the temporary multi parametric stations deployed on 16th July and ECNE station, belonging to the INGV-OE permanent network. **b)** Thermal image of the active vents. The white dotted rectangles indicate the control area defined for thermal analyses (15.9 and 11.6 m wide over the N and S vents, respectively).

and compared with the estimates performed on acoustic recordings from the temporary station and from the permanent INGV-OE network (ECNE station; Fig. 1). During the investigated time, Crater N was characterized by Strombolian activity whereas Crater S alternated Strombolian explosions with puffing. Nonetheless, the overall variation in the recurrence time and amplitude of explosion at the two vents correlates fairly well. The goodness of such relationship was evaluated by the randomized cross-correlation method indicating that the activity at the two vents is not independent, thereby suggesting a shallow partitioning in the plumbing system.

Recycled ejecta modulating Strombolian explosions

A. Capponi, J. Taddeucci, P. Scarlato, D.M. Palladino

Two main eruptive regimes are identified from analyses of high-speed videos collected at Stromboli volcano, based on vent conditions: one where the vent is completely clogged by debris, and a second where the vent is open, without any cover (Fig. 1). By detailing the vent processes for each regime, we provide the first detailed account of how the presence of a cover affects eruptive dynamics compared to open vent explosions. For clogged vents, explosion dynamics are controlled by the amount and grain size distribution of the debris. Fine-grained covers are entirely removed by explosions, favouring the generation of ash plumes, while coarse-grained covers are only partially removed by the explosions, involving minor amounts of ash. In both fine- and coarse-grained cases, in-vent ground deformations of the debris seem to reflect variations in the volumetric expansion of gas in the conduit, with rates of change of the deformations comparable to ground inflation related to pre-burst conduit pressurization. Eruptions involve the ejection of relatively slow and cold bombs and lapilli, and debris is observed to both fall back in the vent after each explosion and to gravitationally accumulate in between the explosions by rolling along the inner crater flanks to produce the cover itself. Part of this material may also contribute to the formation of a more degassed, crystallized and viscous magma layer at the top of the conduit. Conversely, open-vent explosions erupt hotter pyroclasts, with higher exit velocity and with minor or no ash phase involved.

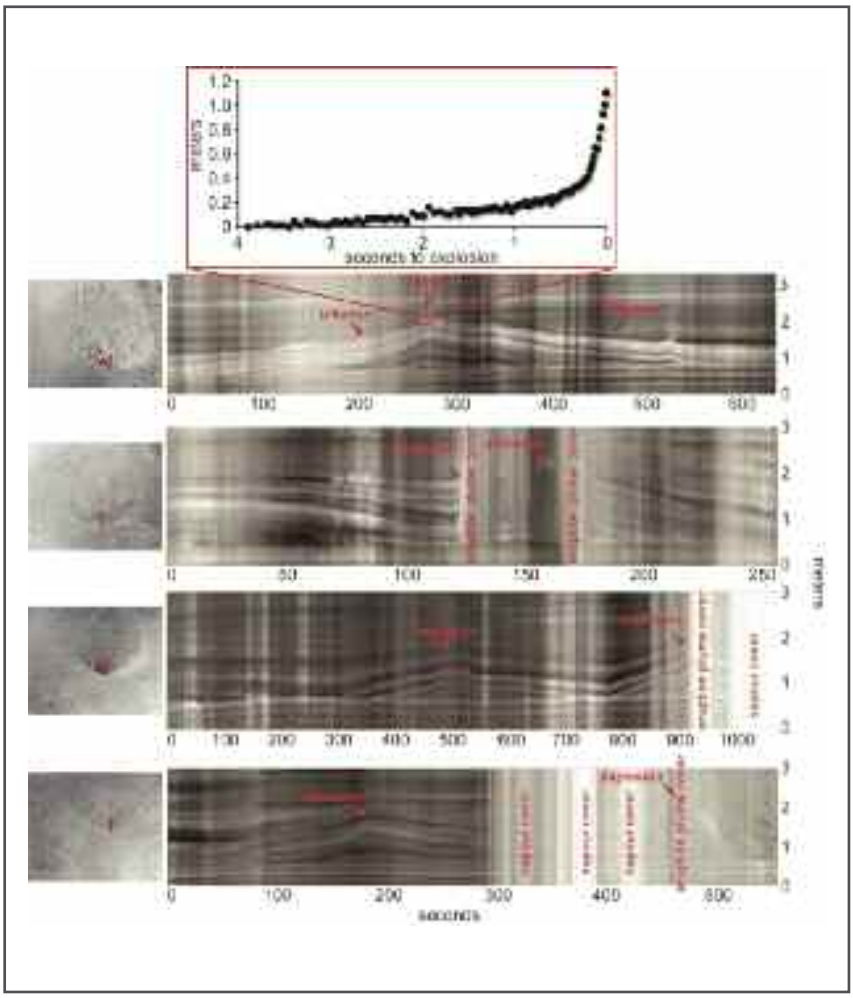

Fig. 1 I Ground deformations of the NE1 vent at Stromboli show that cycles of vent debris inflation-deflation may last several minutes. Each plot displays the temporal evolution of grey levels in the videos along a vertical line crossing the vent (red line, about 3 m long, on the left-hand still frames). Inflation accelerates nonlinearly a few seconds before an explosion (top inset).

3-D high-speed imaging of volcanic bomb trajectory in basaltic explosive eruptions

D. Gaudin, J. Taddeucci, B.F. Houghton, T.R. Orr, D. Andronico, E. Del Bello, U. Kueppers, T. Ricci, P. Scarlato

Imaging in general and high speed imaging in particular are important tools for the study of explosive volcanic eruptions. Traditional 2-D video observations does not allow measuring volcanic ejecta (pyroclasts) displacement in the directions towards and away from the camera, strongly hindering our capability to fully determine crucial hazard-related parameters such as explosion directionality and pyroclasts velocity. In this paper, we adapt stereographic techniques for the study of pyroclasts trajectory in three dimension using multiple synchronized high-speed cameras (Fig. 1). To overcome the difficult observation conditions proper of active volcanic vents, including a large number of overlapping pyroclasts which may change shape in flight, variable lighting and clouding conditions, and lack of direct access to the target, we simplified classical, laboratory-based methodologies by using a laser rangefinder to measure the geometry of the filming setup and manually tracking pyroclasts on the videos. This first order method allows reaching uncertainties down to 10° in azimuth and dipping angle of the pyroclasts, and down to 20% in the absolute velocity estimation. We demonstrate its capability on three examples: a Strombolian explosion showing a clear directionality of the ejection, a bubble burst in Halema'uma'u lava lake showing a complex behavior, and an in-flight collision between two bombs at Stromboli, with generation of lateral momentum.

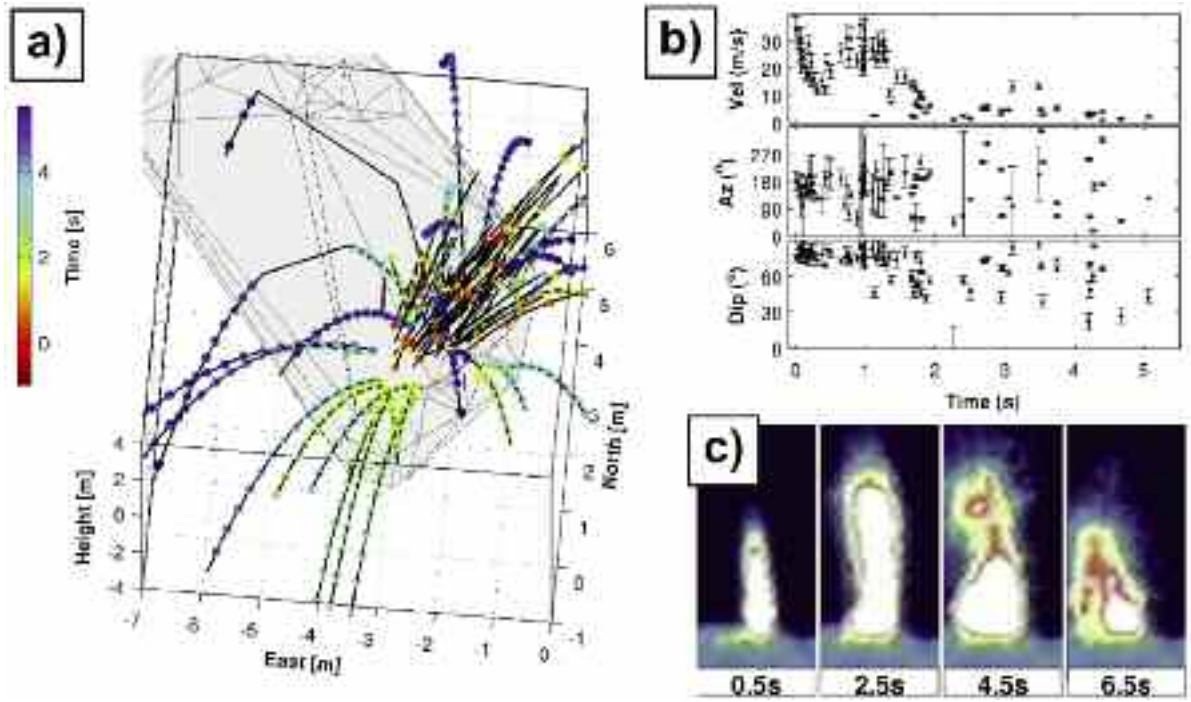

Fig. 1 I Results of the 3-D reconstruction of the 18 May 2014, 11:34:17 GMT explosion at Stromboli. **a)** 3-D reconstruction of the 79 particle trajectories during the explosion, color-coded for time. The dots represent the location of the successive location of the bombs with a time step of 0.10s. **b)** Evolution of the velocity, azimuth and dip angle of the bombs at the exit of the vent. **c)** Detail of the explosion seen by the INGV video monitoring system.

Physical-chemical constraints of the magmatic feeding system of the 2014-2015 explosive eruptive activity at Mt. Etna

P.P. Giacomoni, V. Valenti, S. Mollo, M. Coltorti, C. Ferlito, M. Nazzari

Preliminary compositional data and textural abservations of phenocrysts and glass in products erupted during the 2014-2015 activity from Mt. Etna summit craters have been acquired.

Electron Scansion Microscope observations revealed two distinct textures (Fig. 1): in the first heavily texturized plagioclase of millimetric size are the main phenocryst in tephra from the Voragine Crater; the second, peculiar in products from Bocca Nuova Crater, is characterized by large core to rim compositional profile on dusty plagioclase from Voragine Crater, highlighted an increasing in anorthite content in the dusty, texturized zone; suggesting a reaction with a more basic, hotter and volatile rich magma of a pre-existing plagioclase in equilibrium with a cold (<1050°C) or degassed magma. On contrary, solid assemblage in tephra from Bocca Nuova Crater, suggests an equilibrium at higher-T and high-H_2O content that contributed to lowering the plagioclase liquidus and enhanced the stability of clinopyroxene.

The whole bunch of data gathered during the analytical turn, will be used to calculate crystal-melt equilibria conditions and to estimate the magmatic intensive variables (P-T-fO_2-XH_2O) during magma crystallization inside the Mt. Etna feeding system and to compare the results with those from the 2011-2012 eruptive events.

These events have been characterized by violent strombolian to lava fountains explosions which lasted for few hours and not preceded by significant seismic signals. They represent an important shifting from the prevalently effusive eruptive behaviour of the 2008-2011 events.

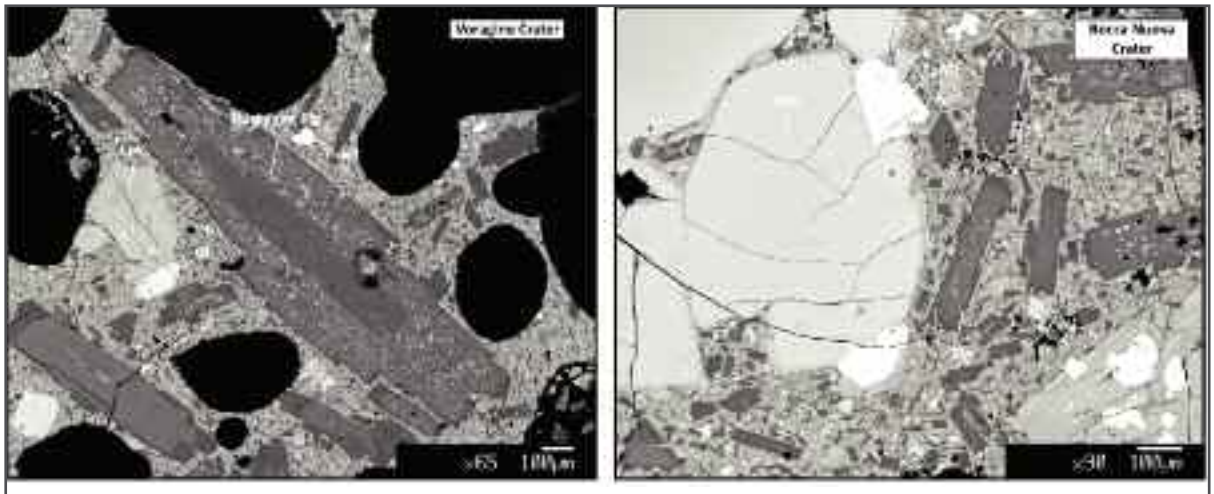

Fig. 1 | **a)** SEM images of tephra from Voragine Crater, characterized by large dusty texture plg and smaller zoned cpx; **b)** SEM images of tephra from Bocca Nuova Crater, the enhanced stability of cpx to respect to that of plg suggesting higher H_2O content and P-T crystallization conditions.

Geochemical characterization of ultramafic xenoliths in North Hartland lamprophyre dikes (New Hampshire-USA)

P.P. Giacomoni, A. Arfè, M. Coltorti, C. Bonadiman, M. Nazzari

The main aim of the project is to characterize the petrographic and geochemical features of some ultramafic xenoliths in lamprophyre lavas from North Hartland (New Hampshire) by electron microprobe (EMP) and electron scanning microscope (SEM). Ultramafic nodules of variable composition in New England have been reported since 70s however, the only two papers describing those outcropping in North Hartland (New Hampshire) are those of Williams and McHone.The host lava is a kaersutite-bearing olivine augite camptonite, and has been dated (whole rock K-Ar) as 130 ± 6 Ma.

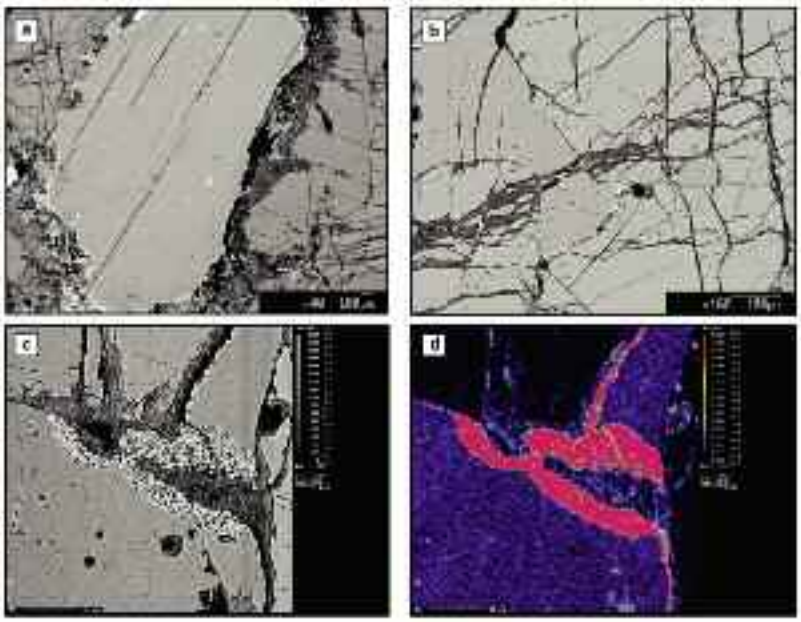

Fig. 1 I SEM microphotographs of xenoliths and host lava. **a)** biotite phenocryst in camptonitic host lava; **b)** harzburgitic mantle xenolits cutted by glassy veins; **c)** reaction zone between intruded glassy vein and ortopyroxene; **d)** map of element.

The three-days analytical turn (28/11-30/11/2016) focused on the geochemical characterization of the main mineral phases (Ol, Cpx, Opx, Sp, Plg, Bt), composition of glasses and on the identification of reaction textures between the ultrafeminc mineral paragenesis and pervasive melts (Fig. 1). Preliminary results reveal the mantle origin of the ultramafic xenoliths. This is an important result, being the literature on mantle xenoliths of Cretaceous age very scarce. Xenoliths are highly heterogeneous with a composite texture predominantly harzburgitic in modal composition, spotted with dunitic enclaves. Clinopyroxene is scarce but present in almost all samples. Two type of glassy veins cut the xenoliths: the first is comptonitic-lamprofiric in composition, comparable with the host lava and contains plagioclase, clinopyroxene and K-feldspar phenocrysts. Biotite is also frequent, sometimes as large phenocrysts (>800 µm). The second type of vein pervades the xenoliths and form complex reaction zones and contains carbonate-bearing mineral phase that we identified as magnesite.

The transition from carbonate to silicate magmas formed by redox melting of a carbonated eclogite

M. Caruso, V. Stagno, M. Nazzari, P. Scarlato

Many experimental studies exist that focused on the effect of CO_2 on phase equilibria within eclogite assemblages with important implications for the deep carbon storage and its contribution to the origin of carbonatitic melts at depths down to the lower mantle. There is evidence of the presence of CO_2-rich oxidized fluids from inclusions trapped in diamonds as well as the major and trace elements distribution in peridotite mantle xenoliths, originated by melting of the subducted volatile-rich crust. On the other hand, thermodynamic calculations would predict carbon (graphite or diamond) being the most stable phase within eclogite rocks even at oxygen fugacity (fO_2) where carbonate is stable within peridotite assemblages. It is, therefore, important to determine the fO_2 and temperature at which diamond (or graphite) turns into carbonate (solid or melts) in typical mantle eclogitic assemblages. The coexistence between elemental carbon and carbonate under subsolidus conditions in eclogite rocks is described by the redox equilibrium,

$$CaMg(CO_3)_2 + 2SiO_2 = CaMgSi_2O_6 + 2C + O_2 \quad [1]$$

dolomite coesite diopside graphite

Although the oxygen fugacity buffered by this reaction can be calculated from thermodynamic data of pure end members, the effect of temperature on the melt composition and the fO_2 buffered by [1] remains unclear. Therefore, we require an assemblage that enables us to measure the oxygen fugacity buffered by carbon/carbonate equilibrium in eclogitic assemblages even above the solidus temperature when CO_2-rich melts form.

We summarize results from experiments at 3 GPa and temperature between 800 and 1200 °C performed using multi anvil presses available at BGI in Bayreuth (Voggenreiter 500 t, Walker-type), Geophysical Lab in Washington DC (1500 t, split sphere) and HPHT lab at INGV in Rome (Voggenreiter 840 t, Walker-type). For all experiments a mixture of synthetic omphacitic glass, SiO_2, natural dolomite and graphite was employed in the system SiO_2-Al_2O_3-MgO-FeO-CaO-Na_2O-C doped with 20 wt% $FeTiO_3$+TiO_2 (1:1 ratio) and 3 wt% iridium. Textural and chemical analyses of all the run products were obtained using the scanning electron microscopy and electron microprobe available at Geophysical Lab and INGV. At 800 °C the recovered run product consisted of a subsolidus mineral assemblage as in [1] with omphacitic clinopyroxene and coesite along with graphite, a dolomitic carbonate phase, ilmenite, rutile and an IrFe alloy (Fig. 1). As the temperature increases a carbonatitic melt forms (900 °C) with 1-5 wt% SiO_2 that evolves to a carbonate-silicate melt (1100 °C) with 25 wt% SiO_2 and, at 1200 °C, to a silicate melt with ~32 wt% SiO_2. The use of IrFe alloy can be used as redox sensor to test the validity of [1] using the equilibrium,

$FeTiO_3 = TiO_2 + Fe + 0.5O_2$ [2]

ilmenite rutile alloy

where [3]

$$\log fO_2 = 2 \cdot \left[\frac{-\Delta G_r^0}{2.3RT} - \log a_{Fe}^{metal} + \log a_{FeTiO_3}^{ilmenite} \right]$$

Figure 3 shows experimental measurements of fO_2 obtained using [3] compared with the fO_2 for DCDG buffer (equilibrium 1) calculated using thermodynamic data for pure end-members. Importantly, such diagram allows also an interlaboratory comparison in terms of target pressures.

In conclusion, preliminary results show that as temperature increases the fO_2 at which carbon and carbonate are equilibrated within eclogite rocks is lower than thermodynamic predictions as result of the dilution of CO_2 in the melt. Magmas from carbonatitic to silicate in composition might originate from a graphite (or diamond)-rich source only when the fO_2 of eclogite rocks crosses the carbon/carbonate equilibrium at solidus temperatures (~900 °C). Further experiments will be performed at 6 and 11 GPa to determine the temperature at which redox melting can occur.

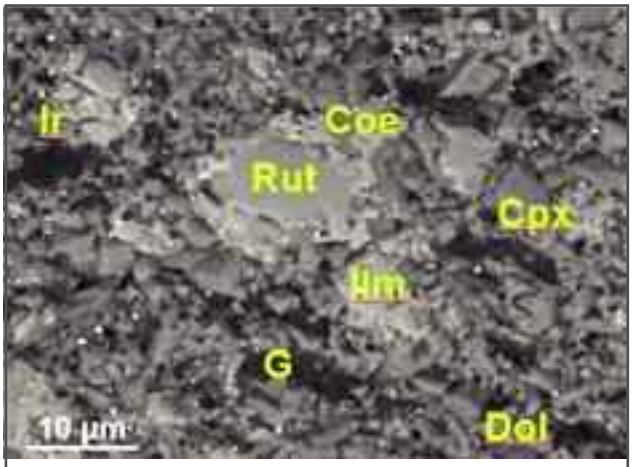

Fig. 1 I BSE image taken by FE-SEM (JEOL-JSM6500F) at Geophysical Lab of the recovered run product from 3GPa/800 °C after 24 hr showing a Ti-bearing assemblage with rutile and ilmenite. Notes: coesite (Coe), omphacitic clinopyroxene (cpx), graphite (G), dolomite (Dol), rutile (Rut), ilmenite (Ilm) and iridium-iron alloy (Ir).

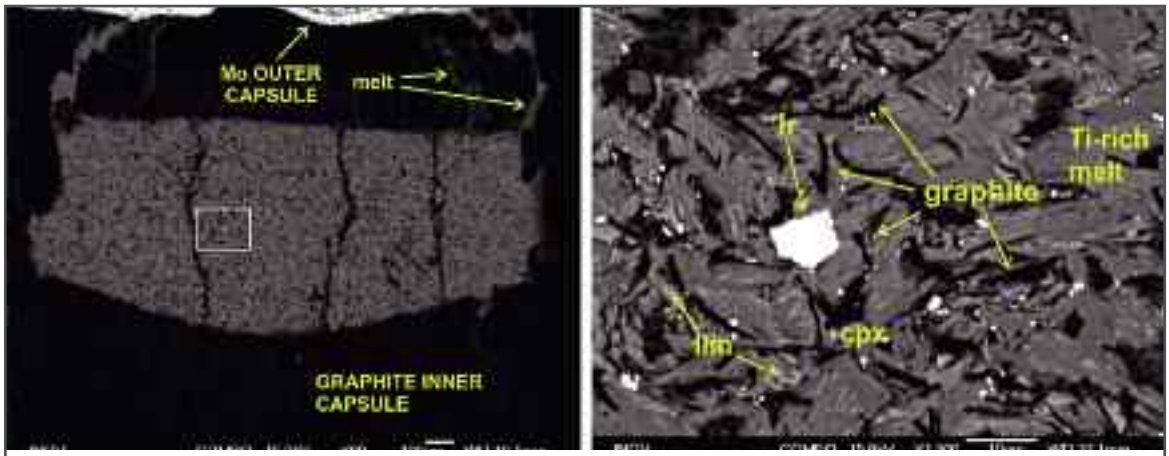

Fig. 2 I BSE images using FE-SEM at INGV that show run product at 3 GPa and 1200 °C (run M76).

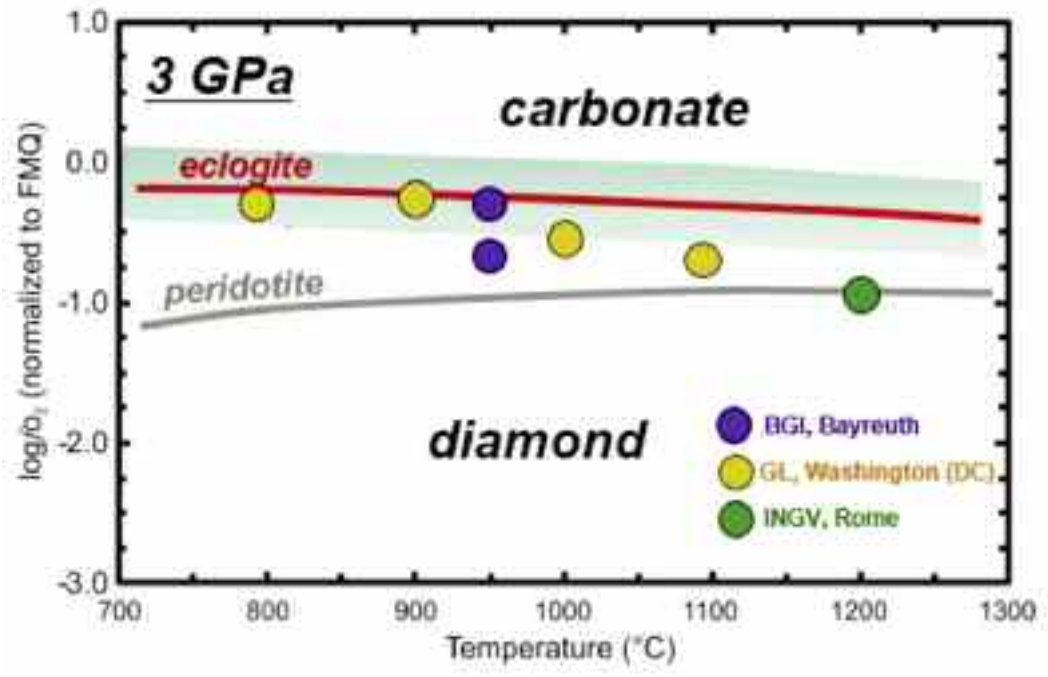

Fig. 3 I Shown is the predicted fO_2 using eq. (1) (DCDG) as function of temperature. The blue-shaded area indicates the standard error for the calculated fO_2. Shown is also the calculated fO_2 for a peridotite assemblage (EMOD). Values are normalized to the fayalite-magnetite-quartz (FMQ) buffer. Circles are the experimental measurements of fO_2 using eq. (3).

Anthropogenic magnetic particulate in the central Apennines snow deposit and Urban area: a comparison

L. Alfonsi, P. Macrì, M. Nazzari

We utilize rock magnetic mineralogy and FESEM and EDS analysis of Fe-particles to investigate characters of the magnetic content of the solid residual contained in snow samples collected in the central Apennines area and in Urban Rome. The snow samples are collected in the Apennines in the late spring season, this to allow the maxim deposition of the possible particulate and taken in both rural and exploited areas (Gran Sasso, Sirente and Campo Felice, and Campo Imperatore natural reserves). For what concerns the sampling in urban district we collected snow samples

Fig. 1 I **A)** Typical sampling locality in the Apennines; **B)** Vacuum filtering system employing a Whatmann filter n.42.

in Rome in February 2012; in that case the samples were taken a week after the snow storm that heavily affected the city of Rome.

The whole set of analyses are devoted to discriminate the anthropogenic contribution to the soil and atmospheric pollution in different environments utilizing the snow as a neutral micro-particles collector. Magnetic particles associated to anthropogenic pollution are often related to heavy metal content and, iron oxides.

A total of 63 samples, snow and terrain samples of the sampling location (this latter aspect was necessary to discriminate between natural provenance of the Fe and Fe-oxides and hydroxides and the anthropogenic contribution on the snow residual). The snow samples were collected with a bottle (one liter volume) on selected snow patches (Fig. 1A), the snow is then melted at room temperature and filter utilizing a vacuum filtering system, specifically designed to fulfill the purposes of this research topic (i.e. the need to retain particles greater or equal than 0,25 micron; Fig. 1B).

The preliminary rock magnetism analysis, necessary to select the suitable samples for the subsequent FESEM and EDS analyses, have been carried out and we are on the way to perform the second step of the research. The rock magnetic analysis carried on the solid residual obtained from the snow showed, unexpectedly, quite high values of magnetic susceptibility, confirming the presence of magnetic material. Titanomagnetite, and in some cases haematite are the magnetic carriers found in the samples analysed. The microscope observations, on selected samples will help to qualitatively characterize the chemical content and identify the morphological aspects of the magnetic fraction. For this the JEOL JSM 6500F Field Emission Scanning Electron Microscope (FESEM, resolution of 1.5 nm), operating at 10/15 kV equipped with detectors for x-ray (EDS, with a resolution of 133 eV) will be used to analyze the material extracted from the snow samples. The shape of the ferromagnetic particles of anthropogenic origin is well known in the literature; the FESEM and EDS analyses of Fe-Particles is a specific technique widely used as a fundamental instrument to identify magnetic particles produced by anthropogenic combustion processes. A suitable result would be to discriminate if any among the natural and anthropogenic content of Fe rich particles in natural environments and urban area and qualitatively characterize it.

Volcanology of the acid magmatism in the Parana Province, Brazil

S.P. De Cristofaro, L. Polo, M. Masotta, S. Mollo, D. Giordano

The study of volcanism has always aroused great academic and social interest, especially in countries where volcanic activity is an important geological risk factor (e.g. Italy and Japan). In recent years, this field has seen a remarkable flowering also in Brazil, where, despite the absence of such risks, past volcanic records are very abundant, and responsible for the generation of some of the most important mineral resources (e.g. gold (in the Nova Lima), iron, lead in the Serra dos Carajas and Minas Gerais). Brazil hosts the dominant part of the Paraná-Etendeka Magmatic Province, the second largest igneous province on Earth covering an area of 1.200.000 km^3 at ages of 131-134 Ma (hereinafter referred to as PMP; Paraná Magmatic Province). The investigation of the PMP volcanism has gained much interest in the international community, especially regarding the recognition of the mantle sources of several distinct basalt magma types, their evolution in the crust and their genetic relations with associated silicic magmas. Although investigation of petrological evolution and dynamics of magma ascent for basaltic volcanism has been already studied in detail in the last 30 years, very little has been done to comprehend those mechanisms that determine the emplacement of the acidic magma bodies of the southern part of the PMP. It is not clear whether the eruptive style of those magmas was explosive or effusive. There has been lot of controversy related to the recognition, origin, transport and emplacement mechanisms of intensely welded to rheomorphic ignimbrites and lava flows. The absence of unequivocal vitroclastic textures frequently complicates the distinction between volcaniclastic (explosive) deposits and lava flows. Few studies have been developed to comprehend those mechanisms that determined the emplacement of the silicic magma bodies of the southern part of PMP. Furthermore, we focused our attention in the Rio Grande do Sul region in the southern border of the PMP. Our interest was in particular aim at the felsic (e.g. rhyolites, dacites) volcanic rocks constituting the Palmas-type eo-

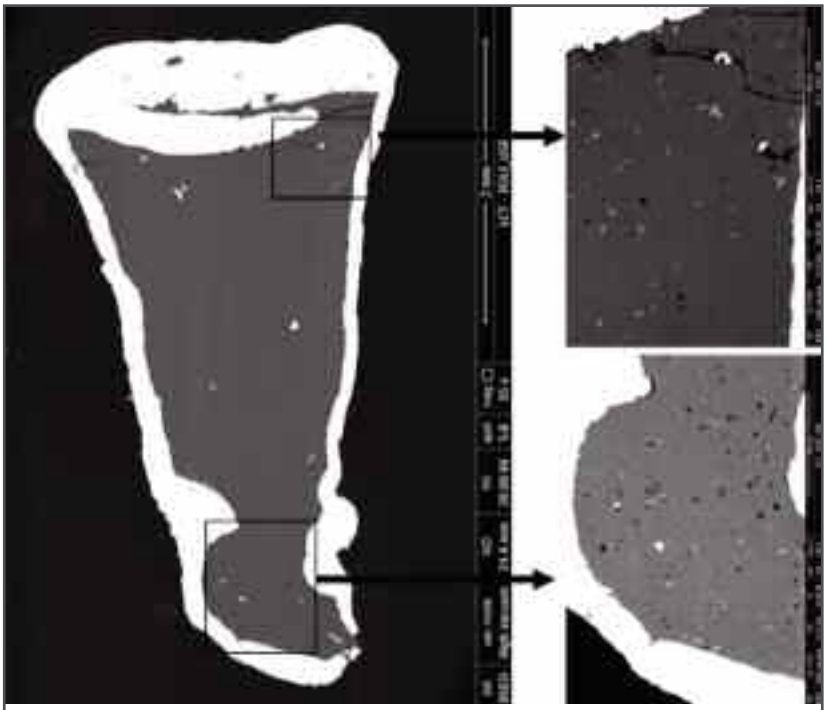

Fig. 1 I Backscattered images of experimental run at P=150 MPa and T= 950°C - heating rate = 80°C/min with 2 wt. % H_2O.

cretacic sequence already well characterized from a geochemical point of view by several authors as it follows: 1) Caixas do Sul constituted by dacitic lava; 2) Barros Cassal sequence represented by basaltic andesite to dacitic rocks with discontinuous emission of lava inter-layered by sedimentary rocks and 3) Santa Maria rhyolitic sequence. To solve the above questions, we selected the most representative felsic samples and we started with the first experimental data addressed to the investigation of the processes of crystallization kinetics in equilibrium conditions (in magma chamber) and eventual disequilibrium (during the magma ascent towards the surface). Further, we started a preliminary experimental campaign devoted to the characterization (at varying water content, H_2O) of the Pressure – Temperature conditions which brought to the formation of the investigated magmas. Phenocrysts (pyroxene, plagioclase and Ti-magnetite oxides) are taken representative of P-T conditions, whereas the analysis of the microlites allow us to constrain the evolution of magma conditions during (cooling and decompression) the ascent toward the surface. We decided to start the first grid of petrological experiments for the first sequence Caxias do Sul (CS). This grid is based on calculations by software Melts (Rhyolite-MELTS) and results of geothermometer and hygrometer. At the begin, we decide to performed 4 hydrothermal syntheses of the glass. We obtained the glass hydrate, reference sample for the CS magma, with two different amount of water (two with 2 H_2O wt. % and two with 4 wt. %). All the experiments were run in a quick press, solid-medium piston cylinder apparatus at pressure of 150 MPa in different ranges of temperature (900°C to 1000°C). We performed 4 runs: in each runs we loaded 3 capsules (each starting material was a mix between natural samples and hydrated synthesis with 0-2 and 4 wt. % H_2O). The addition of natural sample was done to support the kinetics crystallization and accelerate the reaching of equilibrium during the run (only about 10% of the natural crystal-bearing sample). Figure 1 shows some photos studied after the running, where evidence the crystallization of different phases (Px-Pl, Fe-Ti oxides) in a less or more intensively crystallized ground mass. This methodology proves, in the initial datasets, to provide insights for the sample of dynamics in which were unavailable to date.

Viscosity of crystallised silicate melt

F. Vetere, V. Misiti

Magma is natural material which contains mainly silicate melts, crystals and volatile phases. It is of primary importance to study magma properties in order to infer how natural processes, such as the mechanisms of eruption and emplacement take place; for instance lavas flowing on a certain topography will have different velocities reflecting its chemical and rheological status. Thus providing a unique picture of the processes occurring in the interior and exterior of volcanoes is fundamental for better mitigate related risks. On such, magmas will strongly affect volcanic behaviour, and in particular their eruptive mechanisms, when for instance parameters such as crystallinity, varies. The prediction of the viscosity of natural systems at high temperature and pressure is well depicted in literature but still there are shaded areas that need to be investigated. In most cases, magmatic temperature allow magma to crystallize in dependence on the related cooling rate that strongly will affect nucleation and crystallization processes. This means that high temperature magma is formed by an amorphous matrix, where, due to decreasing in temperature or possible volatile loss, ordered phases can nucleate and grow.

The effective viscosity of a system with low crystals content (<10 vol%) can be estimated from the Einstein-Roscoe equation. With the increasing volume fraction of crystals, from 10-50 vol%, the rheology of the system changes abruptly. This implies that the relationship of effective viscosity to melt fraction is non-linear, and particles shape, aspect ratios, concentration, size distribution, and maximum packing fraction can transform magmas from simple Newtonian fluids to more complex rheological materials.

Glass stability (GS) upon heating of non-crystalline solids with sub-alkaline natural compositions by DSC, SEM and EPMA

G. Iezzi, F. Vetere, A.L. Elbrecht, V. Misiti, M. Davis, A. Cavallo, S. Mollo

The reluctance or facility to crystallise of a glass upon heating is called glass stability (GS); GS can be characterised by several methods and parameters and is frequently used to retrieve glass-forming ability (GFA) of corresponding counterpart liquids. Here, GS has been determined for the first time on sub-alkaline glasses, with the most widespread and abundant compositions of volcanic rocks on Earth. The two end-members are a basalt and a rhyolite, labelled B_{100} and R_{100}, whereas the other are intermediate compounds: $B_{80}R_{20}$, $B_{60}R_{40}$, $B_{40}R_{60}$, $B_{20}R_{80}$, for which critical cooling rates (*Rc*) have been already determined. Each glass was heated in a differential scanning calorimetry (DSC) at a rate of 10 °C/min (600 °C/h) to measure T_g (glass transition), T_x (onset of crystallization) and T_m (melting) temperatures, from ambient to liquidus temperatures, then quenched. The *ex-situ* run-products have been characterised by SEM and EPMA to quantify textures and compositions of phases, respectively.

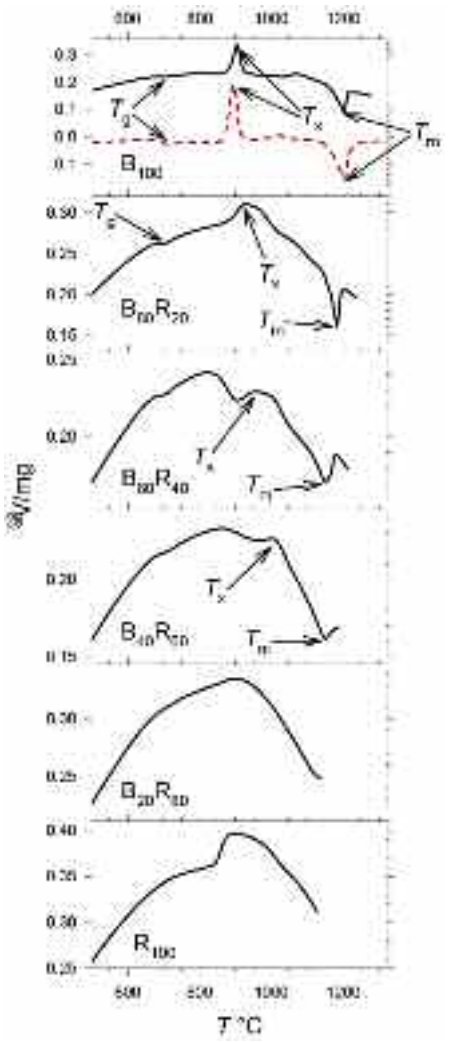

Fig. 1 I DSC spectra of the six glasses heated at 10 °C/min. All glasses were measured using alumina holders, except the B_{100} measured either in Pt (dashed red line) and alumina sample holders. The glass transition, onset of crystallization and melting temperatures (T_g, T_x and T_m, respectively) are indicated by arrows. The $B_{20}R_{80}$ and R_{100} compositions do not shown any peak. From B_{100} down to $B_{40}R_{60}$ the peaks are progressively less prominent.

R_{100} and $B_{20}R_{80}$ do not shown any DSC peak, whereas $B_{40}R_{60}$, $B_{60}R_{40}$, $B_{80}R_{20}$ and B_{100} thermograms display progressive more resolvable spectra. As SiO_2 (wt.%) in the system increases from B_{100} to $B_{40}R_{60}$, T_x almost linearly increases, T_m first decreases and then levels off, whereas T_g poorly changes (Fig. 1). In agreement, from B_{100} to $B_{40}R_{60}$ the amount of glass (gl) increases from 48.5 to 97 area%, clinopyroxene (cpx) decreases from 47.7 to 16 area%, whereas spinel (sp) accounts of only 0.9 to 3.8 area%. R_{100} and $B_{20}R_{80}$ are instead completely glassy. In B_{100} and $B_{80}R_{20}$, plagioclase (plg) crystallises heterogeneously on the Al_2O_3 holders only at a distance < 100 µm from it. R_{100}, $B_{20}R_{80}$, $B_{40}R_{60}$ and $B_{60}R_{40}$ *ex-situ* glasses have chemistries identical or nearly so to their starting compositions, according to the absence or scarcity of crystals formed during heating. Instead, B_{100} and $B_{80}R_{20}$ glasses are enriched in Si, Al and Na and depleted in Fe, Mg and Ca due to internal cry-

stallization of sp and mostly cpx. Cpx in B_{100} is relatively rich in Ca and Mg.

Several GS parameters (K_T, K_H, K_W, K_{LL} and w_2) increase linearly and monotonically as a function of SiO_2, with very high correlations. T_x values and GS parameters highly correlate with GFA *via Rc* values, i.e. GS scales with GFA for natural silicate compositions. In addition, the *in-situ* Rc value of B_{100}, measured with DSC, results > 45 °C/min (> 2700 °C/h), broadly corroborating the *Rc* of about 150 °C/min (9000 °C/h) determined by previous *ex-situ* cooling-induced experiments. Relevant solidification parameters can be obtained by DSC investigations also for chemically complex (natural) systems, similar to simple silicate systems composed of few atoms. These outcomes apply to hot silicate liquids (lavas or magmas) that re-heat glass-bearing volcanic rocks or to glass-ceramic materials based on abundant and very cheap raw materials.

Rheology of suspensions at high shear rates and implications for the flow of slurries, mudflows and sludge

P. Del Gaudio, G. Ventura

The knowledge of rheological properties of water-rich clay to sand suspensions covers an important role in nature as well engineering. Water-rich clay to sand suspensions like mud-flows, slurries and sludge are characterized by a complex, share rate dependent flow behavior. The rheology of such suspensions depends first by rate of deformation then by the size and shape of the suspended particles and by the water (solid) content. The knowledge of the appropriate rheological model (e.g., Netwonian, Bingham or Herschel-Bulkley), which is also a function of particle interaction and lubrication processes, is of primary importance for geological, hydraulic, mining, and civil engineering applications and studies. Our study presents the results of experimental rheological measurements of water-rich (40 to 60 wt.%) clay to silt (population A) and silt to sand (population B) suspensions mixed in different proportions. The data are consistent with the Herschel-Bulkley model. At high shear rates (~200 to 1000 s^{-1}) most of the studied suspensions show a dilatant (shear thickening) behavior with values of the flow index n>1. The viscosity, consistency *K* and yield stress τ_0 decrease as the A+B fraction decreases and the content of B particles increases. This behavior is due to competing effects of the lubrication and frictional processes as function of particle size and water content. Results from an application of the Herschel-Bulkley model to suspensions flowing on an inclined plane show that the flow velocity significantly changes as small variations of water or coarse (fine) fraction occur. In particular we observe that at constant B fraction and total solid fraction flow velocity increases increasing water fraction. Reducing the total water fraction and, therefore increasing the total solid content, the flow velocity stays constant increasing the B fraction (Fig. 1). This has relevant interest for the studies on the hazard related to dam rupture or floods.

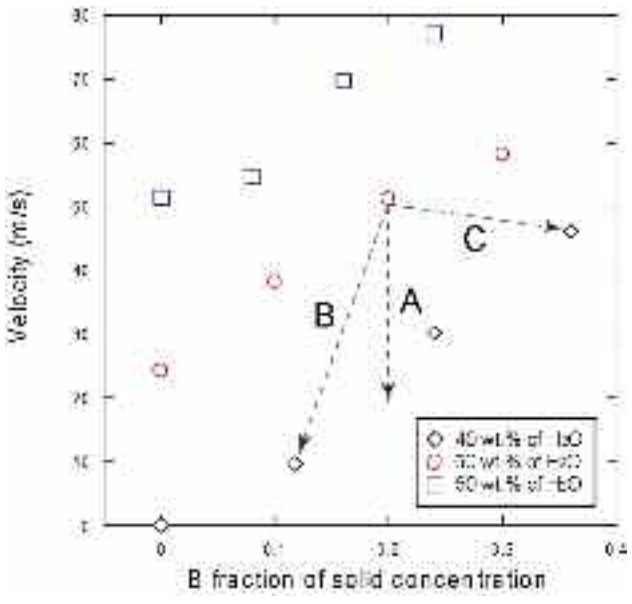

Fig. 1 I The diagram displays the dependence of the flow velocity of water-rich suspensions (40, 50 and 60 wt % of water) as a function of coarse fraction (B fraction).

Effect of particle volume fraction on the settling velocity of volcanic ash particles: insights from joint experimental and numerical simulations

E. Del Bello, J. Taddeucci, M. de' Michieli Vitturi, P. Scarlato, D. Andronico, S. Scollo, U. Kueppers

Most of the current ash transport and dispersion models neglect particle-fluid (two-way) and particle-fluid plus particle-particle (four-way) reciprocal interactions during particle fallout from volcanic plumes. These interactions, a function of particle concentration in the plume, could play an important role, explaining, for example, discrepancies between observed and modelled ash deposits. Aiming at a more accurate prediction of volcanic ash dispersal and sedimentation, the settling of ash particles at particle volume fractions (ϕ_p) ranging 10^{-7}-10^{-3} was performed in laboratory experiments and reproduced by numerical simulations that take into account first the two-way and then the four-way coupling (Fig. 1).

Systematic large-scale ash settling experiments using natural basaltic and phonolitic ash were performed by releasing ash particles at different, controlled volumetric flow rates, in an unconstrained open space and at minimal air movement. Particles terminal velocity, size, and volume fraction was measured with a high-speed camera at 2000 fps.

Results show that the velocity of particles settling together can exceed the velocity of particles settling individually by up to 4 times for $\phi_p \sim 10^{-3}$. Comparisons between experimental and simulation results reveal that, during the sedimentation process, the settling velocity is largely enhanced by particle-fluid interactions but partly hindered by particle-particle interactions with increasing ϕ_p (Fig. 2). Combining the experimental and numerical results, we provide an empirical model allowing correction of the settling velocity of particles of any size density, and shape, as a function of ϕ_p. These results will impact volcanic plume modelling results as well as remote sensing retrieval techniques for plume parameters.

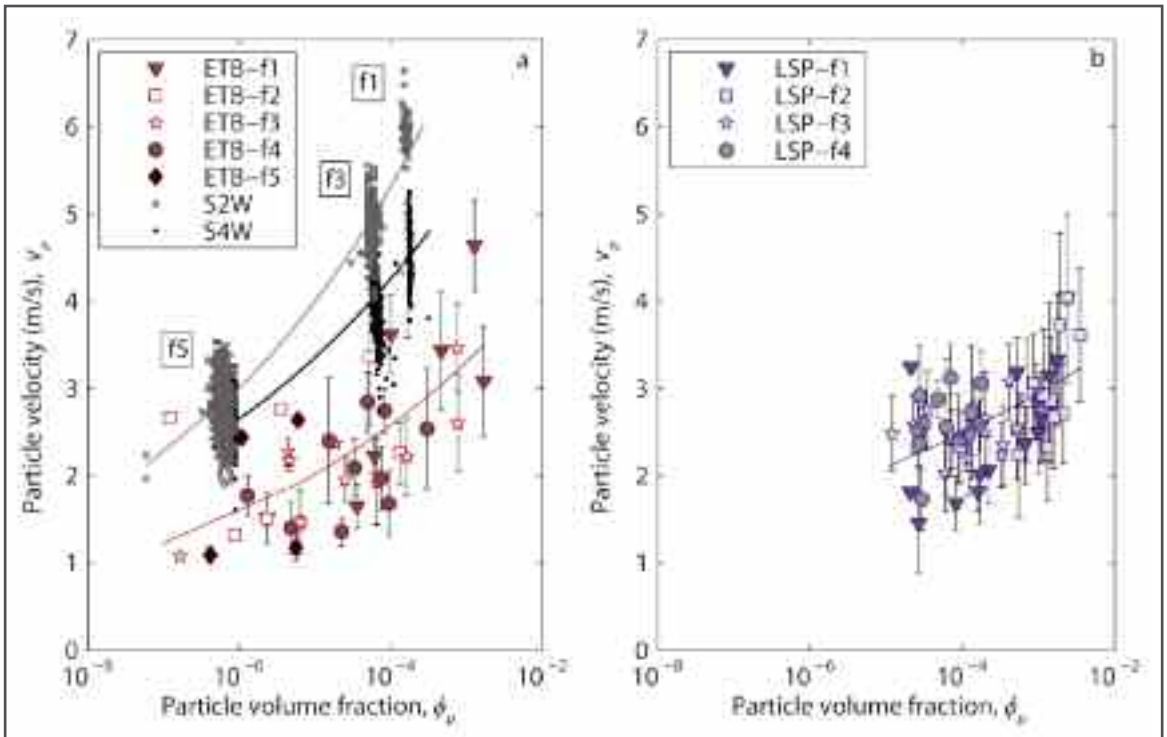

Fig. 1 | Effect of particle volume fraction (ϕ_p) on the settling velocity of particles (v) for the Etna Basalt (ETB, a) and Laacher See phonolite (LSP, b) experiments. Filled symbols denote the mean value with standard deviation (error bar) of data binned (every 5s) for different mass discharge rate runs. The two-way (S2W) and four-way (S4W) numerical simulations are shown for comparison in (a), points representing the mean value sampled every 0.2s of simulation time for the different mass discharge rate runs.

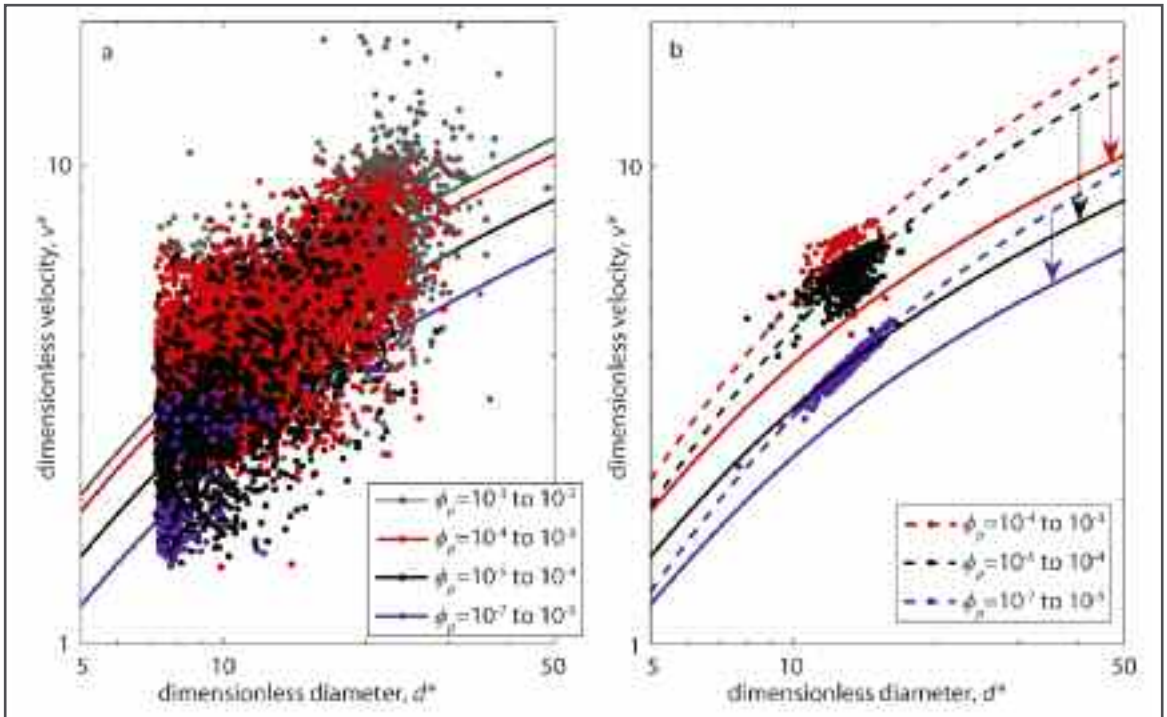

Fig. 2 | Dimensionless particle size versus dimensionless settling velocity for the experimental **(a)** and numerical cases **(b)**. Different colors denote particles settling within variable intervals of particle volume fraction. Fitting curves are solid and dashed for the experimental and numerical cases, respectively. Arrows in **(b)** mark the deviation between spherical and irregular particles.

Experimental viscosity measurements of carbonatitic magmas at pressures and temperatures of the Earth's upper mantle

V. Stagno, V. Stopponi, Y. Kono, M. Nazzari, P. Scarlato

Carbonatites are igneous rocks either intrusive or extrusive that crystallize during cooling of a magma with more than 50 wt% of a carbonate component and less than 10 wt% of silica (SiO_2), likely originated by partial melting of mantle rocks in presence of CO_2 other than shallower processes such as liquid immiscibility and fractional crystallization of magmas during their ascent up to the surface. Although many studies have been carried out over the last decades to understand the origin of carbonatitic magmas at depth, their viscosity as function of pressure result little known yet. The main goal of this preliminary study was to determine experimentally the viscosity of synthetic primary carbonatitic magmas at pressures of 1.5-6 GPa and temperature between 1050 and 1500 °C where the *"falling sphere"* technique combined with the Paris-Edinburgh press was used simultaneously with in situ X-ray radiography at Advanced Photon Source synchrotron facility (Argonne, USA). The starting carbonatitic glass used in these experiments was previously synthesized from a mixture of oxides and carbonates at 3 GPa and 1400 °C using a multi anvil press apparatus. A test experiment was performed at similar pressures and temperatures using the 840t Voggenreiter multi anvil press available at the HPHT lab of INGV (Rome) where the same glass was equilibrated with San Carlos olivine loaded in a graphite capsule to test its buoyancy and equilibrium chemical composition. Both the synthetic starting glass and recovered quenched products from in situ viscosity measurements were analyzed with the JEOL JXA-8200 electron microprobe (INGV) to investigate their texture and chemical composition. The typical quench texture of the carbonatitic melt can be seen in figure 1. Our preliminary data were obtained by converting the velocity of the falling platinum sphere (see Fig. 2) in melt viscosity from the Stokes law. The experimental results show

Fig. 1 I BSE image from EMPA analysis on the recovered carbonatitic melt after viscosity measurements showing quench texture.

an extremely low viscosity for carbonatitic magmas at upper mantle conditions in the range of 0.007-0.02 Pa·s with negligible pressure dependence. It follows that the ascent rate calculated for carbonatitic melts is 30-50 m/y and the estimated time of emplacement of carbonatite deposits is 170.000 y. Additionally, we investigated the structure of the synthetic carbonatitic melt after the viscosity measurement at high pressure and temperature using the multi-angle energy dispersive X-ray diffraction technique. The obtained diffraction data in Figure 3 shows the cation–oxygen and cation– cation distances of the melt at 2.5 GPa at 1200 °C.

The experimental results from this study represent the first preliminary data that can be used in the field of geodynamics modeling of the ascent of primary carbonatitic magmas and carbon speciation from the mantle up to the surface as function of time.

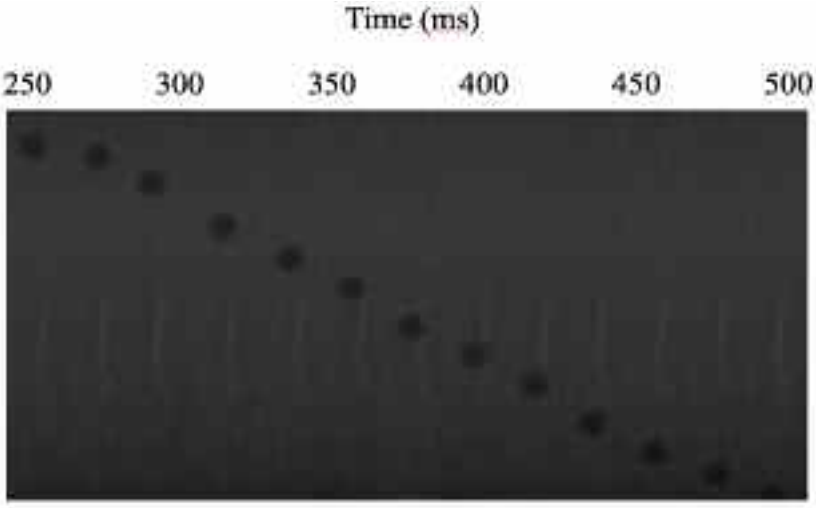

Fig. 1 I In situ X-ray radiography images of the Pt sphere in synthetic carbonatitic melt as function of time for an experiment at 2.5 GPa and 1168°C performed at Argonne National Lab (HPCAT beam line).

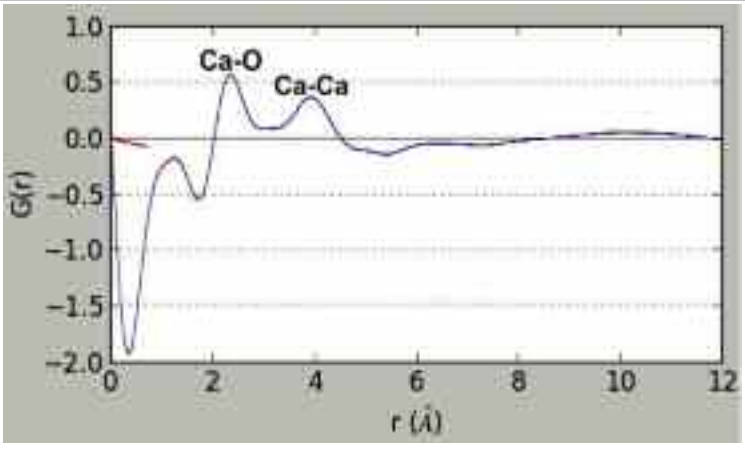

Fig. 2 I Atomic structure of the carbonatitic melt measured at 2.5 GPa and ~1200 °C. The reduced pair distribution function G(r) was measured using the multi-angle energy dispersive X-ray diffraction technique at HPCAT beamline (Argonne National Lab, USA).

An experimental study on carbonate assimilation by ultrabasic magmas

N. Luciani, M. Lustrino, M. Masotta, M. Nazzari, V. Stagno

Carbonatite rocks are extremely rare igneous rocks with more than 50% carbonate minerals, and are generally characterized by less than 10 wt % SiO_2.The entire circum-Mediterranean area is characterized by very scarce outcrops of carbonatite, and one of the best studied Italian case is recorded inthe so-called Italian Intra-Apennine ultra-alkaline Province close to the Polino village (Terni). The Polino rocks are classified in literature as calciocarbonatites, formed by cooling of primary CO_2-rich magmas that variably interacted with peridotitic assemblage before reaching the surface.

However, based on textural compositional evidences, a much shallower origin of these carbonate-rich rocks, following assimilation processes by silicate magmas at expenses of sedimentary carbonate rocks cannot be excluded. In order to explore such possibility, we performed experiments at 2 kbar and 1100, 1200 and 1300 °C using the QuickPress available at HPHT lab of the INGV (Rome). The starting material employed in this study was a silicate glass synthesized by melting a natural polzenite (a melilite-bearing strongly SiO_2-undersaturated rock) from the Bohemian Massif (38.5 wt% SiO_2) at ambient pressure, and mixed with $CaCO_3$ added in different proportions (10, 30 and 50 wt%). The three starting materials were, then, loaded in platinum capsules welded at the bottom and top

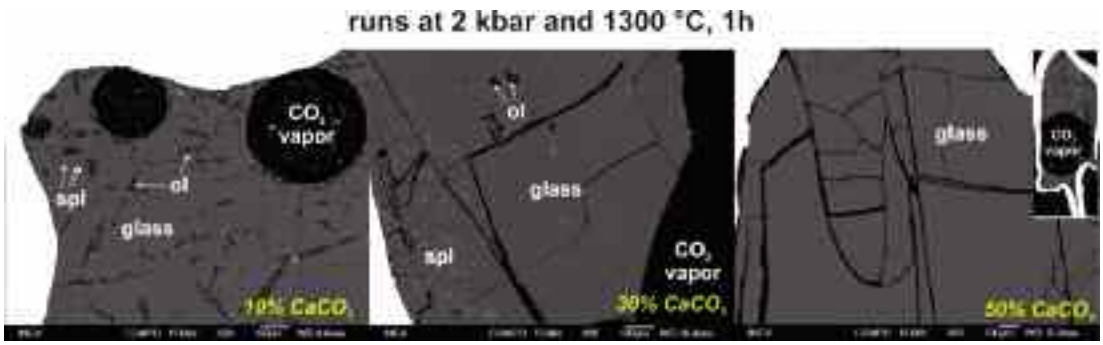

Fig. 1 I BSE images relative to a run at 2 kbar and 1300 °C as function of the $CaCO_3$ content added to the starting glass used for our experiments.

and run simultaneously to ensure the same experimental conditions. The temperature during our experiments was monitored using a C-type thermocouple placed near the bottom of the capsules. The experiments were quenched by shutting off the electrical power after 1h and 6h. The recovered run products were mounted in epoxy resin and polished for textural and chemical analyses using the field-emission scanning electron microscope JSM-6500F, and JEOL JXA-8200 electron microprobe available at the INGV (Rome). Some preliminary results from our experiments are shown in figures 1-3. All recovered products show the presence of bubbles that can be taken as proof of saturation in CO_2. At 1300 °C Mg-rich olivine (Fig. 1) coexists with an ultrabasic glass (37 wt% SiO_2) in run with 10% added calcite; the same phase coexist with 33 wt% SiO_2 glass in runs with 30% added calcite. The addition of 50% calcite to the

starting material results in the formation of a melt with even less SiO_2 (29 wt%) and an estimated CO_2 content of ~8 wt%. The CaO content of the produced melt at 1200 °C increases from ~20 wt% - with 10 wt% calcite added - to ~32 wt% when 50% calcite is mixed with the starting material. Interestingly, a similar amount of CaO is measured in melts produced at 1300 °C, which implies a negligible temperature dependence. The dependence of the CaO content from composition and pressure appears also negligible when the data are compared with data in literature on calcite assimilation from basaltic melt (+1 wt% H_2O; Fig. 2a). Olivine is the liquidus phase in all the experiments (Fig. 2b). Its maximum CaO content is ~2 wt% either at 1200 °C/50% $CaCO_3$ or 1300 °C/30% $CaCO_3$, in agreement with thermodynamic calculations derived from the olivine-monticellite solvus. Similar CaO contents have been measured in olivine rims surrounded by monticellite in Polino rocks. The incorporation of such amount of Ca in the M site of olivine implies a decrease in FeO (Fig. 2c). An assemblage with olivine, spinel, melilite (+ CO_2 vapor) is observed (Fig. 3) in runs quenched at 2 kbar and 1100 °C.

These preliminary results extend our knowledge about the effect of carbonate assimilation on the magma composition, and provide an alternative explanation on the origin of the ultrabasic Ca-rich CO_2-bearing melts of Polino.

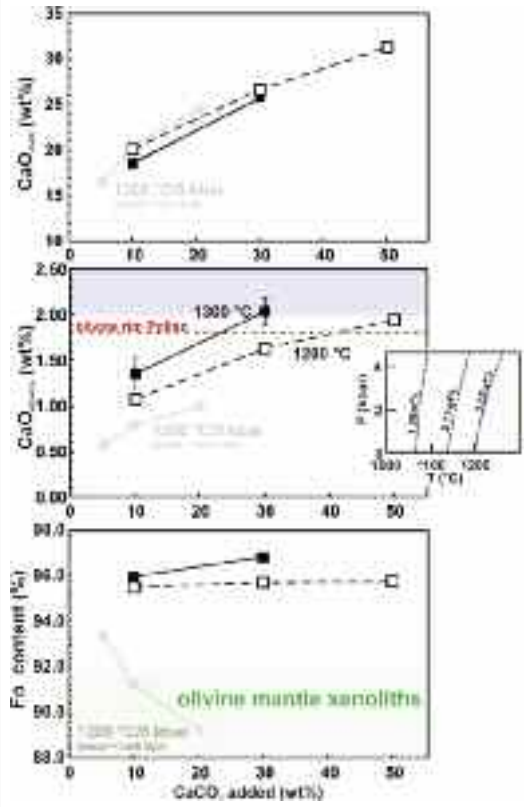

Fig. 2 | **a)** This figure shows the increase of CaO content in the melt as function of the added $CaCO_3$. Only experiments at 1300 °C (continue black line and black squares) and 1200 °C (broken black line and white squares) have been reported, because no analyzable glass pocket has been found in 1100 °C experiments. The grey line and grey squares are the experimental results of Mollo et al. 2010 conducted on hydrated basaltic composition doped with variable amounts of $CaCO_3$. **b)** This figure shows the variation CaO content of liquidus olivine as function of the added $CaCO_3$. The red dashed line indicates the maximum content of CaO in olivine rims in Polino igneous rocks. The pale-violet shaded area is a thermodynamic prediction of the maximum CaO content in olivine equilibrated with monticellite as function of pressure and temperature (see inset). **c)** This figure shows the Fo content [Mg/(Mg+Fe)*100] of liquidus olivine as function of the added $CaCO_3$. Fo content of olivine in worldwide mantle xenoliths is shown for comparison. Gray squares are literature data from similar runs were a hydrated basaltic glass was used as starting material.

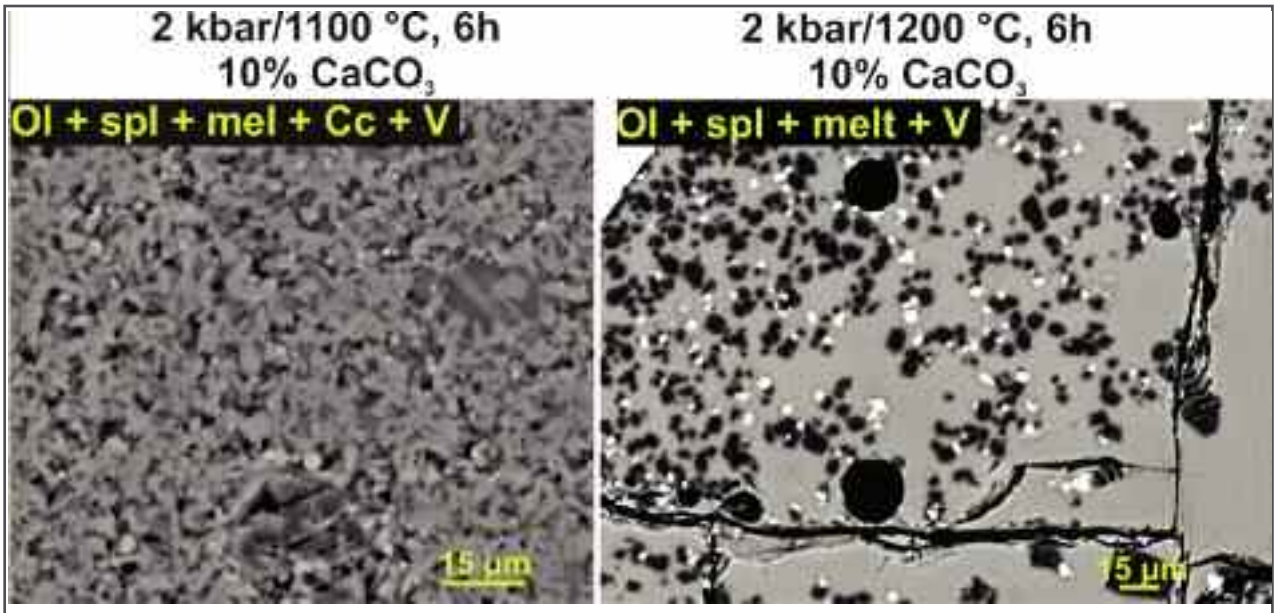

Fig. 3 I BSE images showing the crystallized assemblage at isobaric conditions and 1100-1200 °C by assimilation of 10% wt $CaCO_3$. Ol = olivine, spl = spinel, mel = melilite, Cc = residual calcite, V = CO_2 vapor.

Dynamics of strombolian eruptions at Batu Tara volcano (Indonesia)

E. Del Bello, L. Spina, P. Scarlato, D. Gaudin, J. Taddeucci

The high-speed thermal imaging and acoustic data acquired during the field experiment held in Batu Tara Volcano (Indonesia) in September 2014, were processed aiming at investigating the explosive and degassing dynamics. Using a combination of thermal images, acquired at 50-200 fps with an infrared (FLIR) camera deployed in direct view of the active vent, and synchronized acoustic signals acquired at 10 kHz with two broadband microphones (Freq. range of kHz to 0.1 Hz), we reconstructed the sequence of the eruptive events based on the thermal and acoustic signatures. Thermal images characterization was performed by integrating the amplitude of the thermal images in a box above the vent, and then correcting for the background, obtaining a thermal amplitude signal variation over time (Fig. 1). From this, 146 peak events were discriminated by using a trigger algorithm based on a percentile threshold of 20. Thermally characterised events show a broad unimodal distribution in terms of event duration, and a bimodal distribution of amplitudes (Fig. 2). According to the different eruptive conditions, each explosion can be characterized by a single peak or to a sequence of pulses.

The explosions were also discriminated according to their infrasonic features. Different families of waveforms were retrieved based on a cross correlation method.

Some explosions are characterized by a first, high amplitude transient, with a first positive peak pressure followed by rapid dampening, typical of a Strombolian eruption, while others are characterized by an emergent signal. Such two distinct waveforms types are sometimes overlapping reflecting the variations in i) the timing and ejection of large spatters and bombs, ii) the presence of secondary pulses, and also iii) the amount of ash involved. The different evolutions suggest that there are at least two repeatable explosion dynamics occurring in the conduit, with comparable gas overpressure, source depth and amount of gas involved.

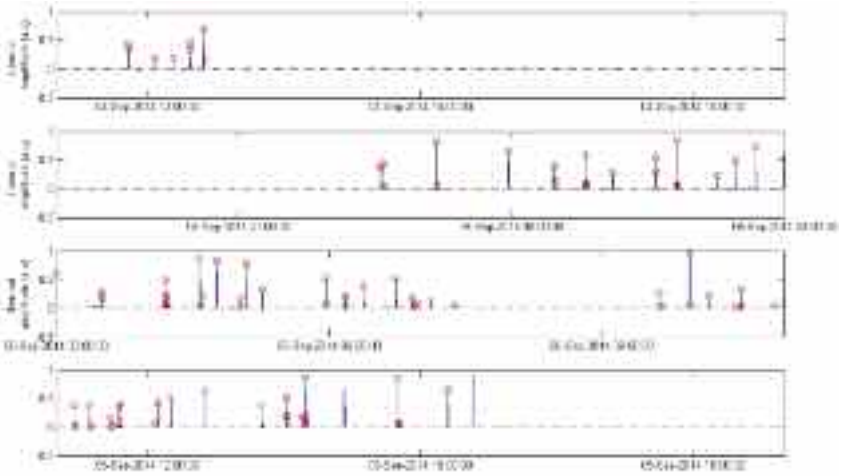

Fig. 1 | Temporal evolution of the explosive activity at Batu Tara over a 28 hours interval based on thermal images data. The blue line represent the integrated amplitude of thermal images on a target window, the red circles represent the events triggered with the percentile-based algorithm.

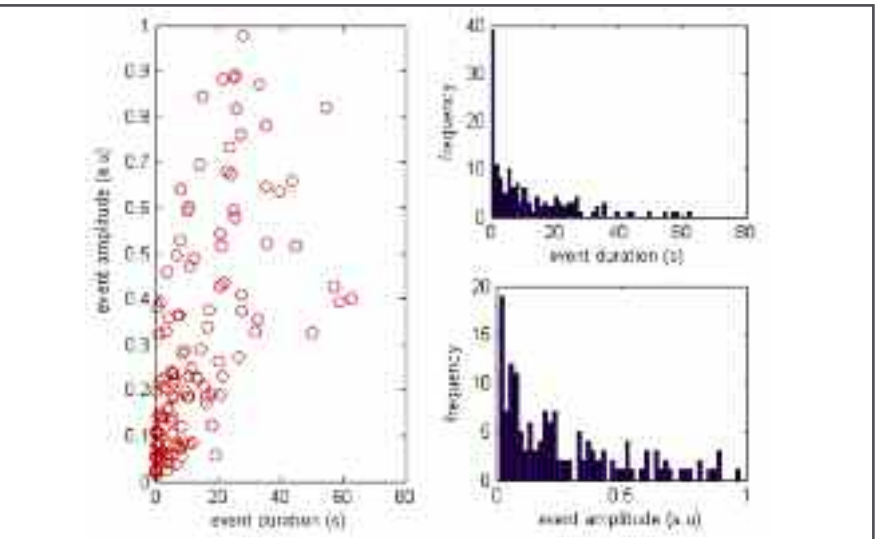

Fig. 2 | Plot of the thermal peak amplitude vs event duration (left panel) retrieved with the percentile-based algorithm. Histograms of the event duration and thermal amplitude measured are also shown (right panels).

Parameterization of volcanic ash remobilization by wind-tunnel erosion experiments

E. Del Bello, J. Taddeucci, J.P. Merrison, S. Alois, J.J. Iversen

The remobilization of volcanic ash from the ground is one of the many problems posing threat to life and infrastructures during and after the course of an explosive volcanic eruption. A proper management of the risks connected to this problem requires a thorough understanding of the factors that influence and promote the dispersal of particles over large distances.

Towards this target, we conducted a series of experiments aimed at defining first-order processes controlling the remobilization threshold of ash particles by wind erosion.

In the framework of the EU-funded Europlanet project, we joinly used the environmental wind tunnel facility at Aarhus University (DK) and the state-of-the art high-speed imaging equipment of INGV experimental lab (Italy) to capture at unparalleled temporal and spatial resolution the removal dynamics of ash-sized (half-millimetre to micron-sized) particles. A homogenous layer of particles was set at on a plate placed downwind a boundary layer setup. Resuspension processes were filmed at 2000 fps and 50 micron pixel resolution, and the plate weighted pre and post-experiment. Explored variables include: 1) wind speed (from ca. 1 to 7 m/s) and boundary layer structure; 2) particle grain size (from 32-63 to 90-125 micron), and sample sorting; 3) chemical and textural features, using basalt and trachyte samples from Campi Flegrei (Pomici Principali,10 ka) and Eyjafjallajökull (May 2010) eruptions; and 4) temperature and humidity, by conducting experiments either at ambient conditions or with a heated sample. We found that the grain size distribution exerts a strong control on the fundamental dynamics of gas-particle coupling. Particles > 90 micron detach from the particles layer individually, also entering the gas flow individually. Conversely, removal < 63 micron particles occurs in clumps of aggregates. These clumps, once taken in charge by the gas flow, are frequently disaggregated and dispersed rapidly (order of few milliseconds). Our preliminary results shows that, for a given size distribution, the boundary between the two dynamics may shift greatly as a function of ambient humidity.

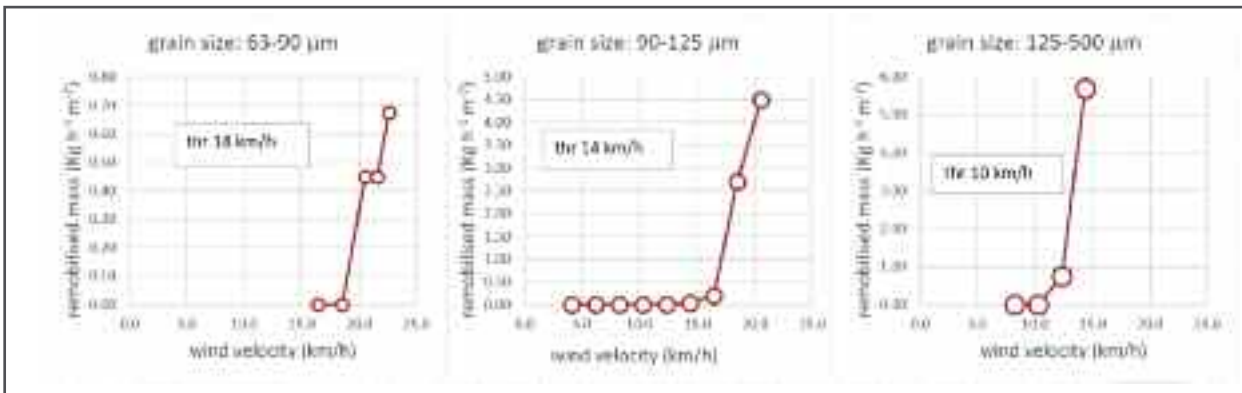

Fig. 1 I Plot showing the remobilised mass of Campi Flegrei ash as a function of wind friction speed at the plate surface during wind tunnel experiments. The three panels illustrate the decreasing remobilization threshold for grain size distributions of the samples increasing from 63-90 µm (left) to 125-500 µm (right).

The third Broadband Acquisition and Imaging Operation (BAcIO3) at Stromboli Volcano

P. Scarlato, J. Taddeucci, E. Del Bello, T. Ricci

The third edition of BAcIO, a multidisciplinary experiment headed by INGV gathering a large combination of worldwide monitoring expertise, was held in Stromboli in May 2016. This year, the experiment involved an international team of 23 researchers from 8 research institutes/universities: 1) Piergiorgio Scarlato, Jacopo Taddeucci, Elisabetta Del Bello, Tullio Ricci, Damien Gaudin, Pierre Yves Tournigand, and Manuela Nazzari from INGV – Roma; 2) Valentino Salvatore from University La Sapienza; 3) Ulrich Kueppers, Valeria Cigala, Sebastian Müller, and Alessandro Pisello from LMU Muenchen; 4) Bruce Houghton, Nick Turner and Bianca Mintz from University of Hawaii; 5) Joern Sesterhenn, Juan Jose Pena Fernandez and Steffen Nitsch from TUB Berlin; 6) Matthias Hort and Lea Scharff from Hamburg University; 7) Federica Lanza and Simone Puel from Michigan Technological University; 8) Stefano Alois from Aarhus University.

Aimed at improving the understanding of Strombolian eruptive dynamics and at favoring the networking and scientific interaction among researchers with different backgrounds, the field experiment comprised this year: 1) the use of up to 4 synchronized high speed cameras for stereoscopic, multi-scale filming of the eruptive activity, 2) the use of 2 high definition cameras for filming the plume dispersal dynamics, 3) the acquisition of thermal images through a high speed IR camera, 4) the acquisition of infrasonic and seismic signals through microphones arrays and infrasonic/seismic stations, 5) the use of a camera-equipped drone for DEM reconstruction of the summit area, and 6) the use of a Doppler radar to measure eruption velocity.

Fig. 1 I Deployment of instruments at Pizzo Sopra la Fossa (Stromboli) on May 26 2016.

KRAFLA MAGMA TESTBED – the contribution of the HPHT experimental laboratory

P. Scarlato, S. Mollo, M. Masotta, E. Del Bello, T. Ricci, E. Spagnuolo, P. Papale

The KRAFLA MAGMA TESTBED (KMT) PHASE I, is a drilling project submitted to the International Continental Scientific Drilling Program. The Steering Committee for KMT is leaded by John Eichelberger (UAF/USA), and comprises members of international institutions (SNL/USA, LMU/Germany, GEORG/Iceland, UL/UK, BGS/UK, LV/Iceland,USGS/USA, BGS/UK, INGV/Italy, SMU/USA, UI/Iceland). This project descends from the The Krafla

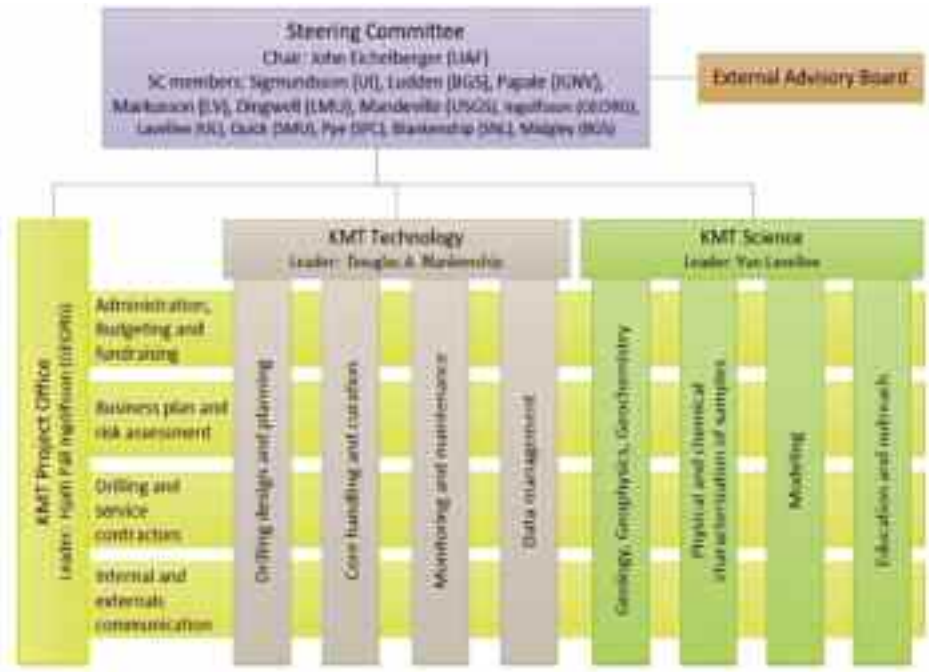

Fig. 1 I Organigram of KMDP. HPHT laboratory leads the task 'Physical and chemical characterization of the sample'.

Magma Drilling Project (KMDP), that is an open multi-national consortium of scientists, geothermal engineers, and Landsvirkjun National Power Co. aimed at coring through the subsolidus – hypersolidus boundary in granite ("felsite") to liquidus rhyolite.

The Krafla site, with its unprecedented 4-D view of a magma-hydrothermal system from source to surface, is a key location to advance geophysical and geochemical volcano monitoring methods including emplacement of sensors in the magma chamber, assess the energy potential and optimal engineering approach for magma energy, investigate magma-hydrothermal coupling through intentional perturbation of the system, benchmark coupled mass-heat transfer reservoir models with self-induced thermal fracturing, and provide experiential learning in fields of volcano hazards and renewable energy. The well is scheduled to be drilled in 2017, and a number of geophysical and geochemical experiments will be conducted in the frame of KMDP prior to, during, and after the drilling. Also, the drilling is conceived to allow the direct recovery of intact samples of rock from the transition zone and of the magma itself.

The HPHT laboratory will have a major involvement into the physical/chemical/mechanical characterization of

magma under Krafla caldera and the geochemical investigation of its relationship to the overlying hydrothermal system. The main goals of the laboratory experiments involve: 1) the origin and anatomy of the igneous system, 2) material properties of the intrusive and hydrotermal environments; 3) thermo-mechanical response of the reservoir to stress and temperature perturbation. The geochemical surveys will characterise the hydrothermal reservoir by monitoring CO_2 diffuse degassing and Radon.

KRAFLA MAGMA TESTBED – geochemical survey and Radon monitoring

T. Ricci, A. Sciarra, G. Galli, A. Piersanti, P. Scarlato, P. Papale

In the framework of the KMT Project a preliminary list of field activities regarding surface fluid geochemistry and thermal imaging were performed in 2015-2016. Main aims of the 2015 geochemical survey, carried out in collaboration with British Geological Survey, Landsvirkjun, and University of Iceland were characterizing the CO_2 diffuse degassing occurring in selected areas inside and on the rims of Krafla caldera (Fig. 1), as well as mapping the thermal anomalies within the caldera, characterizing the chemistry and isotopes of deep and shallow emissions, identifying a suitable site for the installation of a ^{222}Rn monitoring station, constraining the origin of the CO_2 carbon isotopes, and performing an overflight of the Krafla caldera to map thermal anomalies. From 2 to 11 August 2016, new activities were performed in collaboration with Landsvirkjun and additional geochemical measurements were carried out in the Viti crater area aimed at the installation of the ^{222}Rn Barasol multi sensors BMC2 Algade monitoring station, in acquisition since the 8th of August. In addition, new CO_2 flux and soil temperature measurements, real-time soil gas analysis, ^{222}Rn and ^{220}Rn activity concentrations in soil gas were performed during the survey while soil gas samples were collected and then analyzed to characterize the chemistry and isotopes of shallow emissions.

Fig. 1 I Rn characterization.

Experimental constraints on the rheology, eruption and emplacement dynamics of lavas from Mercury Northern Volcanic Plains

F. Vetere, S. Rossi, O. Namur, D. Perugini, D. Morgavi, V. Misiti, P. Mancinelli, M. Petrelli, C. Pauselli

We present new viscosity measurements of a synthetic silicate system considered as analogue for the magmas erupted on the Mercury planet surface. In particular, we focus on the Northern Volcanic Plains (NVP), which correspond to the largest lava flows on Mercury and possibly in the Solar System. High-temperature viscosity measurements were performed at both superliquidus (up to 1736 K) and in subliquidus conditions (1736-1502 K) to constrain the viscosity variations as function of crystallinity (from 0 to 28%) and shear rate (from 0.1 to 5 s^{-1}; Fig. 1). Melt viscosity shows moderate variations (from 4 to 16 Pa s) in the temperature range 1736-1600 K. The effective viscosity evidences a significant increase from 4 to ~10^4 Pa s as the temperature decreases to 1502 K and the crystallinity increases up to 28%. The major increase in viscosity is observed at 1520 K (from 102.2 to 103.1 Pa s) when crystallinity reaches ca. 12%. The system shows a shear thinning behaviour with a decrease in viscosity of ca. 1 log unit as the shear rate varies from 0.1 to 5.0 s^{-1} . Low viscosities of NVP melts can explain their ability in covering long distances in a relatively short time. At liquidus eruptive temperatures, lava flows with thickness from 1 to 5 m are likely to have been emplaced with velocities of 4.8 and 6.5 m/s respectively, on a 5° ground slope. Numerical modelling allows us to infer that high effusion rates (> 5000 m^3 /s) are necessary to cover large distances, as shown by satellite data.

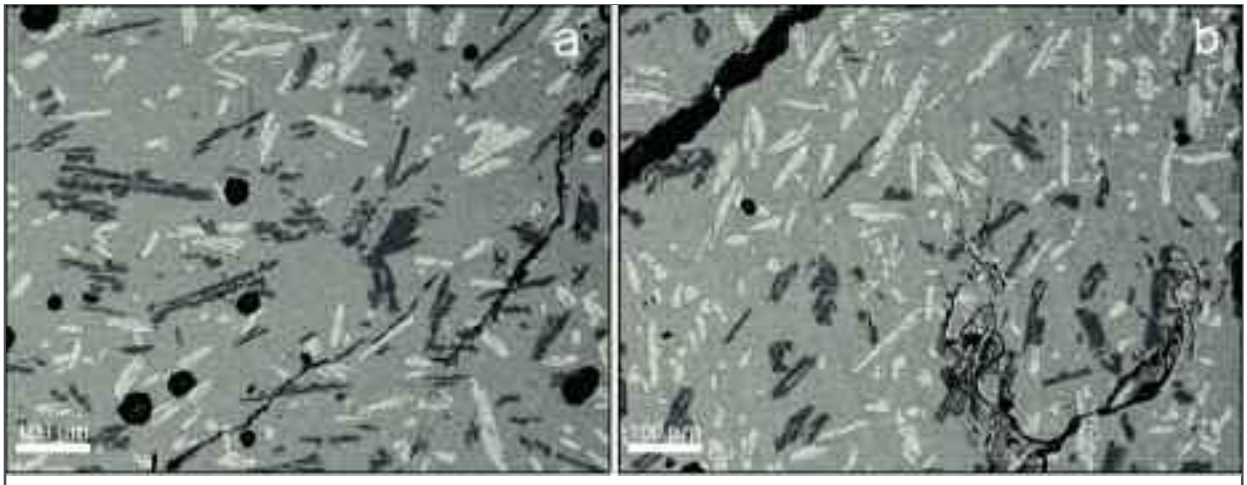

Fig. 1 I Back Scattered Electron images of representative experimental products. a) experiment at temperature of 1502 K and shear rate of 5.0 s^{-1} ; b) same temperature as in (a) but shear rate of 0.1 s^{-1}. The two experiments show comparable crystal contents at the two shear rates.

Tephrochronology of a ca. 60.000 yrs. lacustrine sequence from the Fucino Basin, Central Apennines, Italy

A. Di Roberto, A. Smedile, P. Del Carlo, P.M. De Martini, M. Iorio, M. Petrelli, D. Pantosti, S. Pinzi, A. Todrani

Three cores FUC-S4-S5-S6, have been sampled in the Fucino Basin (central Apennines, Italy), which is a keysite for tephrochronological reconstruction, possibly containing a 2 Ma-long continuous lacustrine sediment succession. The cores have been investigated for tephra content and a total of 11 tephra and cryptotephra layers have been identified. Major and minor element glass chemistry was determined by EPMA at the INGV-Sezione di Roma. Composition have been compared with those of the proximal samples emitted from Italian volcanoes since the Late Pleistocene, most of which are included in the RESET database as well as with composition of distal tephras from the literature. Results in figure 1 indicate that some identified tephras correlate (statistically determined with SC index between 0.95 and 0.98) with (top-down):

T1_169 -<10 ka eruption of Ischia (undetermined);

T4_287 -Napolitean Yellow Tuff (NYT);

T6-T7-T8_463-471-502 - 3 eruptions from the last eruptive cycle of the Alban Hills at < 39 ka;

T9_560 - Campanian Ignimbrite (CI) lower-intermediate flow units + first eruption from the Alban Hills last eruptive cycle < 39 ka;

T10_712 - Pre-Campanian Ignimbrite (Pre-CI TIa/TIc) + undetermined eruption;

T11_722 - Caldera-forming Monte Epomeo Green Tuff (MEGT) eruption;

For some of the identified tephra and cryptotephra the Fucino Basin sediment record provides the first distal occurrence in the central Italy. These key horizons, which span the last ca. 60.000 yrs., improve the present tephrostratigraphic framework for the central Mediterranean area and provide precise tie-points around which an independent age model and the sediment accumulation rate for the Fucino Basin can be constructed.

This research is developed within the framework of a national project focused on the seismic risk of the Abruzzo region (FIRB Abruzzo project, “High-resolution analyses for assessing the seismic hazard and risk of the areas affected by the 6 April 2009 earthquake”; http://progettoabruzzo.rm.ingv.it).

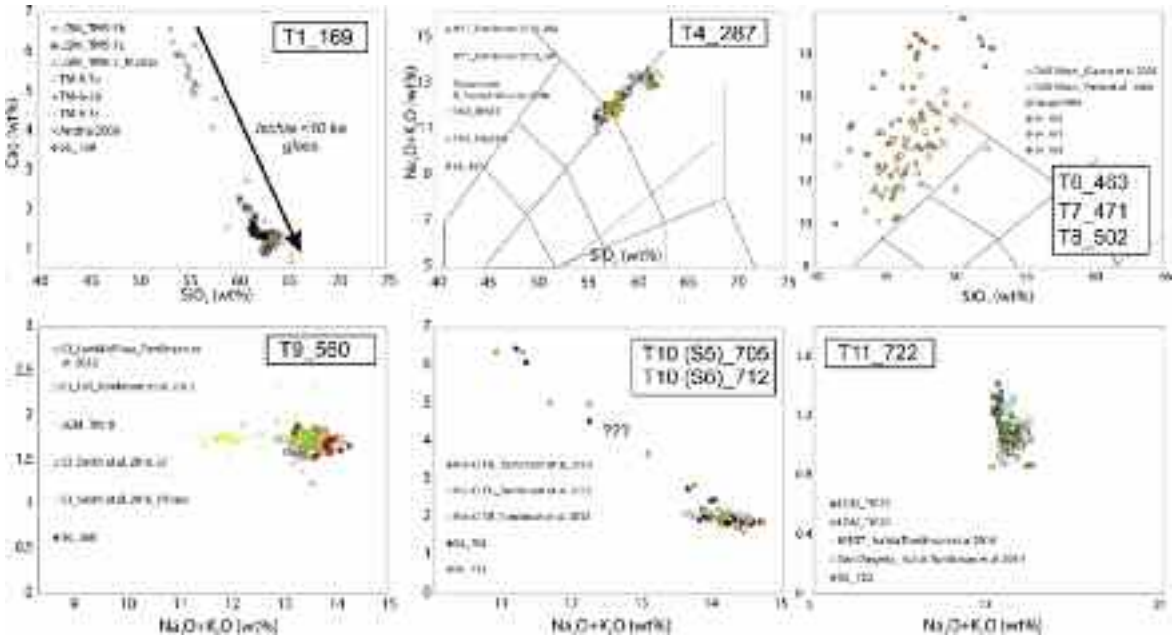

Fig. 1 I Major, minor and trace element variation diagrams showing the composition of some selected tephra and cryptotephra identified in FUC-S4-S5-S6 cores in comparison with the composition of proximal and distal tephra from the literature.

The rhyolites from Ramadas Volcanic Center (Altiplano-Puna, Argentina): origin and interaction with Andean crustal rocks

G. De Astis, V. Misiti, R. Becchio, L. Bardelli

Ramadas volcanic centre (RVC) is a monogenetic calderic depression, that was active in the Late Miocene and produced aplinian eruption in the Altiplano-Puna plateau (Argentina). The RVC generated a rather complex suite of garnet-bearing, rhyolitic pyroclastic rocks dominated by a fall deposit (>35 km^3) and starting with the emplacement of lag breccia, which is visible in a few outcrops. A final obsidian lava flow closed the eruption. The breccia deposit contains abundant crustal rocks (meta-sedimentary lithics and garnet-tourmaline leucogranites) that have been analysed through the use of JEOL JXA-8200 microprobe at the HPHT Laboratory (INGV, Rome) together with the products of pressure calibration experiments performed by a piston cylinder apparatus (Quick-Press; pressure in the range 150 and 500 MPa). It must be recalled that the RVC rhyolites are aphyric rocks - usually tube pumices - with euhedral garnets as micro-phenocryst and that eruptive vent area widely lies on amphitheatre carved in Precambrian–Lower Cambrian meta-sedimentary rocks (Puncoviscana Formation). Moreover, petrographic and microprobe studies on these pumiceous juveniles identify the presence of accessory microlites (zircon and monazite) within the garnet crystals and the presence of micrometric metaigneous fragments (Qtz+Bt+Kfs+Mt+Tur) in the groundmass or in the vesicles. In the groundmass, microlites of feldspar, quartz, tourmaline and platy bare randomly present. Previous studies by SEM revealed garnets traversed by cracks, micro-fractures at the glass-garnet boundary and shear structures in glass due to crystals dragging (features supporting the idea of a mineral already crystallized and then mechanically transported by magma during the eruption). In general, it's known that: a) garnet (typically rich in Alm molecule) is a common mineral in metamorphic rocks, whereas its origin in igneous rocks is controversial and restricted to certain P-T conditions; b) most occurrences of magmatic garnet are in felsic pegmatites ($SiO_2 \geq 70\%$) associated with peraluminous/metaluminous granitoids; c) the presence of Zr and Mnz is associated with both magmatic and high-T metamorphic processes.

In order to unravel a "classic" dilemma between magmatic vs. xenocrysts origin of garnets in our rhyolitic magma, we have studied garnet (and included microlites) compositions, as well as the garnet compositions in crustal rocks, taking into account that also the garnet isotopic compositions and those of the host-rocks are decisive to finally obtain the correct physical-chemical conditions of their formation. The new set of mineralogical data collected on RVC rhyolites have revealed that garnets haveFe-Ca rich homogeneous compositions ($Alm_{72-71}Sps_{24-23}Grs_{4-3}Pyr_{0-1}$) and are basically unzoned. Among the crustal xenolith collected in RVC breccia, the leucogranite (poikilitic texture - min. assemblage: Qz, Fd, Bt, Ms and accessory tourmaline, sillimanite) is

the only containing also garnet as accessory, whose analyses display a more Mn-Mg-rich composition ($Alm_{55-61}Spe_{38-33}Pyr_{5-6}$). It is worth noting that also the experimental products from the Quick-press have never shown the presence of newly formed garnet crystals. Therefore, no result has become crucial and has provided decisive evidence in favour of either hypothesis. However, with a view to expand our mineralogical data set and strengthen our interpretation, we lean to a thermo-metamorphic process and no genetic relationship between garnet crystals and rhyolitic magma. This magma may have been generated as the final effect of the thermo-metamorphism, giving rise to the partial melting of upper crustal rock (Fe-MnO-rich metapelitic rocks or re-melting of older acid volcanics?) with the extraction of volatiles-rich peraluminous rhyolitic melts, able to produce the plinian eruption.

Unrest at Turrialba volcano: chemistry of the ashes emitted during 2014 and 2015

A. Di Piazza, A. Rizzo, M. de Moor, G. Alvarado, G. Avard, M. Carapezza

Since 2010, the reawakening of Turrialba volcano has been characterized by sporadic explosions occurred at the summit craters, becoming more frequent with time and erupting fragments of altered preexisting material with a minor percentage of suspected juvenile components.

The identification of juvenile material in erupted products is crucial to volcano studies because it represents the fundamental threshold to distinguish magmatic or phreatomagmatic events from purely phreatic ones. The problematic in distinguishing phreatomagmatic from phreatic ashes also regards the Turrialba eruptive activity, which poses the question if the current activity will progress along the same pattern as the 1864-1866 eruption with a final clear magmatic stage. In order to reveal the possible existence of juvenile material in the recent ashes emitted by the explosive activity of the volcano, we performed detailed petrographic observations and chemical microanalysis of the products erupted between October 2014 and May 2015. These data were compared with those of scoriae and ashes erupted in 1864-1866, to identify features associated to the current eruptive period.

Seven ash samples erupted during the sequence of explosive events occurred in October 2014 – May 2015 have been collected at Turrialba summit area. Back scattered electron (BSE) imaging of these samples reveal that the outline of the clasts is variable from irregular to angular. Most of the clasts are porphyric, and only few display fresh glasses (Fig. 1a). Microanalysis on fresh glasses reveal that most of the samples are basaltic-andesite to trachy-andesite in composition (Fig. 1b). The ashes of October and November 2014 are characterized by a broader major element composition, compared to the products of the period December 2014-May 2015. The analyzed clasts display different degrees of alteration, except those from the explosion of May 6, which are the glassiest and aphyric of the entire suite. For the chemical characterization of minerals and glasses (Fig. 1c), only the freshest clasts from each explosive event were selected. These samples are characterized by the same mineral assemblage made of plagioclase (An_{50}-An_{67}), augitic to diopsidic clinopyroxenes (Wo_{4-47}, En_{43-72}, and Fs_{8-23}) phenocrysts of olivine crystals (Fo_{72-75}), and oxides (Mt_{56-69}). Substantially, the composition of mineral phases found in the fresh ashes of 2014-2015 explosions matches that of 1864-1866 eruptive products.

According to these observations, altered and reworked material with a variable composition dominate the eruptive products in the first eruptive stages (Oct.-Nov. 2014). Fresh ashes emitted during the December 2014–May 2015 activity, display a narrow chemical composition (basaltic-andesite to trachy-andesite, SiO_2 ~55-60 wt%) and thus are considered as the best candidates to be representative of a fresh juvenile magma increasing with time. Their mineral chemistry and major element chemical composition resembles that of the 1864-1866 eruptive products, suggesting that the composition of the magma involved in the unrest of Turrialba volcano should be similar to that

erupted in 1864-1866. Compared to the evolutionary stages that led to the magmatic eruption of 1864-1866 (phreatic explosions transitioned to phreatomagmatic and Strombolian activity), the occurrence of explosions with a juvenile component could indicate that the eruptive activity at Turrialba is currently at an intermediate stage preceding more magmatic eruptions.

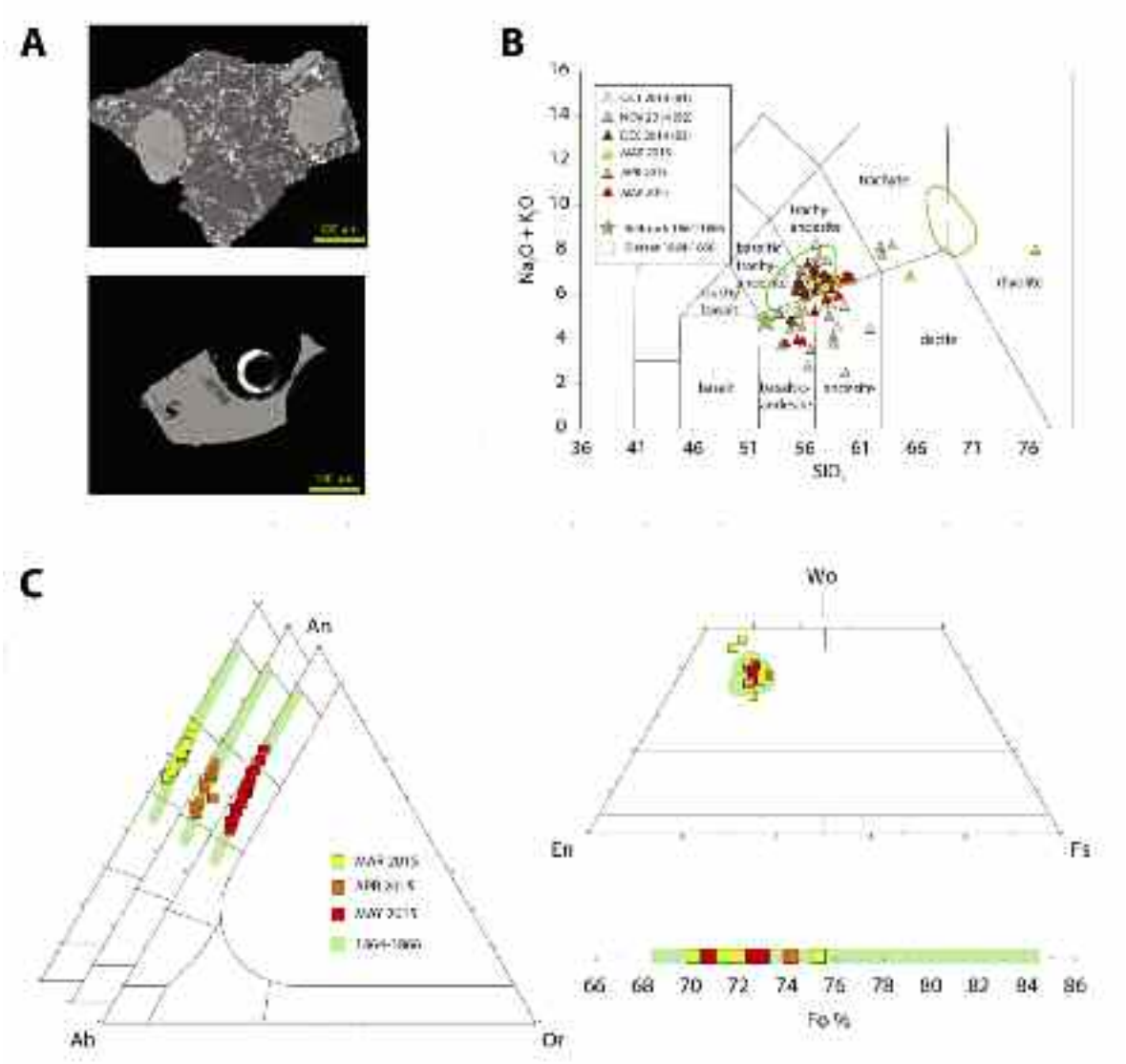

Fig. 1 | **a)** BSE images of two clasts belonging respectively to the early (Oct.-Nov. 2014; uppermost, altered clast) and late stage of explosive activity (May 2015; lowermost, fresh glassy clast). **b)** Diagram of the total alkali versus silica content comparing the compositions of the samples collected in this study with those of bulk rocks and glasses of the 1864–1866 eruption. **c)** Classification diagrams of the main mineralogical phases of Turrialba rocks contained in ashes erupted in 2015, compared with phenocrysts of Turrialba products erupted in 1864–1866: a pyroxene ternary diagram; the olivine forsteritic molar percentage; and a plagioclase ternary diagram. It was not possible to analyze mineral phases in the 2014 samples.

Cannonballs: a peculiar feature of basaltic monogenic volcanoes?

A. Di Piazza, E. Del Bello, S. Mollo, A. Vona, G. Alvarado, M. Masotta

Cannonballs are spherical to sub-spherical eruptive products associated with the basaltic explosive activity of monogenic volcanoes and strato-volcanoes worldwide. The origin of cannonballs is still debated and subjected to a wide spectrum of different interpretations: from post-impact mechanical attrition while rolling down on the flank of a scoria cone or a volcano, to recycling processes at vent. We investigated the textural and chemical characteristics of cannonballs from a monogenic volcano in Costa Rica (Cerro Chopo), to understand the physicochemical mechanisms controlling the formation of these sub-spherical explosive products and to propose a general model for their genesis. These explosive products ubiquitously show a core domain with large, coalesced bubbles (30.2-36.5 % porosity) wrapped by a dense rim domain with small, isolated bubbles (20.7-27.6 % porosity). The different textural characteristics of the cannonball core and rim denote a variable degassing history for the two domains. The dense rim domain is characterized by micro-vesiculation, a complex mosaic of groundmass crystals, a high vesicle number density (2.6-3.3×10^6 cm^{-3}), and a steep crystal size distribution, all features suggesting rapid volatile exsolution and cooling. Conversely, the high-porosity core domain shows hour glass outlines of the larger vesicles in concert with the perturbed shapes of the smaller ones, a skewed distribution of the vesicle volumes towards the larger sizes, and a gently sloping trend of the CSD, all features pointing out continuous coalescence and growth of vesicles upon the effect of a slow cooling condition. According to thermo-barometric calculations, the sub-rounded shape of the ejected material was attained at very shallow levels via a solidification process controlled by magma decompression and volatile exsolution. On this basis, most of the cannonball textural variations can be rationally addressed to physical mechanisms that took place during magma fragmentation and eruption to the surface. Both rim and core domains are virtually identical in terms of bulk rock composition and mineral chemistry, being portions of the same magma batch. According to thermo-barometric calculations, the sub-rounded shape of the ejected material was attained at very shallow levels via a solidification process controlled by magma decompression and volatile exsolution. Modeling results indicate that a low-viscosity ($10^{1.24}$ Pa s) melt containing early-formed olivine phenocrysts (~8 vol.%) ascended at a decompression rate of 0.51 MPa s^{-1} up to a depth of ~150 MPa. At this pressure condition, the melt underwent rapid decompression (0.74 – 2.62 $MPas^{-1}$) accompanied by H_2O exsolution (1-3 wt.%) driving the final groundmass crystallization. The fast ascent velocity obtained by calculations (33-110 m/s), induced turbulent ($Re>10^3$), annular flow development in the uppermost region of the conduit. Therefore, here we propose that cannonballs represent blebs of fluid magmas that underwent shear-driven detachment from the annulus of magma lining the conduit walls. The formation of cannonballs is dictated by magma fragmentation and transport dynamics of low-viscosity, phenocryst-poor and gas- rich melts that rapidly accelerate within the shallow conduit.

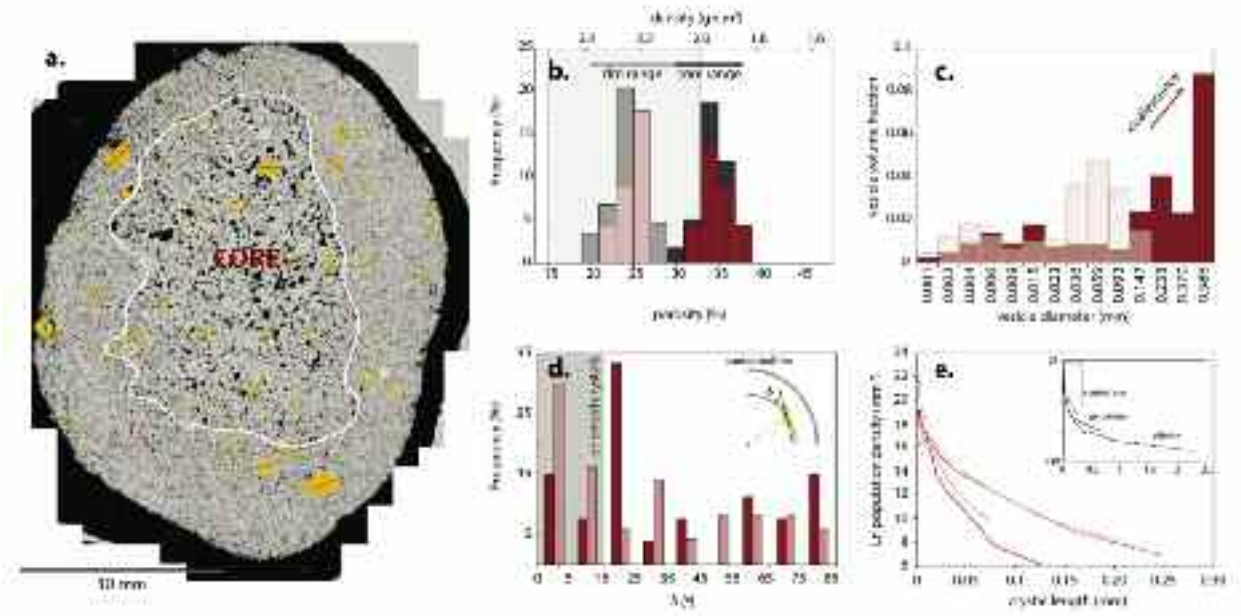

Fig. 1 I **a)** BSE mosaic of the Cerro Chopo Cannonball; scale bar is indicated. White line delimit rim (light red) and core (dark red) domains. Olivine phenocrysts are highlighted in orange with their major axis orientation indicated by black lines. **b)** Density and porosity distribution of core and rim domains measured on 100 sub-fragments of Cerro Chopo samples (in gray) and on the rim (light red) and core (dark red) fragments of the studied sample. The shaded area indicates the porosity range of cannonballs. **c)** Vesicles volume distribution of rim and core domains. **d)** Frequency distribution of d angle (i.e. angle between olivine long axis and the perimeter of the sectioned cannonball); crystals at rim display a higher orientation dispersion respect to those at core. **e)** Crystal size distribution of plagioclase (dotted line) and pyroxenes (solid line) in the range of crystal lengths 0 - 0.30 mm; inset displays the CSDs of all mineral phases in the range 0 - 2.5 mm.

Textural characterization of natural and experimental samples of mugearitic mega-crystic lavas from Mt Etna volcano

A. Di Piazza, A. Vona, E. Nicotra, C. Romano, M. Viccaro, G. Giordano

At Mt. Etna, megacryst-bearing lava flows, locally known as "cicirara" due to their chick-pea-like appearance, appear in several periods of the volcanic history. A peculiar textural feature of these magmas is the abundance of cm-size plagioclase crystals (megacrysts) together with smaller size crystals (phenocrysts and microlites), yielding very wide crystal size distributions. In order to investigate the multiphase rheology of these mega-crystic lavas, we performed rheological measurements at high temperatures (1000-1200°C) combining rotational and compressional rheometry. In addition, to obtain useful information on the deformation mechanisms occurring at high temperatures on such peculiar magmas, we performed a detailed textural analysis of pre-run and post-run samples.

The studied "cicirara" lava sample (Fig. 1a) is characterized by a porphyritic texture made of euhedral rectangular prismatic plagioclase megacrysts with size > 3 mm. Phenocryst assemblage is composed of rectangular prismatic plagioclase (~8 %) and rare sub-rounded olivine (< 3 %). The groundmass is almost holocrystalline and made of rectangular prismatic to acicular plagioclase (dominant), sub-rounded olivine, equant to elongate augitic pyroxene and rounded Fe-Ti oxide often forming polycrystalline clots. The total crystal fraction was determined through textural analysis by integrating measured crystallinity of images from different magnifications, following the same approach proposed for vesicles by Shea et al. (2010). Results indicate an overall crystal content of 68 % (referred to melt area).

A global overview of post-experimental samples allows two main observations (Fig. 1b-h): i) increasing degree of partial melting with increasing experimental temperature; ii) textural features recording the sample deformation history. With increasing temperature, the continuous decrease of total crystal fraction is mainly associated with the resorption of the femic phases. The plagioclase phase is not significantly affected up to temperatures between 1100-1200 °C. Among the femic phases, pyroxene smallest sizes (< 10 μm) sensibly decrease starting from 1050 °C, whilst the larger sizes disappear completely between 1100 °C and 1200 °C. Olivine content is generally slightly lower than in the natural sample, and remains quite constant at T 1000-1100 °C, disappearing completely at T = 1200 °C. Oxide content remains quite constant in all the investigated temperature range, with the exception of the highest temperatures where a slight increase in their amount is observed. The analysis of BSE images in Fig. 1 (b-h) reveals a clear effect of deformation on the sample bulk geometry. In general, a continuous increase of ductile over brittle deformation can be observed by the change of the core geometries with increasing temperature.

Partial melting experiments revealed that plagioclase megacrysts are preserved up to 1200 °C, where they are only slightly resorbed. Considering the eruptive temperatures inferred for lava flows of mugearitic compositions (1075-1085 °C), this suggests that megacryst population ($\phi X \sim 0.20$; melt-referenced) is already present at the moment

of the eruption. In addition, experiments performed at T=1075-1085 °C indicate that also a substantial part of the smaller crystals (phenocrysts and microlites, ϕX ~ 0.35-0.40; melt-referenced) is in equilibrium at these temperatures. This means that the studied "cicirara" lavas are most likely erupted at high crystal content (ϕX ~ 0.55-0.60%; melt-referenced).

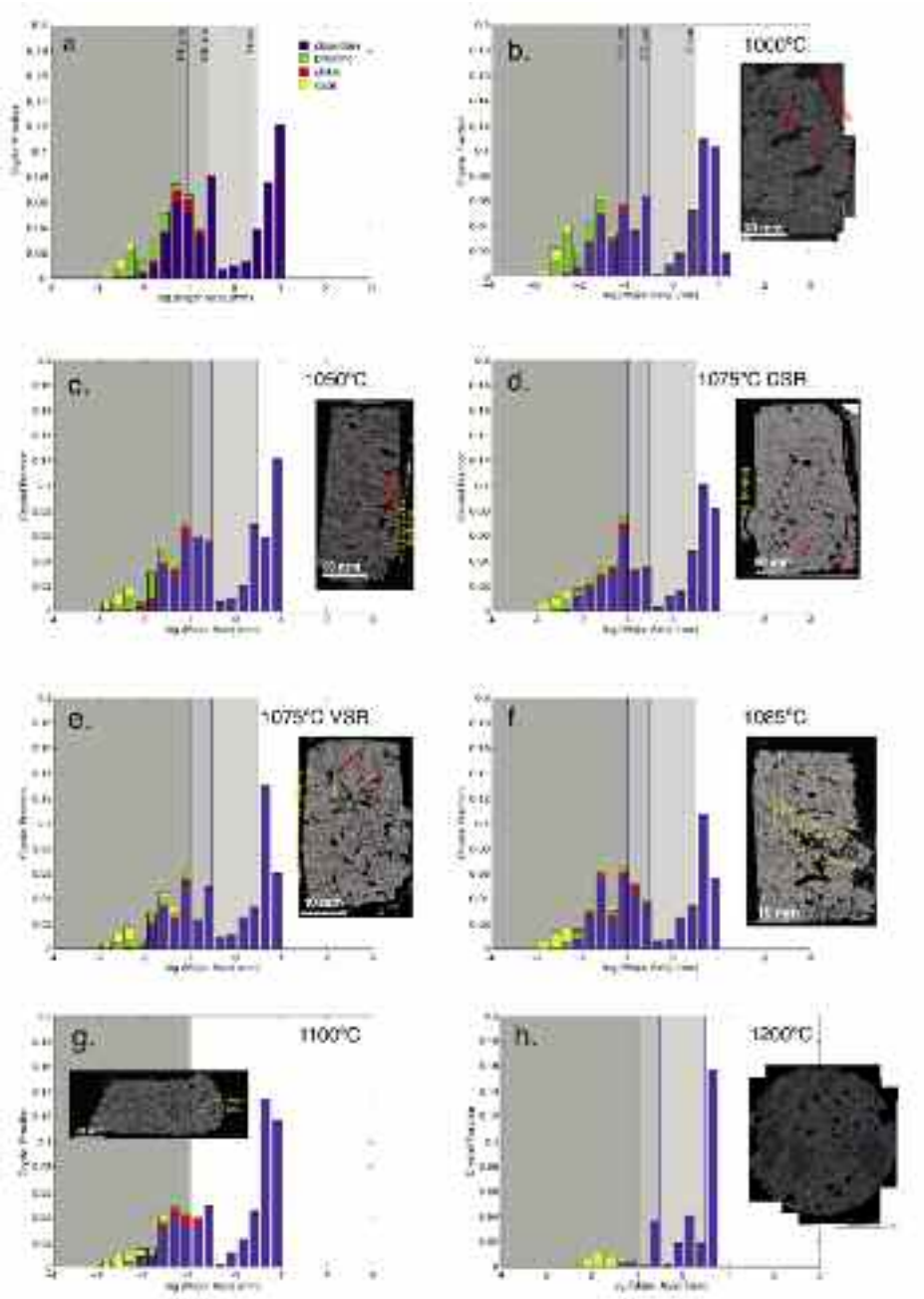

Fig. 1 I. Summary of 2D phase fraction distributions obtained by image analysis of "Cicirara" natural sample **(a)** and post-run samples **(b-h)**. Mineral phases are indicated in the legend. Vertical dashed lines indicate size thresholds of different crystals population (microlites <100 μm; microphenocrysts <300 μm; phenocrysts <3 mm; megacrysts >3 mm). In each graph a mosaic of BSE images taken at magnification 60X is shown, representing the entire thin section of the experimental cores, cut parallel to the deformation axis. Brittle (red) and ductile (yellow) main textural features associated to deformation are indicated. The BSE image of the post-run sample at 1200°C is a mosaic of images taken at magnification 70X, representing a section of the sample cut orthogonal to the spindle position.

Solidification of a rhyolitic magma beneath the Krafla caldera

M. Masotta, P. Scarlato, M. Nazzari, S. Mollo

The Krafla caldera is located in the north of Iceland and is bisected by a NNE–SSW fissure swarm that marks the North Iceland Rift Zone. Basaltic lavas and hyaloclastites fill the caldera (8 km wide), which originated by collapse approximately 110 ka. Rhyolite volcanism occurred in two main phases, each of which emplaced about 1 km^3 of magma, plus a third, small and more recent phase (i.e., younger than 24 ka). The most recent eruption is the famous 1975-1984 "Krafla Fires", a basaltic fissure eruption associated to rifting. The caldera was the site of extensive drilling for geothermal development since 1974. The geothermal exploration unveiled the subsurface geology of the caldera, consisting of effusive products in the shallow part (down to about 1000 m) and intrusive bodies at greater depths. Magmatic intrusions include dolerites and felsite, with the grain size increasing with depth.

The perforation IDDP-1 was originally designed to intercept supercritical fluids at about 4000 m depth, slightly above a magma body inferred by geophysical surveys. The drilling was interrupted at 2100 m depth, when loss of circulation occurred due to unexpected drilling of a magma intrusion. The well was side-tracked twice but the intrusion made impossible drilling to depths greater than 2104 m. The drilling logs and the recovered cuttings identified the magma body as a rhyolitic lens intruded into felsites.

In order to better constrain the physico-chemical conditions of the rhyolitic magma intercepted by the IDDP-1 and the hosting felsite, we have carried out a detailed petro-chemical analysis of the fragments sampled during the perforation and an experimental investigation of the conditions of the origin of the rhyolite.

The rhyolitic glassy samples quenched by the drilling fluids are poorly vesiculated and show a phenocryst assemblage composed of plagioclase, augite, pigeonite and titanomagnetite (Fig. 1). The mineral assemblage of the felsite includes mostly quartz and feldspars, and minor clinopyroxene and oxides. A temperature between 850 and 920 °C has been inferred for the rhyolite by a two-pyroxene geothermometer and crystallization modelling. However, such temperature estimate may be inaccurate, due to the fact that exchange reaction between pyroxene and liquid indicate that minerals are in disequilibrium with the melt.

Fig. 1 I Microscope (left) and backscattered electron (centre-right) images of the rhyolitic fragments collected at the IDDP-1. Legend: plagioclase (Pl), augite (Cpx), pigeonite (Pig).

Phase equilibria experiments were performed at 150 MPa and 3 wt.% H_2O over experimental time from 24 to 72 h. The mineral assemblage of the natural rhyolite is reproduced at <850°C (Figure 1), which suggests that the temperature of the rhyolite is lower than that estimated using the two-pyroxene geothermometer (850-920 °C). Partial melting experiments were performed at 150 MPa, over experimental time from 24 to 72 h (Fig. 2). The amount and composition of partial melt does not change with experimental duration (up to 72 hours) and temperature (up to 850 °C). The composition of the partial melt approaches the composition of the rhyolite only at higher degrees of partial melting (T=950 °C).

The rhyolitic magma intercepted by the IDDP-1 well probably formed at high degree of partial melting of the hosting felsite. The rhyolitic melt accumulated into lenses and eventually cooled at temperature below 850 °C when it was intercepted by the IDDP-1 drilling.

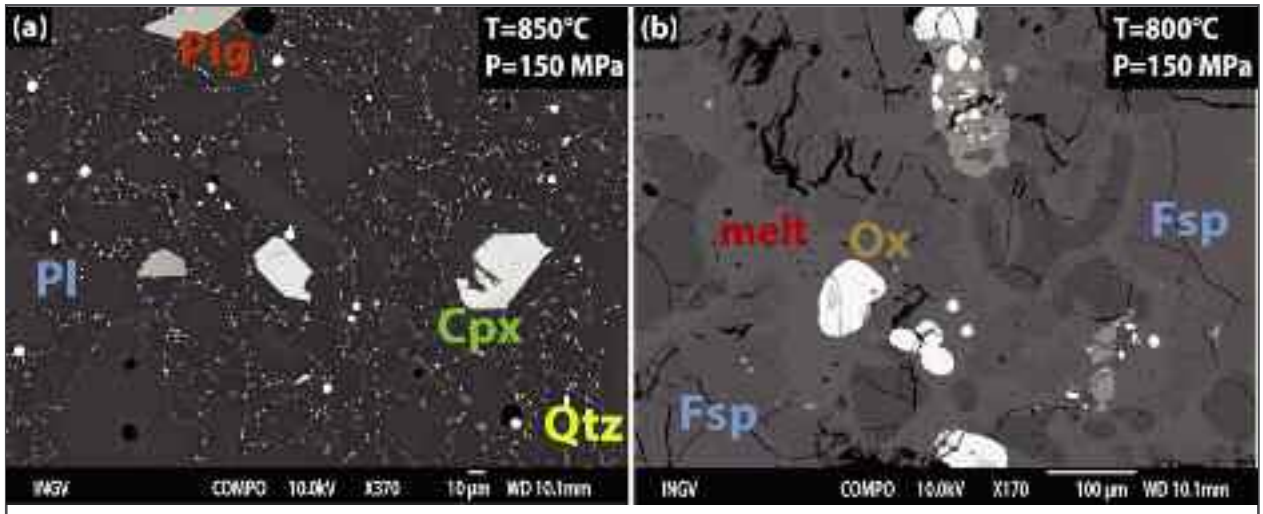

Fig. 2 I Backscattered electron image of a phase equilibria experiment (a) and a partial melting experiment (b).

Trace element partitioning between clinopyroxene and trachy-phonolitic melts: A case study from the Campanian Ignimbrite (Campi Flegrei, Italy)

S. Mollo, F. Forni, O. Bachmann, J.D. Blundy, G. De Astis, P. Scarlato

The partitioning of trace elements between crystals and melts provides an important petrogenetic tool for understanding magmatic processes. We present trace element partition coefficients measured between clinopyroxene phenocrysts and trachy-phonolitic magmas at the Campi Flegrei (Italy), whose late Quaternary volcanism has been characterized by two major caldera-forming events (Campanian Ignimbrite at ~39 ka, and Neapolitan Yellow Tuff at ~15 ka). Our data indicate that the increase of trivalent rare earth elements and yttrium into the crystal lattice M2 site is facilitated by the charge-balancing substitution of Si^{4+} with Al^{3+} on the tetrahedral site. Higher concentrations of tetravalent and pentavalent high field strength elements on the M1 site are also measured when the average charge on this site is increased by the substitution of divalent cations by Al^{vi}. In contrast, due to these charge balance requirements, divalent transitional elements become less compatible within the crystal lattice. On the basis of the lattice strain theory, we document that the incorporation of rare earth elements and yttrium in clinopyroxene is influenced by both compositional and physical parameters.

Data from this study allow to update existing partitioning equations for rare earth elements in order to construct a self-consistent model for trachy-phonolitic magmas based on the lattice strain theory. The application of this model to natural products from the Campanian Ignimbrite, the largest caldera-forming eruption at the Campi Flegrei, reveals that the complex rare earth element pattern recorded by the eruptive products can be successfully described by the stepwise fractional crystallization of clinopyroxene and feldspar where the clinopyroxene–melt partition coefficient changes progressively as a function of the physicochemical conditions of the system (Fig. 1).

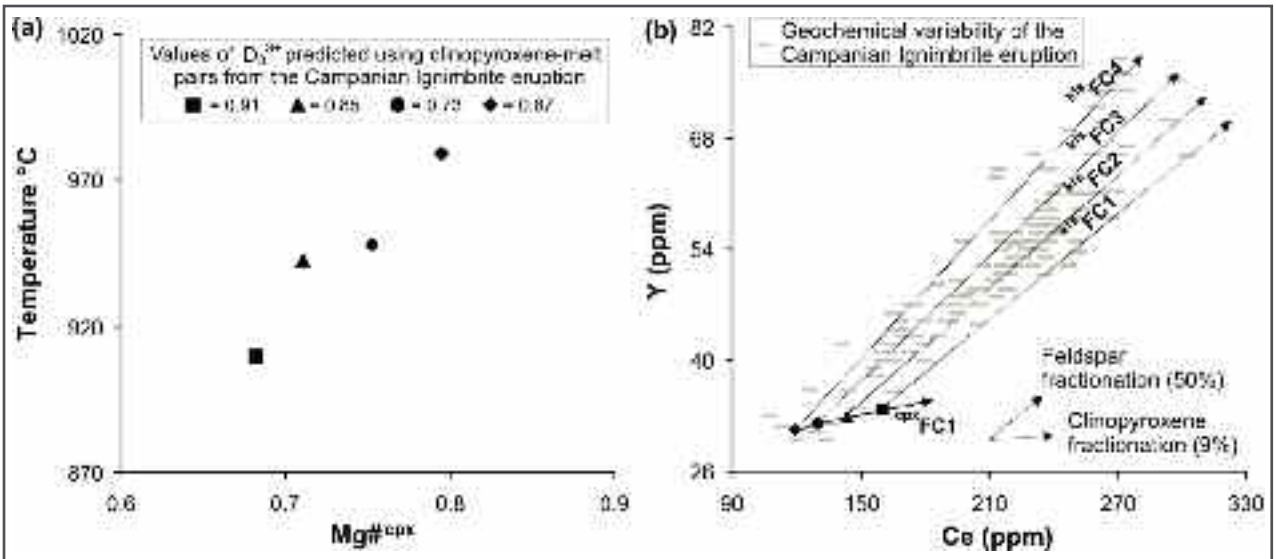

Fig. 1 | Natural clinopyroxene–melt pairs from the Campanian Ignimbrite have been used as input data for the thermobarometer of Masotta et al. (2013) and the trace element model presented in this study. **(a)** Temperature vs. Mg #^{cpx} diagram shows that the geochemical evolution of clinopyroxene parallels the decreasing temperature of magma. Each symbol plotted on the diagram refers to the value of D_0^{3+} predicted. This value is found to increase from 0.60 to 0.85 with decreasing both T and Mg #^{cpx}. **(b)** Ce vs. Y diagram showing the geochemical evolution of the Campanian Ignimbrite modeled through the Rayleigh fractional crystallization equation. At the beginning of the modeling, low degrees of clinopyroxene fractionation (i.e., 3%, 5%, 7%, and 9%) have been considered. Stepwise calculations were performed changing the clinopyroxene composition and temperature at each step of fractionation. Modeled Ce and Y concentrations were used to draw the ^{cpx}FC vector. Fractional crystallization calculations were further developed accounting for the segregation of ~50% of K-feldspar from the solidifying magma. Modeling results are aligned along four different FC trajectories (i.e., from ^{kfs}FC1 to ^{kfs}FC4).

The 2013 eruption of Chaparrastique volcano (El Salvador): Effects of magma storage, mixing, and decompression

P. Scarlato, S. Mollo, E. Del Bello, A. von Quadt, R.J. Brown, E. Gutierrez, B. Martinez-Hackert, P. Papale

On December 29, 2013, an isolated vulcanian-type eruption occurred at Chaparrastique volcano (El Salvador) after 12 years of inactivity. The eruption was classified as VEI 2 and produced an ash plume with a maximum height of ~9 km. Textural and compositional data from phenocrysts from the erupted products have been integrated with geochemical and isotopic information from bulk rocks to elucidate the magmatic processes responsible for the reawakening of volcanic activity.

Phenocrysts consist of Fo-rich poikilitic olivines hosting high-Mg titanomagnetites, and Fo-poor olivines coexisting with low-Mg titanomagnetites. Mineral-melt equilibria suggest an origin for the distinct phenocryst populations by mixing between a high-T (~1130–1150 °C), basaltic magma with fO_2 (NNO buffer) typical of the lower crust in arc systems and a low-T (~1060–1080 °C), basaltic andesitic magma with fO_2 (NNO+1 buffer) commonly encountered in shallower, more oxidized crustal reservoirs. Thermobarometry based on Fe-Mg exchange between orthopyroxene and clinopyroxene constrains the crystallization before eruption at relative low-P (~150–250 MPa) and low-T (~1000–1050 °C). Mixing between two chemically distinct magmas is also evidenced by the occurrence of reverse zoned plagioclase phenocrysts with resorbed sodic cores and re-growth of sieve-textured calcic mantles. Conversely, plagioclase rims exhibit disequilibrium compositions addressed to decompression kinetics (~10^{-3} MPa/s) driven by rapid magma ascent to the surface (~0.03 m/s).

Major and trace element modeling excludes fractional crystallization as the primary mechanism controlling the bulk rock variability, whereas geochemical data align along a mixing trend between two end-members representative of the primitive basalt and the differentiated basaltic andesite. Trace element and isotope data indicate that the primary source of magmatism is an enriched MORB-like mantle with the contribution of fluxes of metasomatic fluids and/or melts produced by the subducted slab (Fig. 1). The role played by slab-fluid inputs of carbonate origin and slab-melts from the hemipelagic sediments seems to be minimal. Assimilation/contamination processes of magmas by crustal rocks are also negligible. In contrast, the geochemical signature of magmas is greatly influenced by slab-derived aqueous fluids produced prevalently by progressive dehydration of marine sediments and altered basaltic crust (Fig. 1).

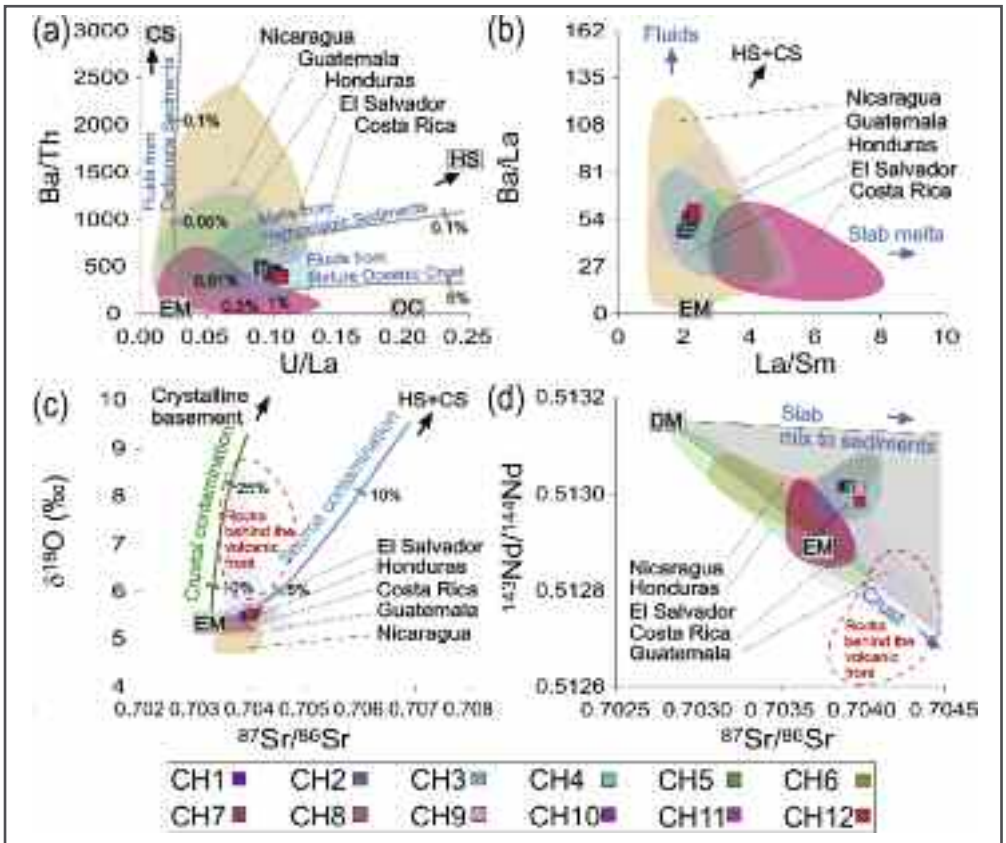

Fig. 1 | U/La vs. Ba/Th diagram based on soluble/insoluble element pairs. **(a)**. La/Sm vs. Ba/La diagram based on ratios of elements that are not highly fluid mobile in arc systems, such as the REE and HFSE. This diagram allows to evidence the contribution of to the mantle wedge of melt-like components derived from the subducted slab **(b)**. $^{87}Sr/^{86}Sr$ vs. $\delta^{18}O$ diagram that serves to discriminate crustal and source contamination **(c)**. $^{87}Sr/^{86}Sr$ vs. $^{143}Nd/^{144}Nd$ diagram shows evidence of crustal contamination for rocks in Guatemala that are behind the volcanic front. However, most of the volcanic products in Central America define an array with positive slop that represents a mix between the enriched MORB source and the subducted slab (d). EM, enriched MORB source. OC, oceanic crust. CS, carbonate sediments. HS, hemipelagic sediments. DM, depleted MORB source.

An improved clinopyroxene-based hygrometer for Etnean magmas and implications for eruption triggering mechanisms

C. Perinelli, S. Mollo, M. Gaeta, S.P. De Cristofaro, D.M. Palladino, P. Armienti, P. Scarlato, K.D. Putirka

We have refined the clinopyroxene-based hygrometer published by Armienti et al. (2013) for a better quantitative understanding of the role of H_2O in the differentiation of Etnean magmas. The original calibration data set has been significantly improved by including several experimental clinopyroxene compositions that closely reproduce those found in natural Etnean products. To verify the accuracy of the model, some randomly selected experimental clinopyroxene compositions external to the calibration data set have been used as test data. Through a statistic algorithm based on the Mallows' CP criterion, we also check that all model parameters do not cause data overfitting, or systematic error.

The application of the refined hygrometer to the Mt. Etna 2011–2013 lava fountains indicates that most of the decreases in H_2O content occur at P < 100 MPa, in agreement with melt inclusion data suggesting abundant H_2O degassing at shallow crustal levels during magma ascent in the conduit and eruption to the surface (Fig. 1).

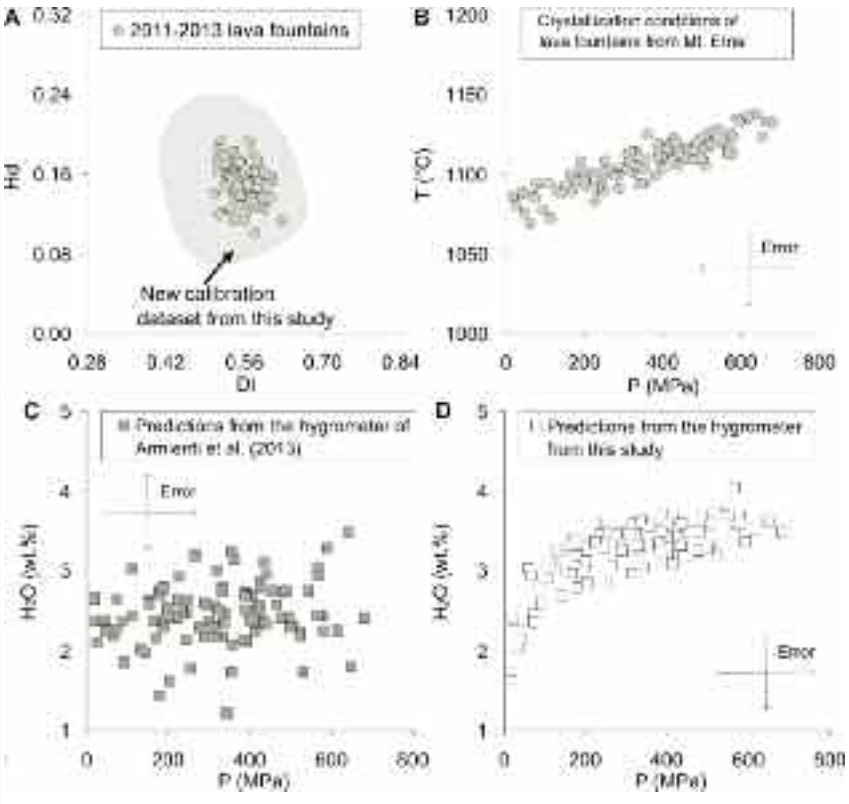

Fig. 1 | (a) Di (diopside) vs. Hd (hedenbergite) diagram showing the compositions of natural clinopyroxene phenocrysts reported by Mollo et al. (2015) for scoria clasts erupted during 2011–2013 lava fountains. (b) Estimates of the magma crystallization conditions performed by Mollo et al. (2015) using the compositions of clinopyroxene rims and coexisting melts as input data for the thermobarometric models of Putirka (2008). Error bars correspond to ±25 °C and ±180 MPa, i.e., the uncertainties of the thermometer and barometer of Putirka (2008). (c) H_2O predictions obtained through the original hygrometer of Armienti et al. (2013) are not very accurate showing scattered estimates and no clear correlation with the pressure decrease during magma upward migration. (d) H_2O predictions obtained through the refined hygrometer from this study show melt-H_2O concentrations that progressively decrease with decreasing pressure. Most of the H_2O decrease occurs at P < 100 MPa, in agreement with independent melt inclusion data.

Clinopyroxene-melt element partitioning during interaction between trachybasaltic magma and siliceous crust: Clues from quartzite enclaves at Mt. Etna volcano

S. Mollo, J. D. Blundy, P. Giacomoni, M. Nazzari, P. Scarlato, M. Coltorti, A. Langone, D. Andronico

A peculiar characteristic of the paroxysmal sequence that occurred on March 16, 2013 at the New South East Crater of Mt. Etna volcano (eastern Sicily, Italy) was the eruption of siliceous crustal xenoliths representative of the sedimentary basement beneath the volcanic edifice. These xenoliths are quartzites that occurred as sub-spherical bombs enclosed in a thin trachybasaltic lava envelope. A high-temperature reaction corona developed at the quartzite-magma interface in which alkaline differentiated melts of hybrid origin coexist with newly-formed clinopyroxene crystals different to those found in the host trachybasaltic lava. This characteristic makes it possible to quantify the effect of magma contamination by siliceous crust in terms of clinopyroxene-melt element partitioning.

For clinopyroxenes from both lava flow and hybrid melt expected relationships are observed between the partition coefficient, the valence of the element, and the ionic radius. However, for the hybrid melt, there is a decrease in the partition coefficients for transition metals (TE), high-field strength elements (HFSE) and rare earth elements including yttrium (REE+Y), and an increase for large ion lithophile elements (LILE) due to coupled substitutions one the M1, M2 and T sites of the type M1(Al, Fe^{3+}) + TAl = M2(Mg, Fe^{2+}) + ^{T}Si. The different incorporation of trace elements into clinopyroxenes of hybrid origin is controlled by cation substitution reactions reflecting local charge-balance requirements. According to the lattice strain theory, simultaneous cation exchanges across the M1, M2, and T sites have profound effects on REE+Y and HFSE partitioning, whereas temperature and melt composition have only a minor effect. As a consequence, partition coefficients for REE+Y and HFSE diverges significantly from those derived by magmatic differentiation, causing unexpected elemental overprints on the primary geochemical signature (Fig. 1).

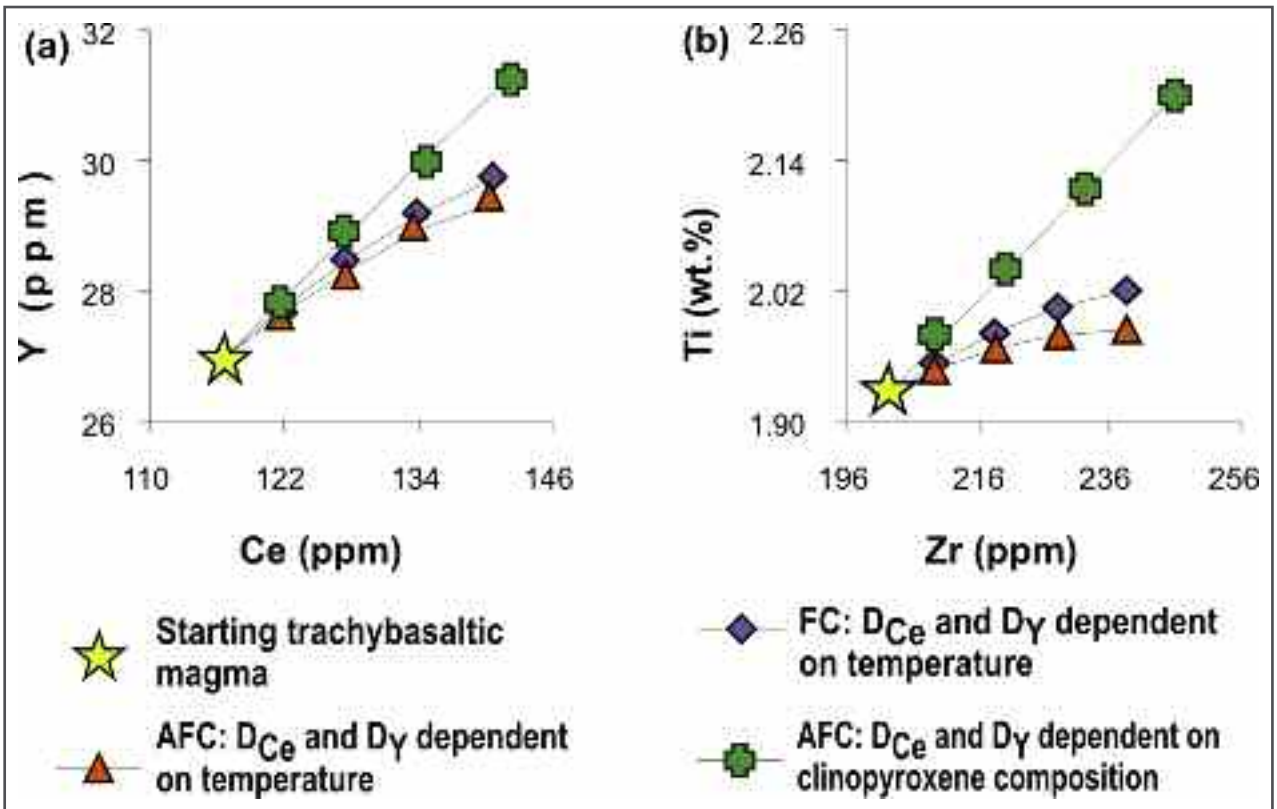

Fig. 1 | Ce and Y **(a)**, and Ti and Zr **(b)** partition coefficients as a function of temperature and clinopyroxene composition are used to illustrate magma dynamics driven by fractional crystallization (FC) and assimilation and fractional crystallization (AFC) processes.

Initial development of transient volcanic plume as a function of source conditions

P.Y. Tournigand, J. Taddeucci, D. Gaudin, J.J. Peña Fernandez, E. Del Bello, P. Scarlato, J. Sesterhenn, Y. Akihiko

Vent conditions are the key parameters to understand unsteady volcanic plume dynamics from which arise a wide range of different hazards, such as human health issues, building and aircraft's engine damages. Indeed, it has been experimentally evidenced that plume development and stability over time are largely driven by the source behavior. In this study we use high-speed videos of transient volcanic plumes in the visible (Optronis CR600x2 1280x1024 pixels definition, 500 Hz frame rate camera) and the thermal (FLIR SC655 640x480 pixels definition, 50 Hz frame rate camera) spectral range of Strombolian to Vulcanian explosions from three different volcanoes: Sakurajima (Japan), Stromboli (Italy) and Fuego (Guatemala). Figure 1 displays several events from those three volcanoes, sorted up to down from the longest to the shortest ejection phase, and left to right from the most spread sources to the most focused ones. This figure illustrates the great diversity of plume types present in this dataset. This diversity and the relationship between shape evolution and source behavior highlighted by the plume parameterization pushed towards the setting of a new method of mass eruption rate (MER) estimations based on high-speed imagery. Results show a direct relation between shape evolution and mass eruption rate with more sustained sources generating well-collimated plumes while more discontinuous sources generate chaotic shape evolution that might even lead to partial collapses of the structure. Time (e.g. duration and/or interval between pulses) and space (e.g. number of active vents and angle of ejection) variability are first order parameters involved in transient plume dynamics.

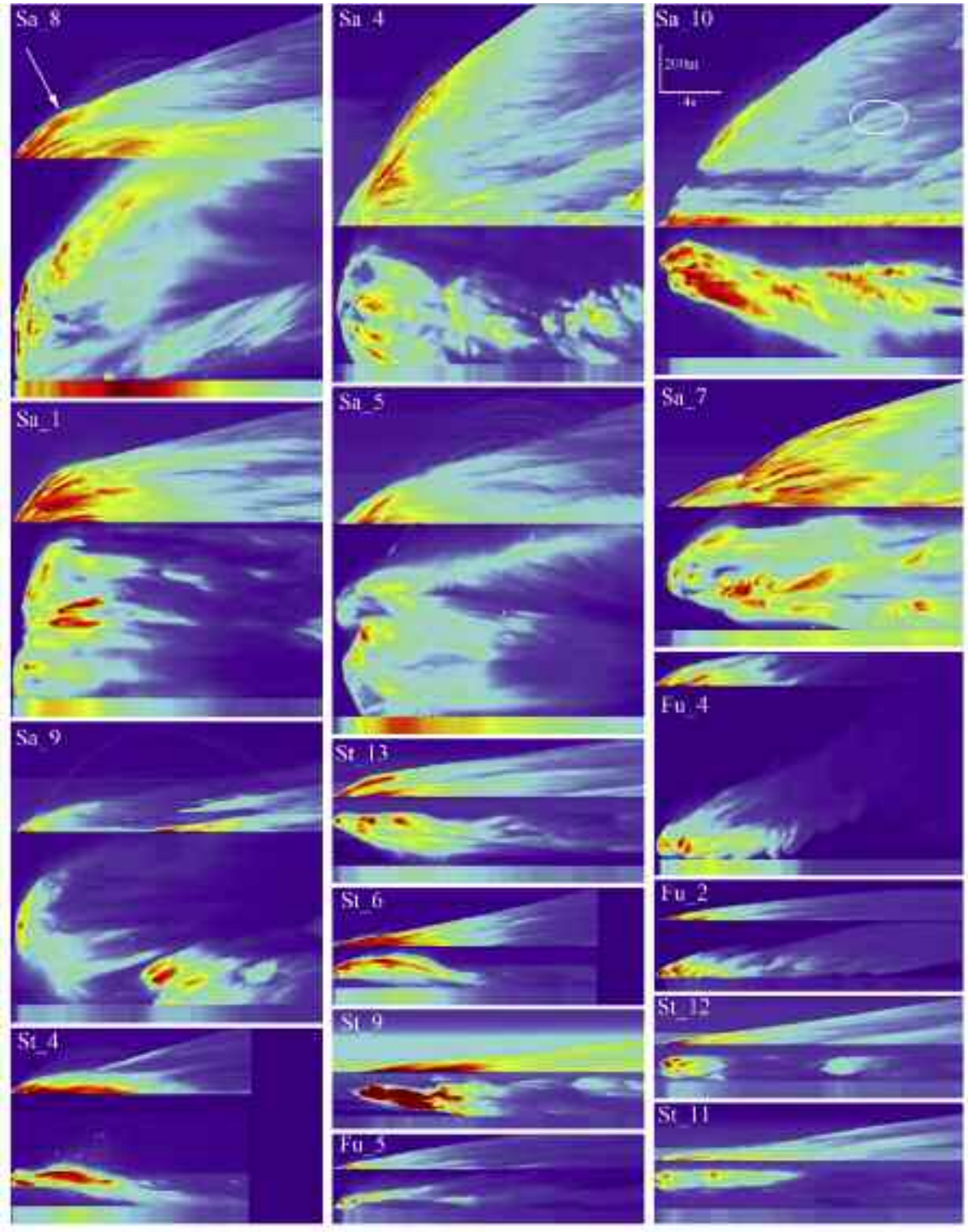

Fig. 1 | Thermal pixel line extracted over time. The color code of each picture correspond to the relative temperature evolution over time. For each volcano, the explosions are sorted up to down, from the longest ejection phase to the shortest one and left to right from the most spread sources to the most focused ones. Space and time scales are the same for each explosions, and the considered period of time is from second 0 to second 20.

Fractal analysis: A new tool in transient volcanic ash plume characterization

P.Y. Tournigand, J.J. Peña Fernandez, J. Taddeucci, D. Perugini, J. Sesterhenn

Transient volcanic plumes are time-dependent features generated by unstable eruptive sources. They represent a threat to human health and infrastructures, and a challenge to characterize due to their intrinsic instability. Plumes have been investigated through physical (e.g. visible, thermal, UV, radar imagery), experimental and numerical studies in order to provide new insights about their dynamics and better anticipate their behavior. It has been shown experimentally that plume dynamics is strongly dependent to source conditions and that plume shape evolution holds key to retrieve these conditions. In this study, a shape evolution analysis is performed on thermal high-speed videos of volcanic plumes from three different volcanoes Sakurajima (Japan), Stromboli (Italy) and Fuego (Guatemala), recorded with a FLIR SC655 thermal camera during several field campaigns between 2012 and 2016. To complete this dataset, three numerical gas-jet simulations at different Reynolds number (2000, 5000 and 10000) have been used in order to set reference values to the natural cases. Turbulent flow shapes are well known to feature scale-invariant structures and a high degree of complexity. For this reason we characterized the bi-dimensional shape of natural and synthetic plumes by using a fractal descriptor. Such method has been applied in other studies on experimental turbulent jets as well as on atmospheric clouds and have shown promising results. At each time-step plume contour has been manually outlined and measured using the box-counting method. This method consists in covering the image with squares of variable sizes and counting the number of squares containing the plume outline. The negative slope of the number of squares in function of their size in a log-log plot gives the fractal dimension of the plume at a given time. Preliminary results show an increase over time of the fractal dimension for natural volcanic plume as well as for the numerically simulated ones, but at varying rates. Increasing fractal dimension correspond to an increase in the overall complexity of plume shape and thus to an increase in flow turbulence over time. Accordingly, numerical simulations show that, fractal dimension increases faster with increasing Reynolds number. However, other parameters seem to play a role in volcanic plumes evolution. The features of the eruption source (e.g. vent number, size and shape, ejection duration, number and time interval between the different ejection pulses that characterize unsteady eruptions) seem also to have an effect on this time evolution with for example a single vent source generating a faster increase of the fractal dimension than in the case of a plume fed by several vents over time. This first attempt to use fractal analysis on volcanic plume could be the starting point towards a new kind of tools for volcanic plume characterization potentially giving an access to parameters so far unreachable by only using more traditional techniques. Fractal dimension analysis applied on volcanic plumes could directly link a shape evolution to source conditions and thus help to constrain uncertainties existing on such parameters.

Noble gases in fluid inclusions (FI) of olivine and pyroxene crystals from active volcanoes along subduction zones

A.L. Rizzo, P. Robidoux, A. Di Piazza, A. Aiuppa, A. Battaglia, M. Liuzzo

Volcanic systems along Central and South America Arc have been studied for $^{3}He/^{4}He$ ratios in fluids outgassed from fumaroles and geothermal areas. High temperature fumaroles with high Rc/Ra values (>7) are found for volcanoes belonging to the Trans Mexican Volcanic Belt (TMVB) (Colima, Ceboruco) with the highest values measured at El Chichón in 1998 (8.09 Rc/Ra). In the Central American Volcanic Arc (CAVA), fumaroles from different volcanoes have variable Rc/Ra values, but the maximum values continue to be strictly in the mantle range (>7 Ra) from Guatemala to Costa Rica, and in South America.

The pristine signature of He isotopes in high and low temperature fluids outgassed at the surface from fumaroles and geothermal areas fed by volcanic arcs is sometimes modified by the contamination of crustal and atmospheric fluids mixed with those magmatic at shallow levels of the volcanoes plumbing system. This means that the $^{3}He/^{4}He$ ratios measured in these fluids are somehow lower than the range of values typically expected in the mantle wedge (8±1Ra). For this specific reason, the study of noble gases in FI hosted in mafic minerals separated from rocks becomes crucial for understanding the magmatic/mantle features beneath the studied volcanoes and for recognizing those processes susceptible to modify the pristine signature at crustal levels. Indeed, FI well preserve the magmatic conditions at which the crystals growth, avoiding shallow contaminations by hydrothermal or atmospheric fluids. A few studies of noble gases in FI have been already carried out in CAVA who compared FI with the same measurements in surface gases, but lot of information is still missing for most of the volcanic front (Central and South America).

In order to deepen the knowledge on the mantle features and those processes involving magma along its rise within the crust, the study of noble gases has to be integrated by the investigation of mineral and whole rock chemistry (major and trace elements). For this reason, in this project we studied the mineral chemistry of olivine and pyroxene crystals already studied for noble gases in FI. The chemistry of the minerals hosting FI, particularly their Mg# is in fact crucial to evaluate the extent of magma differentiation, the equilibrium conditions as well as the presence of possible xenocrysts in the rock matrix. This information can be acquired by measuring the relative amount of major oxides by electron microprobe survey (EMPA).

For this purpose, we selected a series of mineral crystals (n~300) in the fraction 0.5 – 1.0 mm. We recall that the rocks from which we separated crystals have been collected from the following volcanoes: Lastarria and Lascar (Chile), Barú (Panama), Irazú (Costa Rica), Momotombo (Nicaragua), Pacaya (Guatemala), and a few Mexican scoria cones and Maars (Cintura-Alberca-Solis-Pelagatos). We plan to measure the major elements composition of each crystal with a couple of spots on the core and the rim, in order to verify the composition during its growth. We

would like to make these measurements within the end of June 2016.

An intense revision of mineral chemistry from different Central/South American volcanoes was possible at HPHT laboratories of INGV-Roma by using the electron microprobe (EMP) JEOL JXA-8200 equipped with 5 wavelength dispersive X-ray spectrometers and 1 energy dispersive X-ray spectrometer (EDS) analyzer. Olivine and (clino/ortho) pyroxene phenocrysts from different tephra layers were handpicked, and sieved to the 0.5 – 2.0 mm granulometry fraction, all prepared on different mounts. In some cases, thin sections from the scoria lapilli fraction and lava fragments were added to study the composition from the mineral assemblages. The EMP analytical conditions were a beam current of 7.48 – 7.50 nA, accelerating voltage of 15 kV, and beam diameter of 5 µm. The counting times for the minerals were 10 and 5 s at the peak and background, respectively. Crystal reference materials were used for quantifying the major elements.

Lascar contains the most primitive mineral assemblage among all sampled stratovolcanoes, consisting of mostly dark scoria of lapilli-to-bomb size from a pyroclastic flow emitted during the strong vulcanian eruption of April 1993, but large scoria from a ~9 years old scoria flow are also considered (olivine, Fo_{74-90}; augite, $Wo_{5-17}En_{39-46}Fs_{38-52}$; hypersthene, $Wo_{1-3}En_{63-75}Fs_{16-35}$; plagioclase, An_{45-71}). Lastarria generally represents heterogeneous material that were sampled in pyroclastic flow deposits (scoria, heterogeneous banded-black-beige pumice, blocks, bombs), but the mineral assemblage indicates differentiated magmas (olivine, Fo_{82} (only n = 1); augite, $Wo_{9-14}En_{3}8-44Fs_{41-48}$; hypersthene, $Wo_{1-3}En_{62-70}Fs_{23-35}$; plagioclase, An_{38-52}).

Lava flows from the Barú volcano oldest basement were also sampled (0.011 to 0.213 Myrs) and represent diverse mineral assemblages (Forsterite, Augite, diopside, labradorite-bytownite, biotite, amphibole, apatite, spinel, etc.), but various degrees of diffentiation are measured depending on the layer (e.g. olivines with Fo_{74-90}), while Pacaya samples (scoria of coarse ashes-to-lapilli size) show bimodal compositions for their olivines (Fo_{64-78} and Fo_{83-90}). A similar behavior is observed for mainly coarse ashes sampled at scoria cones from Valle of Santiago and Mexico (moderate to violent strombolian style activity), but with the oldest layers passing from mafic (Fo_{83-94}) to more evolved (Fo_{67-82}) olivines generally at the top of their respective stratigraphic sequence.

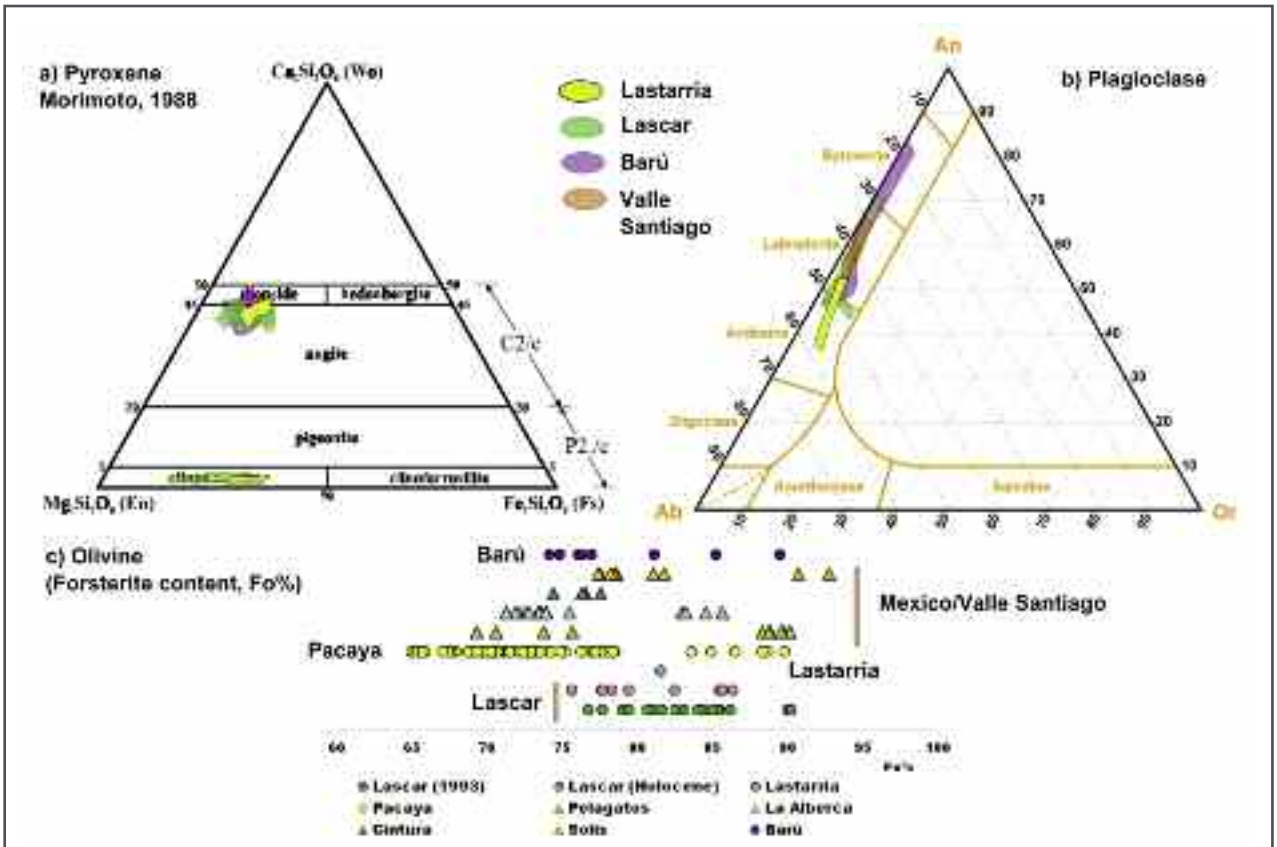

Fig. 1 I a-b-c presents results (systematically core and rim spots) from 157 spots on olivines, 197 on clinopyroxenes, 78 on orthopyroxenes (hyperstene) and 76 on plagioclases. The mineral chemistry indicates a certain degree of magma differentiation, unique for each eruption and volcano. The hyperstene group, for example, shows Enstatite (Mg-rich) and Ferrosilite (Fe-rich), while the clinopyroxene group shows Augite with higher or lower Mg (Fig. 1a). Plagioclase are considered to crystallize in mafic magmas when calcium (Anorthite pole - An) is relatively enriched compared to sodium (Albite pole - Ab) (Fig. 1b). High forsterite contents (Fo%) from olivine indicate relatively rich Mg content (Fig. 1c).

Petrological constrains on the coarse-grained, high-Mg basaltic enclaves of Capo Marargiu (Sardinia, Italy)

V. Tecchiato, M. Gaeta, S. Mollo, P. Scarlato

We present results from a textural and geochemical study conducted on calc-alkaline volcanic and hypabyssal rocks from the Oligo-Miocene Capo Marargiu Volcanic District (CMVD; Sardinia, Italy).

Stratigraphic units of CMVD consist of lava domes, a pyroclastic breccia interbedded with lava flows, and dikes. The pyroclastic breccia is in lateral contact with a low crystallinity (~15 vol.% phenocrysts), massive hypabyssal body hosting decimetre-sized, coarse-grained enclaves with porphyritic textures (~50 vol.% phenocrysts).

These crystal-rich enclaves and the host rock exhibit phase assemblages of clinopyroxene + plagioclase + amphibole + olivine + magnetite + low-Ca pyroxene, and plagioclase + clinopyroxene + magnetite + low-Ca pyroxene, respectively. Clinopyroxene phenocrysts (≤5 mm in size) in the crystal-rich enclaves show two compositionally distinct populations: type 1 clinopyroxenes are diopsides ($Mg\#_{85-90}$), whereas type 2 clinopyroxenes are augites ($Mg\#_{74-82}$). Plagioclase phenocrysts (≤1 mm in size) from crystal-rich enclaves and the host rock are normally zoned with An_{75-96} cores grading to An_{50-75} rims. The composition of amphibole phenocrysts (≤20 mm in size) is Mg-hastingsite. The mineral texture is poikilitic suggesting early crystallization of amphibole with respect to plagioclase. In fact, the primitive (~$Mg\#_{76}$), high-T amphiboles include clinopyroxene, whereas the more evolved (~$Mg\#_{65}$), low-T phenocrysts host plagioclase. Amphiboles are also surrounded by characteristic reaction coronas, consisting of tiny microlites (<5 µm in size) of clinopyroxene, low-Ca pyroxene, plagioclase, magnetite and ilmenite. Olivine occurs as phenocrysts (≤1 mm in size) with Fo_{79-87} cores surrounded by Fo_{66-79} rims.

The bulk-rocks of crystal-rich enclaves are high-Mg basalts (i.e., 10 wt.% MgO), whereas the host rock is a more differentiated basaltic andesite (i.e., 5 wt.% MgO). Major oxides and compatible trace element modelling suggest that the basaltic andesitic magma originates by crystal fractionation of olivine + clinopyroxene from a high-Mg basalt. In turn, compatible trace elements in the high-Mg basalt are low (330 ppm Cr, 130 ppm Ni) relative to picritic arc magmas, as the result of crystal fractionation of olivine ± Cr-spinel from a primary magma at depth.

Thermobarometric calculations on phenocrysts from the crystal-rich enclaves in equilibrium with the high-Mg basalt yield pressures (600-400 MPa) and temperatures (1200-950 °C) consistent with phase diagrams derived by experiments conducted on primitive arc liquids. Nevertheless, (i) the breakdown of the opacitic amphibole rim, (ii) the late appearance of plagioclase, and (iii) the correspondence between ~$Mg\#_{65}$ natural amphiboles and mineral compositions experimentally-derived at 200 MPa, indicate that the crystal-rich enclaves experienced a decompression path started at higher crustal depths. In this view, the high-Mg basalt and the basaltic andesite represent two different regions of a chemically zoned magma chamber formed by crystal fractionation of a primary magma ponding at ~500

MPa. Subsequently, buoyancy forces associated with density gradients caused upward migration of the basaltic andesite carrying portions of the adjacent high-Mg basalt to shallower crustal levels.

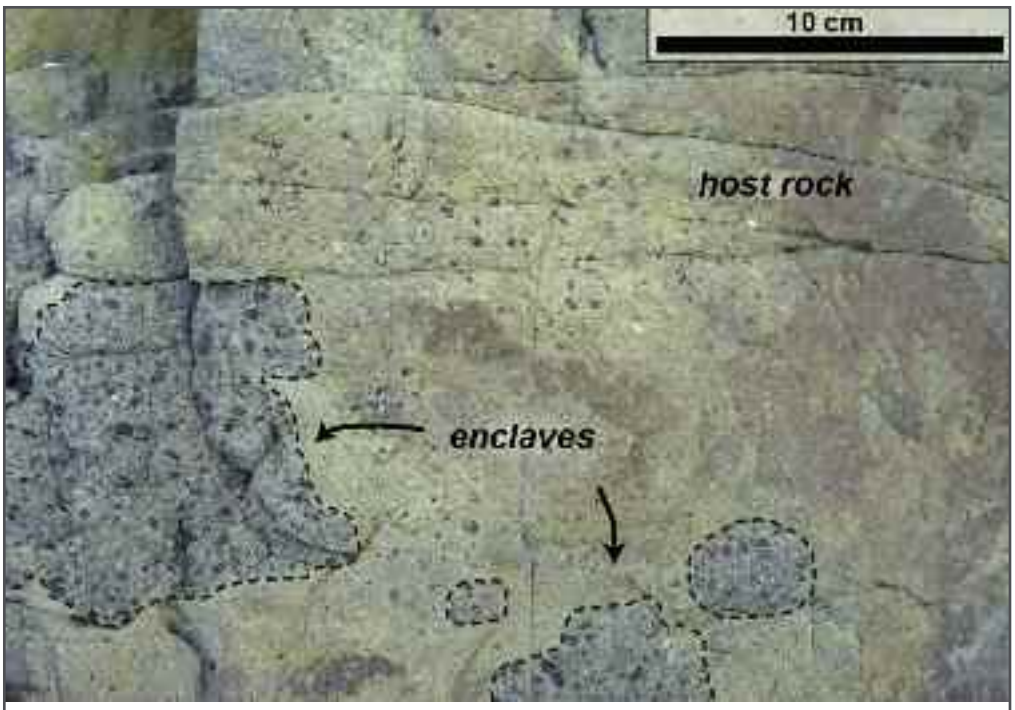

Fig. 1 I A detail of the outcrop where the basaltic andesite hosts the crystal-rich enclaves. The picture clearly show the striking textural differences of crystallinity and crystal-size between these rocks.

Generating phonolitic magmas by trachy andesite fractionation

M. Brenna, M. Masotta, S. Mollo

Magmas with phonolitic compositions erupt at intraplate alkaline volcanoes. The origin of such magma types is still controversial, with different models invoking variable degrees of fractional crystallization, crustal assimilation, magma mixing, and/or direct derivation from melting of mantle peridotite.

Single eruptions, originated from a relatively primitive end-member, are frequently characterized by heterogeneous bulk rock compositions shifting towards more differentiated phonolitic terms. In this scenario, the role played by fractional crystallization process may potentially explain the formation of such phonolitic magmas. An intriguing case study is represented by Al Shathaa volcano, in the Harrat Rahat volcanic field (Kingdom of Saudi Arabia), where a continuous eruption sequence (i.e., pyroclastic flows and surges)exhibits bulk rock compositions ranging from trachyandesitic to phonolitic products (Fig. 1).

In order to elucidate the physico-chemical conditions driving the magmatic differentiation, a preliminary set of experiments was designed to identify the pressures and temperatures that potentially controlled the natural liquid line of descent. These experiments were performed at 200 and 500 MPa, and 900 and 1000°C, at both anhydrous and hydrous (~4 wt.% H_2O) conditions, using as starting composition the most primitive trachyandesite end-member. Run-products obtained at 200 MPa (both anhydrous and hydrous) resulted in residual glasses with trachytic compositions (Fig. 1), whereas run-products equilibrated at 500 MPa (both anhydrous and hydrous) resulted in residual glasses with dacitic to rhyolitic compositions. At hydrous conditions glass was mostly dacitic (at 900 °C) with minor rhyolite (at 1000 °C), whereas dry conditions generated rhyolitic glass (Fig. 1). Notably, the run-products share a common paragenesis of K-feldspar, clinopyroxene and Fe-Ti oxides, whose variable mineral abundance controls the residual glass composition.

Preliminary results evidence as the primitive trachyandesitic end-member may potentially feed the trachytic eruptions at pressures around 200 MPa, but undoubtedly lower than 500 MPa. Conversely, the addition of H_2O up to 4 wt.%, does not produce residual melts substantially different from those derived under anhydrous conditions. On the other hand, none of the run-products reproduce the natural shift from trachyte to phonolite. Consequently, further experiments should be carried out using the rock sample named SH5C as starting composition (Fig. 1). This to explore the possibility that phonolitic melts result, indeed, by fractional crystallization of trachyandesite/trachyte magmas.

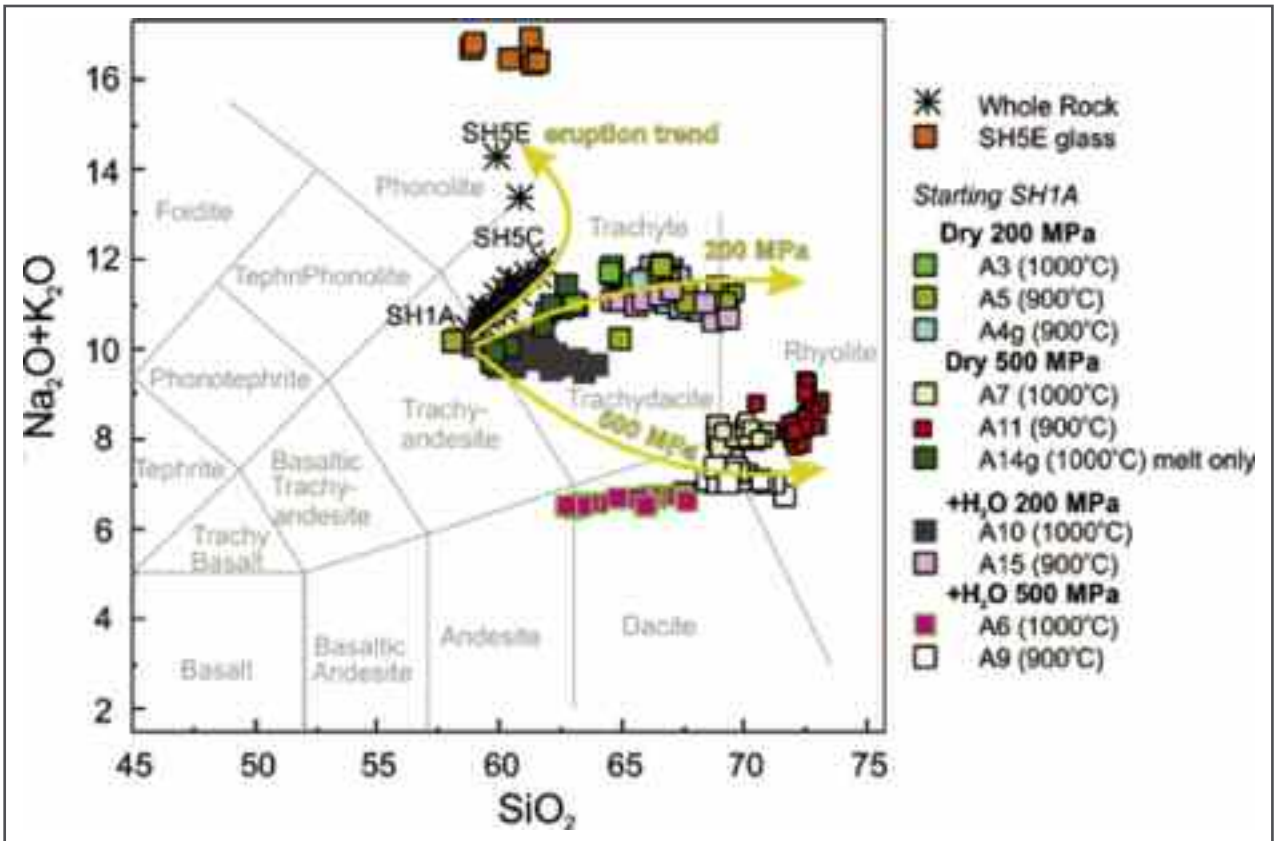

Fig. 1 | Experimental glass compositions are compared with the bulk rock analyses and natural glasses from the Al Shathaa eruption. The trachyandesitic sample named SH1A was used as starting material. The sample named A14g consists of a glassy material that did not crystallize.

Compositional variations of clinopyroxene in natural silicate melts induced by cooling rate

G. Iezzi, F. Vetere, V. Misiti, A. Cavallo, G. Ventura, H. Behrens, J. Knipping, S. Mollo, L. Giuliani

Clinopyroxene compositional variations induced by different cooling rates are evaluated for five natural silicate melts on the basaltic-dacitic join. Dynamic cooling experiments have been run under six different rates (150, 30, 3, 1, 0.116 and 0.0167 °C/min) from superliquidus (1300 °C) to solidus (800 °C, quenching) conditions. The composition of clinopyroxenes and other crystals was analysed by EPMA-WDS and SEM-EDS.

In all the crystal-bearing run-products, spinel is always present (few vol.%), whereas clinopyroxene occurs only in the run-products with a crystal content > 2-3 vol.%. Plagioclase is systematically outclassed by clinopyroxene, although the former phase should be the most abundant one under equilibrium conditions in all the run-products. In the less evolved starting compositions and at the highest cooling rates (> 3 °C/min), olivine, orthopyroxene and melilite crystals also occur.

In all the considered compositional systems, clinopyroxene is strongly and systematically enriched in Al_2O_3 as the cooling rate increases, whereas CaO and MgO evolve in a similar way but with a lesser marked dependence. SiO_2, Fe_2O_3 and Na_2O follow more scattered and articulated trends as a consequence of the co-precipitation of spinel and plagioclase with clinopyroxene. The chemical and derived molecular variations of clinopyroxenes can be used as speedometers, as well as to design glass-ceramic materials with tune able textural and compositional features.

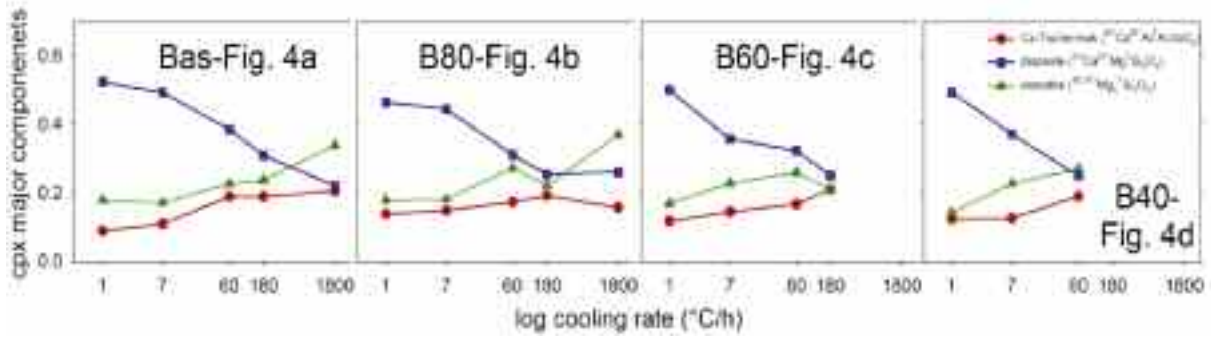

Fig. 1 I The increasing of cooling rate invariably determines a decreasing of the average diopsidic (Di) component and an increasing of enstatitic (En) and Ca-Tschermark (CaTs) molecules.

Mineralogy and textures of Riebeckitic asbestos (crocidolite): the role of single *vs* agglomerated fibre in toxicological experiments

S. Yao, C. Petrarca, F. Lazzarin, G. Della Ventura, F. Bellatreccia, M. Di Gioacchino, M. Nazzari, G. Iezzi, A. Marcelli, C. Petibois

Exposition to asbestos may cause adverse effects, but a clear relationship between mineralogy and texture of fibres vs. their toxicity is still lacking. Toxicological studies can be properly interpreted and compared only if quantitative features of fibres are determined. Here, Riebeckitic ("crocidolite") amphibole fibres were analysed by XRPD, FTIR, SEM-EDS and EMP-WDS, showing that only crystals with stoichiometry close to $^{A}\square^{B}Na_2^{C}(Fe^{2+},Mg)_3CFe^{3+}{}_2)Si_8O_{22}(OH)_2$ are present in the staring material used for the experiments.

Fibres deposited from solutions of 0.1, 1, 10, 25, 50, 75 and 100 mg/L were counted by image analysis using SEM images (Fig. 1). At 0.1 and 1 mg/L the fibres are well separated, whereas between 1 and 10 mg/L they start to agglomerate. *In-vitro* tests performed on fibres deposited at the same mg/L concentration show that the toxic potential follows a curvilinear increasing trend with a decreasing rate. Considering that the mineralogy is constant, the decreasing rate of toxicity suggests that the hazardous potential must be attributed mainly to the single fibres, while the agglomerated fibres, whose amount increases strongly for increasing total fibres have a minor effect.

The analytical protocol proposed here is valuable for any aero-dispersed dust, in polluted environments, as well as in the interpretation of experimental studies.

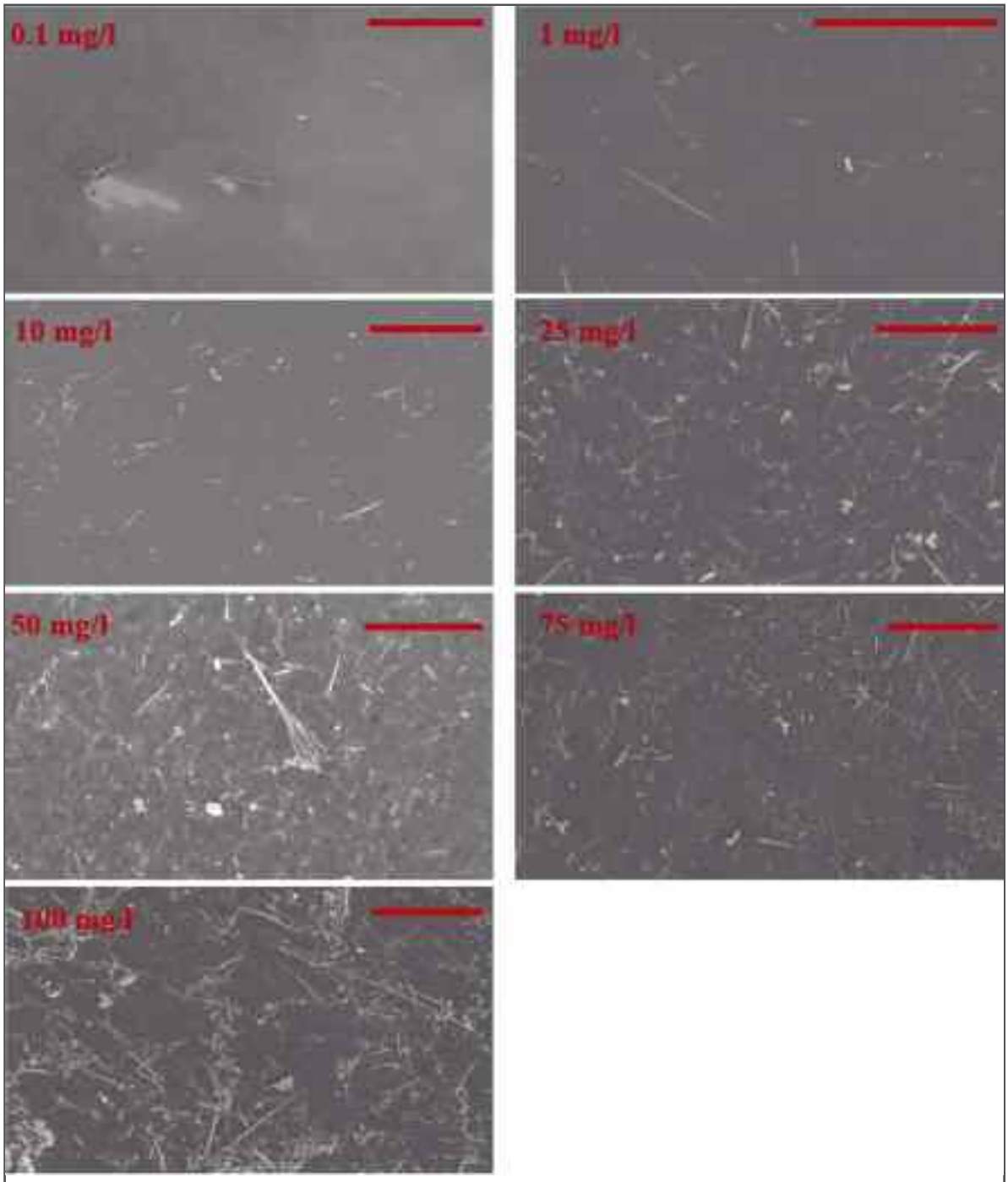

Fig. 1 | SEM micro-photographs of representative whole textures of Riebeckitic fibres sonicated at different concentration (0.1 to 100 mg/l) for 10 minutes and deposited on Si-foils for the counting of number of fibres per area (#fibres/area). The red bar is equal to 50 µm (all micro-photographs were collected at 550-620 X, except the 1 mg/l concentration acquired at about 800 X). Qualitatively, the #fibres/area increases as the mg/l also increases; in parallel, the impingement and/or agglomeration of fibres increase progressively as the #fibres/area or the mg/L increases.

Solidification and turbulence (non-laminar) during magma ascent: insights from 2D and 3D analyses of bubbles and minerals in an Etnean dyke

G. Lanzafame, G. Iezzi, L. Mancini, F. Lezzi, S. Mollo, C. Ferlito

Numerical models envisage laminar and turbulent regimes in basaltic dykes. In this work, non-laminar characteristics of intrusive magma at Mount Etna have been documented by bi-dimensional (2D) and three-dimensional (3D) analyses conducted on both bubbles and minerals. A 4.3-m-thick aphyric dyke (DK) solidified at depth of 100-300 m below the pristine surface level has been investigated. Textures and fabrics of seven rock samples from dyke rim (DK1) to core (DK7) have been analysed in 2D by using a high-resolution scanner, a transmission optical microscope, and scanning electron microscopy imaging with back-scattered electrons, and in 3D by microfocus X-ray computed tomography (Fig. 1).

The amount, size and shape of bubbles, irregularly change from dyke rim to core, in contrast with the limited changes documented for plagioclase (plg), clinopyroxene (cpx), titanomagnetite (timt), and olvine (ol). Bubble and plg contents depict opposite saw-like trends due to solidification from different portions (even as low as a few cm3) of magma enriched in dissolved H_2O and *vice-versa*. Bubbles with anisotropic shapes (average aspects 3:1) are randomly oriented in space, with strong variations in abundance, dimension, and form. All these features have been attributed to transitional to turbulent, i.e. non-laminar, regimes (Reynolds number > 1000).

Water solubility, volume of bubbles, magma density and viscosity models reveal that at depth > 100-300 m, i.e. P > 10 MPa, a virtual crystal-free magma containing 1 wt.% H_2O intruded, whereas at P < 10 MPa magma significantly degassed and crystallized. Results indicate that a rapid volatile exsolution at very shallow level induced sudden and marked crystallization, coupled with increase of viscosity and rapid deceleration or even arrest of magmatic suspension; the bubbles were frozen in, whereas crystals continued to grow under the effect of cooling rate increasing from inner to outer dyke portions. Despite the low H_2O content, the trachybasaltic magma was close to its liquidus temperature and the estimated ascending velocity of a few m/s led to hypothesize transitional to turbulent regimes during the emplacement of the dyke.

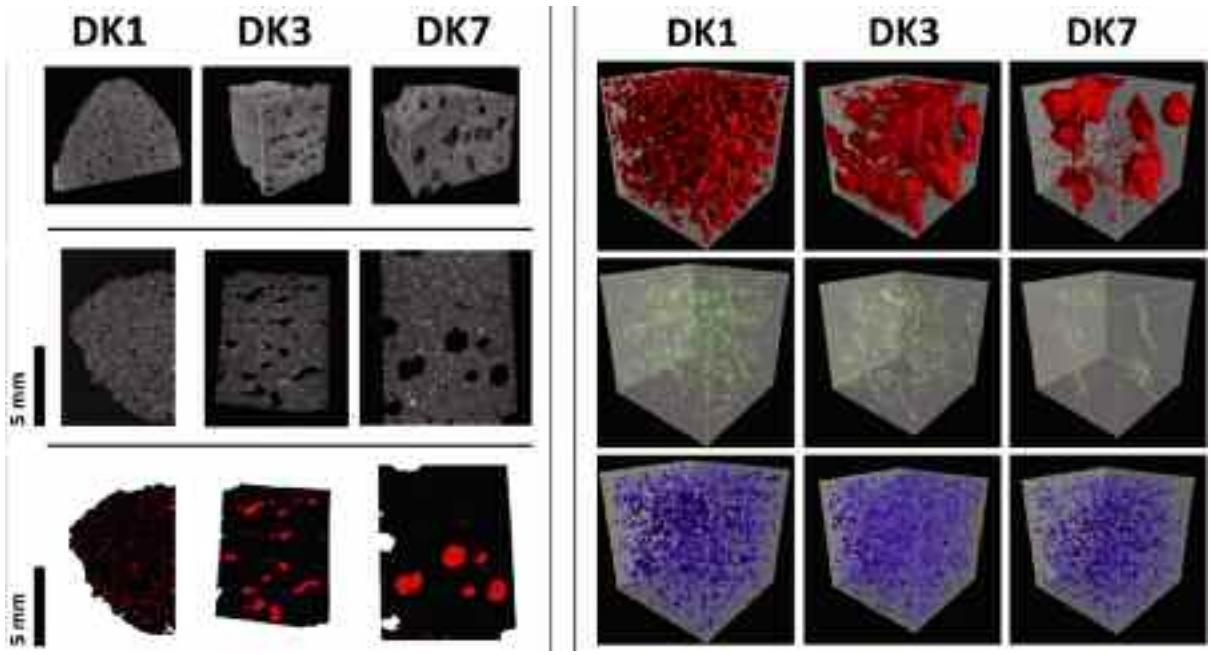

Fig. 1 | **left)**. Volume renderings of the selected investigated samples. Middle row: reconstructed assial slices. Bottom row: the same slices reported in the middle row where bubbles (red) and timt (blue) not connected with the borders have been segmented. **right)** 3D renderings of 500x500x500 voxels volumes of selected samples. Up row: isosurface renderings of the bubble phase; Middle row: skeletons of the bubble network, in green node-to-node connections, in red end-to-end branches. Bottom row: isosurface rendering of the timt phase.

Volcanic gas-ash interaction: an in vitro study of respiratory health effects

I. Tomašek, C.J. Horwell, D.E. Damby, A.S. Casas, P.M. Ayris, C.J. Ottley, C.Bisig, A. Petri-Fink, B. Drasler, M.J.D. Clift, B.Rothen-Rutishauser

Volcanic plumes are complex, heterogeneous environments composed of gases, aerosols and ash particles, where various reactions occur. By processes of chemical reaction and adsorption onto the surface of ash particles, volatiles are subsequently scavenged *i.e.* removed from the atmosphere and dispersed into the environment, commonly in the form of soluble salts adhered to ash surfaces.

These interactions between gases and ash particles in volcanic eruption plumes have been previously studied in order to understand the influence they might have on volcanic volatile budgets, surface properties of the ash and chemistry and dynamics of a plume. The aim of our study is to gain a first understanding of the effects of high-temperature in-plume processing on the respiratory health hazard of salt-laden ash particles, using a model of human lungs in vitro.

To simulate chemical reactions between ash surfaces and hot volcanic gases, we used an analogue system (i.e. powdered volcanic glass and pumice) in a novel Advanced Gas-Ash Reactor (AGAR) at the Department of Earth and Environmental Sciences of Munich University, Germany. This device is capable of generating a chemically-diverse atmosphere of volcanic gases (SO_2, HCl, CO_2) at temperatures ranging from 200 to 900°C, and can be used to demonstrate the gas uptake by volcanic particles.

As a result of the uptake of SO_2 at temperatures above 300°C, which occurs via rapid adsorption onto reactive surface sites, anhydrite ($CaSO_4$) is formed. At INGV Rome, preliminary imaging, by FE-SEM at the HPHT Laboratory, of generated ash particles confirmed the presence of salt coatings on the particle surfaces (Fig. 1).

Fig. 1 I The anhydrite coating of volcanic glass particles exposed to SO_2 in the Advanced Gas-Ash Reactor (AGAR) at University of Munich, Germany.

The biological effects of these particles are being investigated at the Adolphe Merkle Institute of the University of Fribourg, Switzerland.

8.2 ROCK PHYSICS AND EARTHQUAKES

Tsunamigenic earthquake simulations with experimentally derived friction laws

S. Murphy, G. Di Toro, S. Lorito, F. Romano, A. Scala, E. Spagnuolo, G. Festa, S. Aretusini, S. Nielsen, A. Piatanesi

The Tohoku fault has historically produced a range of different types of earthquakes from the M 8.2 1896 Menji tsunami earthquake to the Mw 9 2011 Tohoku mega-thrust earthquake with a number of traditional major thrust events in between. Using dynamic rupture simulations with 2D spectral element methodology we aim to reproduce these events within a single numerical model. To do this, we apply a thermal slip distance friction law that is based on high-velocity rock friction experiments. The choice of frictional parameters varies from clay-like near the surface with a transition to rock-like at depth. A variable effective normal stress is imposed in the wedge based on the dynamic critical taper theory. By varying the location of a high stress asperity up and down the fault the numerical model can reproduce a number of depth-dependent features (e.g. increasing static stress drop with depth) and the three most destructive types of earthquakes observed on the Tohoku fault (i.e. mega-thrust earthquakes, tsunami earthquakes and traditional thrust earthquakes). When the asperity is located at depth, rupture is constrained to the zone around the asperity and thus standard thrust earthquakes

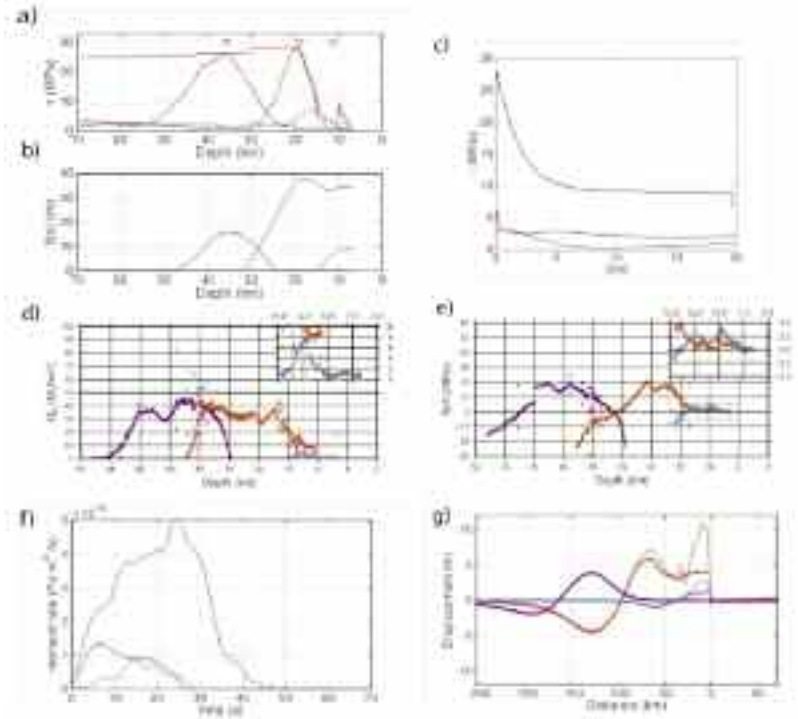

Fig. 1 I Case study setup and results. **a)** The different solid colours relate to the initial stress distributions used in the three simulations which reproduce a tsunamigenic megathrust (orange), tsunami earthquake (blue) and traditional thrust earthquakes (purple). The triangles refer to nucleation location with the colour corresponding to the initial stress distribution of the same colour. The red line is the yield stress. **b)** slip distributions where the colours relate to the initial stress distributions in **a). c)** Stress evolution with slip at three different depths taken from the simulation where nucleation occurs at a depth of 19 km (i.e. orange line in **b)**. The black line is evolution of stress with slip at 25 km depth where the frictional conditions are 'rock-like', the blue line is at a depth of 12 km which is in the transition between rock- and clay-like and is in the zone where the fluid pore pressure is very high, i.e. $\lambda = 0.95$. The red line denotes the stress evolution at 9 km depth where the frictional conditions are clay-like and $\lambda = 0.65$. **d)** Breakdown energy calculated at each point along the fault. Insets are expansions of the data inside the red dashed boxes. **e)** Static stress drop has been calculated using $\Delta\sigma=\tau o-\tau f$ where τf is the shear stress at the end of rupture and τo is the initial shear stress. **f)** Moment release rate with time for the four earthquakes. **g)** Vertical seafloor displacement for the different earthquakes are depicted by dotted lines, estimated tsunami source accounting of seafloor slope steepness and horizontal displacement {Satake:1999fs} are depicted with solid lines. Distance is horizontal distance from the point where the fault reaches the seafloor.

are produced. Near the surface, it is difficult for rupture to propagate down-dip from the clay-rich to the rock-rich layer meaning asperities in the wedge are constrained by the clay to rock transition. Conversely, rupture propagating up-dip can easily rupture into clay-like material producing large, mega thrust earthquakes. Due to these features, those earthquake that nucleate within a particular depth range (the lower end of the transition between the clay - and - rock like material) can produce larger earthquakes compared to those nucleating elsewhere on the fault.

Characterisation of the mud emissions occurred after M 6.5 earthquake in Central Italy

T. Ricci, A. Sciarra, V. Misiti, D. Di Naccio, S. Amoroso, B. Cantucci, S. Pinzi, P. Monaco, P.M. De Martini

Mud volcanoes are geologically important manifestations of fluid flow and mud eruption in sedimentary contexts worldwide. Their formation is predominantly ascribed to release of overpressure from clay- and organic-rich sediments, leading to impressive build-up of mud mountains in submarine and subaerial settings. Here we report on a newly mud emissions as a consequence of the 30th October earthquake and on the activity of preexistent mud volcanoes affected by the recent Central Italy seismic sequence (Fig. 1).

The emission points are situated in an farming plot of land. The emission started in the late morning of the 1st November 2016.

A geochemical survey was conducted on these mud emissions and CO_2, CH_4, O_2 and H_2, temperature measurements, as well as measurements of Radon and Thoron activities, were carried out. We also measured the pH and conductivity of the samples.

Fig. 1 I Newly formed mud emissions.

Textural analysis of fault rocks: a multi-scale investigation

A. Merico, M. Cremona, M. Nazzari, M. Scafa, B. Pace, G. Iezzi, L. Ferranti, A. Colella

Shear zones in carbonate fault rocks are frequently quantified by sieving and sedimentation methods or using etching of grain rims from mildly acid solution. However, these methods have some limitations; sieving can be performed only on loose faulted rocks and etching can alter the original size and shapes of grains, as well as selective dissolution of phases, for instance carbonates versus silicates, can alter their actual abundances. Owing on these limitations, we test a multi-scale approach on a secondary fault sample collected into the Venere quarry outcrop, along the San Benedetto–Gioia dei Marsi (SBGM) fault (Fucino Plain, central Italy).

This faulted carbonate lithic sample has been first analysed by XRPD, unravelling that the entire rock is made of only calcite. Then, part of it was used to prepare a relative large polished mesoscopic section plus a standard thin section, as shown in Figs. 1a and 1b. These two surfaces were used to analyse the relative large (≥ 1 mm) and tiny (< 1 mm) tectonic grains, respectively, thus capturing size variations from cm down to µm dimensions. We imaged the sample at the following magnifications: 1, 2.5, 10, 95, 550, 1900 and finally 7000 X. Grains ≥ 1 mm were manually recognised and drawn on a transparent sheet (Fig. 1a). Transmission optical microscopy (TOM) was used to acquire digital images at both 2.5 and 10 X and quantifiable grains again coloured manually on transparent sheets (Figs. 1c and 1d). Instead, grains imaged by SEM were directly measured automatically due to their distinguishable features (Figs. 1e, 1f, 1g, 1h, 1i). Thereby, image analysis has been conducted on reproduced grains on transparent sheets at their corresponding mesoscopic and TOM scales. By contrast, digital SEM images allowed us directly counting textural features of carbonate grains by image analysis. In addition, we collected adjacent SEM images at 95 X, labelled SEM-PUZ, to analyse a relative large portion of this faulted rock and fill a possible size gap between mesoscopic and 95 X imaged grains (Fig. 1e).

The measured grains acquired by 2.5 and 10 X with TOM versus corresponding ones with SEM-PUZ and SEM 95 X are plotted and compared (insets in Figs. 1j and 1k); these two plots show very similar trends and values of regressions. This consistency indicates that two different methods attain the same result, corroborating mutually them. In other words, image analysis results of calcitic grains collected by TOM and drawn manually are virtually identical to those obtained directly on SEM micro-photographs. On this basis, we extended image analysis on a wider range of calcitic grain sizes, such as those displayed in figures 1j and 1k. These textural outcomes and their comparable results testify that cm to µm textural data of carbonate fault rocks have a straightforward and significant interpretation when obtained using mesoscopic large sample surface and related thin section. Back-scattered SEM images recorded at increasing magnifications can be rapidly and automatically used for image analysis to count textures of carbonate rocks.

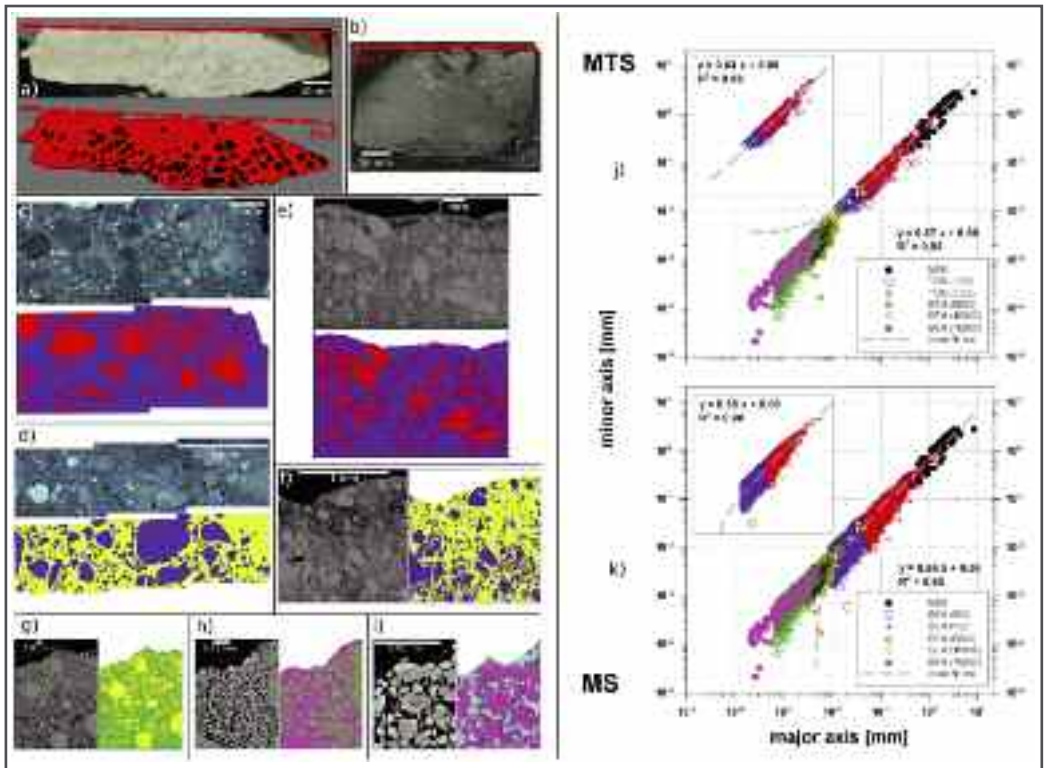

Fig. 1 | **left)** original and corresponding binary digital images at variable magnifications: a) mesoscopic; b) thin section; c) TOM 2.5X; d) TOM 10X; e) SEM-PUZ; f) SEM 95X; g) SEM 550X; h) SEM 1900X; i) SEM 7000X. **right)** diagrams and related regressions of length and width of grains obtained by image analysis using MTS (j: mesoscopic + TOM + SEM) and MS (k: mesoscopic + SEM); the two insets relate to grain sizes obtained by only TOM and SEM-PUZ plus SEM 95X. The trends of these grain distribution are very similar, also according to their regression equations.

Textural variations of carbonate fault rocks: the San Benedetto-Gioia dei Marsi (Fucino, central Italy) shear zone

A. Merico, M. Cremona, M. Nazzari, L. Ferranti, B. Pace, G. Iezzi, A. Colella, M. Scafa

Shear zones in carbonate fault rocks are frequently defined in terms of grain-size features collected on few selected, loose samples by sieving methods. In turn, possible textural variations along the strike of the main fault plane and moving away from the fault core into the damage zone, are relatively less studied, whereas lithified tectonised rocks are unanalysed. Thereby, we have tested an alternative protocol of 2D textural analysis able to measure cm to µm carbonate grains on lithified sample (see Merico et al. contribution in this report). We focus on the San Benedetto–Gioia dei Marsi (SBGM) normal fault and related shear zone (Fucino Plain, central Italy; Fig. 1). The central portion of this fault is exposed in the Venere quarry, where it is possible to investigate the structure responsible of the large 1915 earthquake (Mw 7.0). This ~ 100 m wide shear zone consists of fault planes and cohesive, fractured and pulverised carbonate rocks. In detail, we have analysed in the field, collected and studied in laboratory several oriented samples along the main fault and within both its core and the pulverised rocks inside the damage zone (Fig. 1). We quantified the textural parameters using mesoscopic and microscopic images. Mesoscopic data were obtained on detailed field measurements (scan areas), photos and polished rock sample surfaces (few dm^2), whereas microscopic data were studied on thin sections (35 cm^2) using integrated and scaled MTS (mesoscopic + transmission optical microscopy + SEM data) and alternatively MS (mesoscopic + SEM data). Tectonic grains or particles were investigated by image analysis, to obtain long and short axes of equal-area ellipses. Therefore, we detailed the textural variations in a very broad size scale, from microns to centimetres. The relative abundance of grain sizes evidences that these fault rocks are cataclastics.

In detail, the main fault rocks show the largest average grain sizes Dm (Fig. 1) by both approaches; the relative lowest Dm size from the main fault samples (V13 and V14) partially overlaps with two samples with the relative highest Dm from the cataclastic zone (V15 and V17) (Fig. 1). The grain distribution features around Dm quantified by $\sigma 1$, Sk and K are instead poorly indicative of the various tectonic rock samples collected along the SBGM main fault (V5, V12, V13 and V14), from secondary fault planes (V6, V8 and V10) and in the cataclastic zones (V15, V16, V17, V18 and V19). The “fractal D-values” show similar behaviour of the Dm one (Fig. 1).

These results point out that rock textures in the shear zone, but also along the same main fault, are very variable and reflect complex deformation processes. In turn, one or few samples collected in a shear zone could be poorly representative of the experienced deformation fabrics.

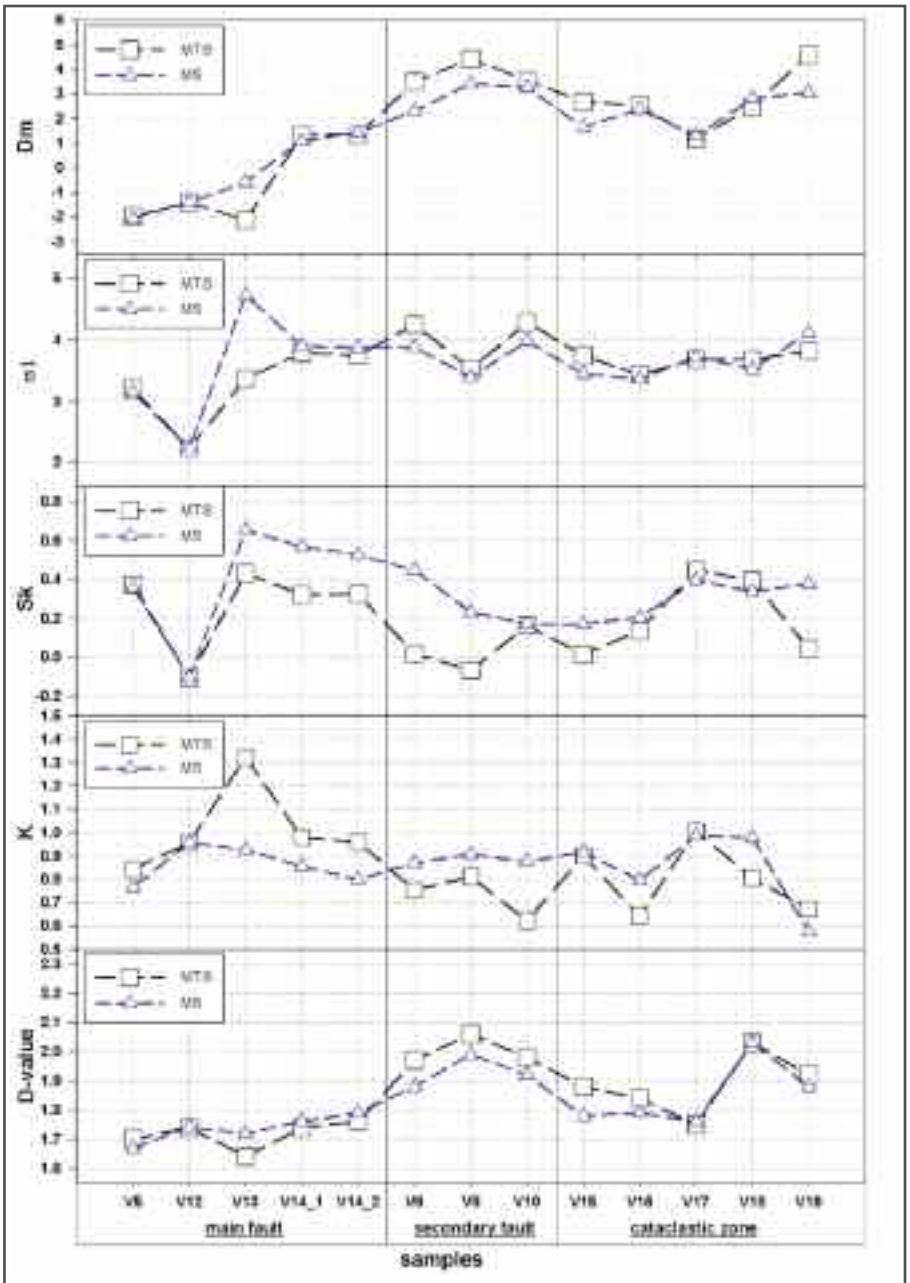

Fig. 1 | (top) Geographical location of the shear zone and of the investigated samples into the quarry of Venere. The four stacked diagrams of Dm, σ1, Sk and K refer to whole grain size parameters obtained by 2D image analysis. The bottom diagram is the so-called fractal D-value; it is the angular coefficient of the regression of the distribution of log range of clast sizes with their corresponding log number of clasts. The main fault samples are characterised by higher % amounts of large clasts with respect to tiny ones.

2016 Annual Report | 92

"Reddish patinas" from shear zones

A. Merico, L. Smeraglia, M. Nazzari, B. Pace, A. Billi, A. Cavallo, G. Iezzi

Reddish patinas are peculiar planar bodies, with thicknesses variable between ~ 1 mm and ~ 1 cm. They inhomogeneously mantle fault planes cropping in central Apennines, as well in some other carbonate brittle shear zones. They are easily observable due to their colours, changing from red to brown. Although their widespread and intriguing occurrences, they have not been characterised in depth. To shed light on their textural and chemical-physical peculiarities, we have characterized some of them, by means of XRPD and EPMA.

We sampled and analysed some of these patinas from the main faults of the following shear zones: San Benedetto-Gioia dei Marsi (SBGM-5p), Tre Monti (TMt), Val Roveto (VlRov), plus a patinas located into the SBGM tectonic structure (SBGM-patina). These patinas occur exclusively, albeit irregularly, along fault planes irrespective of significant or moderate suffered slip. In parallel, patinas invariably show kinematic features, i.e. slickenside structures, indicative of their involvement in tectonic processes. Representative powders of these patinas were analyzed by XRPD and thin sections cut normal to their thickness were investigated by EPMA. The X-ray diffraction data show that calcite (cc) is the unique detectable crystalline phase in the patinas of the SBGM tectonic zone (Fig. 1, left). The TMt and VlRov XRPD spectra unveil that also quartz (qz) and interestingly goethite (gh), besides than cc, are present in them. The VlRov patinas is instead mainly composed of gh, while cc is completely lacking (Fig. 1, left).

To corroborate these XRPD outcomes, several EPMA-WDS chemical maps have been performed on three patinas, two from the SBGM and one from TMt; the other ones will be acquired in the next period. The obtained maps show that patinas occur both on and almost normal to their faults, in agreement with mesoscopic observations. Patinas are made mainly of FeO, plus moderate quantities of both Al_2O_3 and SiO_2, plus a tiny amount of TiO_2 (Fig. 1, right). The SBGM-patina chemical maps, collected on the secondary fault with minor apparent slip, shows that carbonate and patinas are perfectly separated in their respective zones (Fig. 1, right). By contrast, the other two ones shows that patinas and their veins have an heterogeneous compositions; in fact, calcite grains (CaO-rich zones), with variable sizes and irregular rims, are contained into injected veins of Fe-, Al- and Si-bearing phase(s) (Fig. 1, right). The chemical and mineralogical features of these reddish patinas suggest that they originate from relative deep circulation of brines and were injected in these carbonate rocks under the same tectonic stress field that produced these faults. Generation of patinas from dissolution of cc appears unrealistic due to the very low amount of Fe, Al, Si and Ti in these carbonates. Moreover, precipitation of patinas from meteoritic waters appears unsupported from our data, since them occur only in tectonic fractures and are rich in chemical element that can be dissolved only at very high ph. It is thus of capital importance to constrain the composition of fluids that deposited them and which phases potentially recorded tectonic pulses.

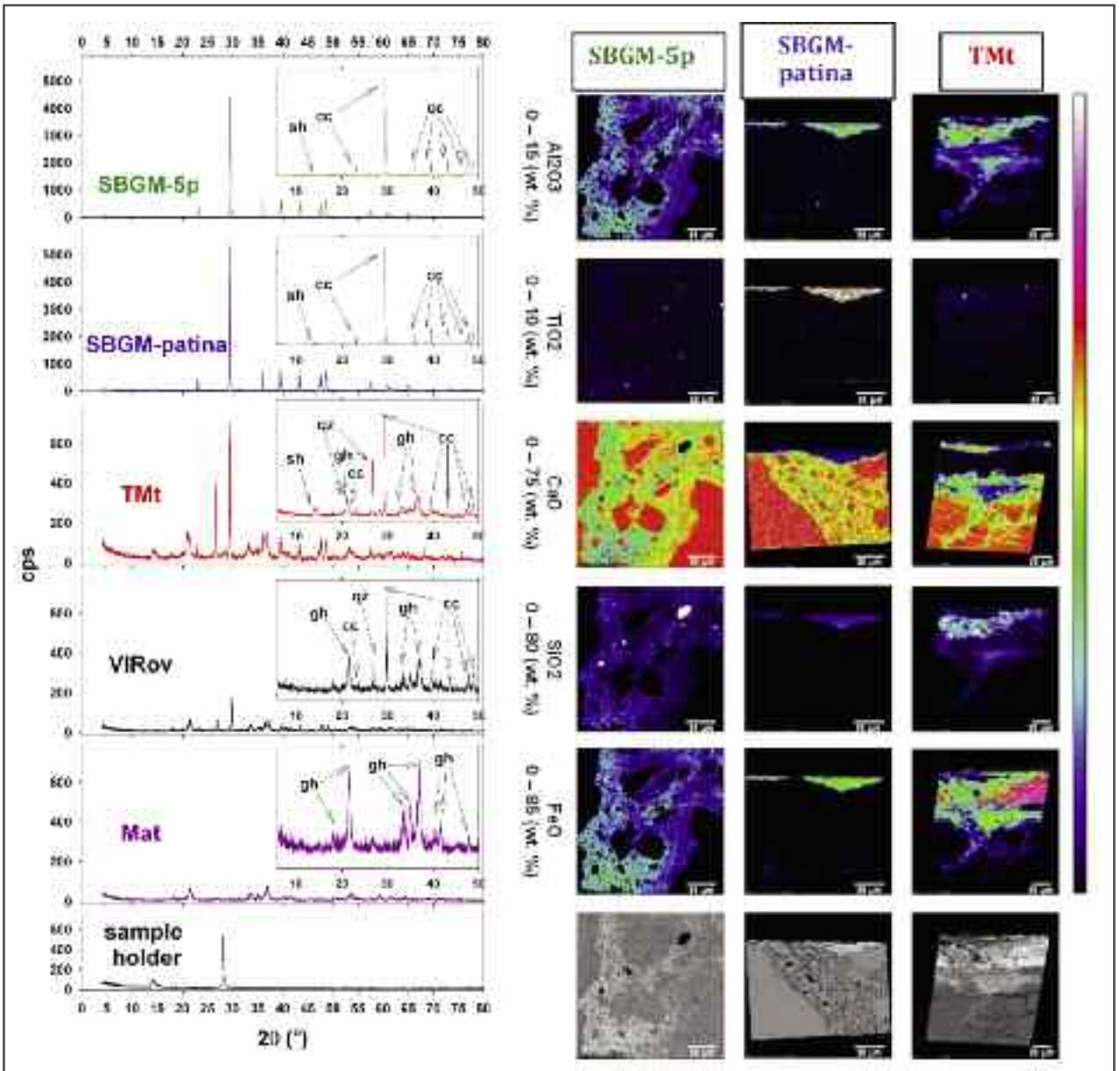

Fig. 1 I **left)** XRPD patterns of reddish patinas, showing that SBGM ones are composed of mainly calcite (cc), whereas other crystalline phases responsible for their mesoscopic reddish appearance are not detected; TMt and VIROV have both cc plus significant amount of goethite (gh) and quartz (qz); finally, Mat is entirely made by gh. **right)** EPMA maps of the three SBGM-5p, SBGM-patina and TMt show that reddish patinas occur on the fault, but also penetrate into the shear zone along veins nearly perpendicular to their fault planes; patinas are composed (in order of abundance) of FeO, Al_2O_3, SiO_2 and minor TiO_2 and are surrounded by only CaO, i.e. cc. At the same time, inside some patina cc grains are also present.

3D multi-scale velocity structure of an active seismogenic normal fault zone (Central Apennines, Italy)

M. Fondriest, T. Mitchell, M. Vassallo, G. Di Giulio, F. Balsamo, F. Passelegue, M. Pischiutta, G. Di Toro

The characterization of physical properties of fault zones (e.g., ultrasonic velocities, elastic moduli, porosity and fracture intensity of the fault zone rocks) is a relevant topic in reservoir geology (exploration and exploitation) and fault mechanics, for the modelling of both long-term quasi-static and fast dynamic fault zone evolution with time. Here we characterized the shallow subsurface velocity-elastic structure of the active Vado di Corno normal fault zone (Campo Imperatore, Central Apennines, Italy) which is up to > 300 m thick. Based on a detailed structural mapping of the fault footwall block covering a 2 km long fault segment, four main structural units separated by principal fault strands were recognized: (i) cataclastic unit, (ii) breccia unit, (iii) high-strain damage zone, (iv) low-strain damage zone (Fig. 1). The single units were systematically sampled along a transect (ca. 200 m) orthogonal to the average strike of the fault and characterized in the laboratory in terms of petrophysical properties (i.e. Vp, Vs, static and dynamic elastic moduli, porosity). The cataclastic and breccia units (Vp = 4.68±0.43 kms^{-1}, Vs = 2.68±0.24 kms^{-1}) were significantly "slower" compared to the damage zone units (Vp = 5.43±0.53 kms^{-1}, Vs =3.20±0.29 kms^{-1}).

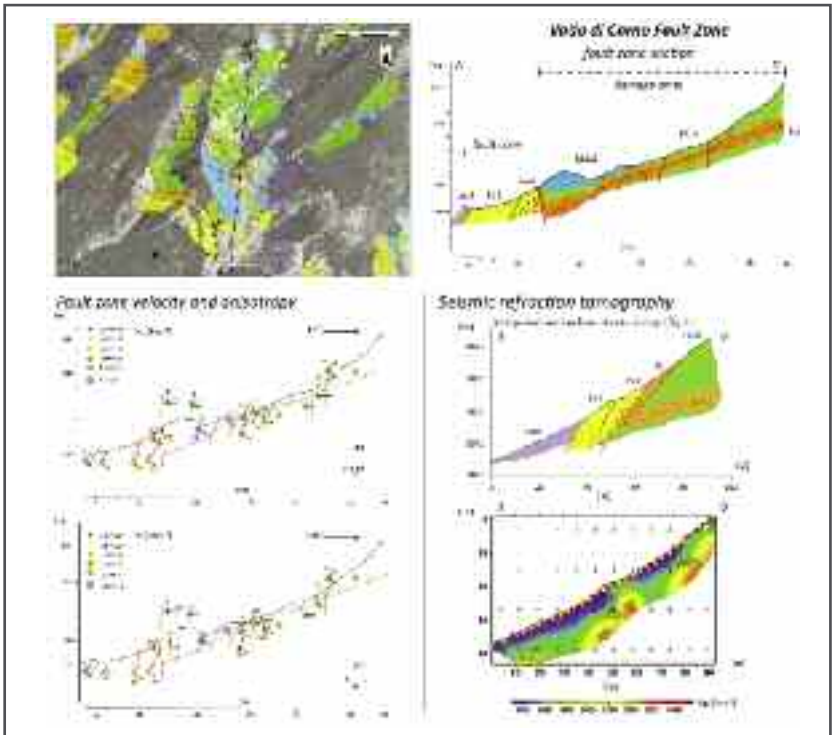

Fig. 1 I **(a)** Structural map of the Vado di Corno Fault Zone (on the left; see Demurtas et al., 2016, for details). White and red circles indicate the sampling location of the fault rocks for which acoustic properties (Vp and Vs) were measured in the laboratory. Section across the Vado di Corno Fault Zone (on the right) highlighting the geometry of the different fault rock unit. The breccia unit (orange in colour) represents an older thrust zone which is cut and locally reactivated by late and currently active normal faults. **(b-c)** Section across the Vado di Corno Fault Zone with Vp, Vs values of the fault rocks measured in the laboratory. The cataclastic-fault core units are significantly slower compared to the damage zone units. Velocity anisotropy is generally low (on average < 10 %). **(d-e)** Seismic refraction Vp tomography across the Vado di Corno Fault Zone (section b-b'). The seismic tomography illuminated fault-bounded rock bodies with different velocities and geometries that match with the ones inferred from the structural mapping of the fault zone exposures (section e of the figure).

A general negative correlation between ultrasonic velocity and porosity values was reported. Moreover three dimensional acoustic anisotropy was quantified within the different units with respect to the mapped fault strands, and related to the deformation fabrics (i.e. open fractures, veins) observed at the sample scale. A Vp - Vs seismic refraction tomogra-

phy was then performed in the field along a profile (ca. 90 m) across the fault zone. The tomographic results clearly illuminated fault-bounded rock bodies characterized by different velocities (i.e. elastic properties) and geometries which match with the ones deduced from the structural analysis of the fault zone exposures.

Fracture intensity measurements (both at the sample and outcrop scale) were performed to investigate the scaling relation between laboratory and field measurements. These results were then coupled with ultrasonic velocity vs. confining pressure (0-30 MPa) profiles measured in the laboratory to extrapolate the subsurface velocity structure of the fault zone to larger depths (up to ca. 1 km). The final dataset of physical properties was used to build a three dimensional velocity-elastic model of the Vado di Corno fault zone based on the fault zone structure inferred from the mapping.

This type of studies are extremely relevant to better understand the petrophysical evolution and geophysical expression of active fault zones during the seismic cycle and represent the base for modern and robust fault mechanics models developed both in quasi-static or dynamic rupture scenarios.

Effect of fluid viscosity on fault frictional behavior

C. Cornelio, M. Violay, E. Spagnuolo, G. Di Toro

Fluids play an important role in fault zone and in earthquakes generation. Fluid pressure reduces the normal effective stress, lowering the frictional strength of the fault, potentially triggering earthquake ruptures. Fluid injection induced earthquakes are direct evidence of the effect of fluid pressure on the fault strength. However, the frictional fault strength may also vary due to the chemical and physical characteristics of the fluid as discussed here.

Here we performed two series of experiments on precut samples of Westerly granite to investigate the role of fluid viscosity on fault frictional behavior. In the first series, we performed 20 rotary shear experiments with the machine SHIVA (INGV, Rome) on cylindrical (50 mm external diameter) at slip rate ranging from 10 µm/s to 1 m/s at effective normal stress of 10 MPa and pore pressure varying from 0 (i.e., dry conditions) to 2 MPa. Three different fluid viscosities were tested using pure distilled water (η =1 mPa s), 60% water/40% glycol (η =10.5 mPa s) and 15% water/85% glycol (η =109 mPa s) mixtures (all reported viscosities at 20 °C). In agreement with theoretical argumentations (Stribeck curve) we distinguished three lubrication regimes. At low product of slip-rate per fluid viscosity, steady state friction coefficient (µss) was about 0.7 and independent of both fluid viscosity and velocity (velocity neutral, or boundary lubrication regime). At intermediate products of slip-rate per viscosity, steady state friction coefficient was strongly influenced by both viscosity and slip rate, with µss dropping from ca. 0.7 to 0.2 (velocity weakening or mixed lubrication regime). In this regime, samples underwent stick slip motion. At high product of slip-rate per fluid viscosity, µss slightly increased with increasing slip rate (hydrodynamic lubrication regime).

In the second series of experiments, we reproduced the stick-slip motion of the mixed lubrication regime. To this end, we performed direct shear experiments at 1 MPa effective normal stress, using the same fluids and at 20°C ambient temperature. During stick-slip, the magnitude of the static stress drops were controlled by both normal stress and viscosity. When fluid viscosity was ten time higher (e.g., 60% water/40% glycol mixture vs. pure distilled water), stress drops were 1.5 higher.

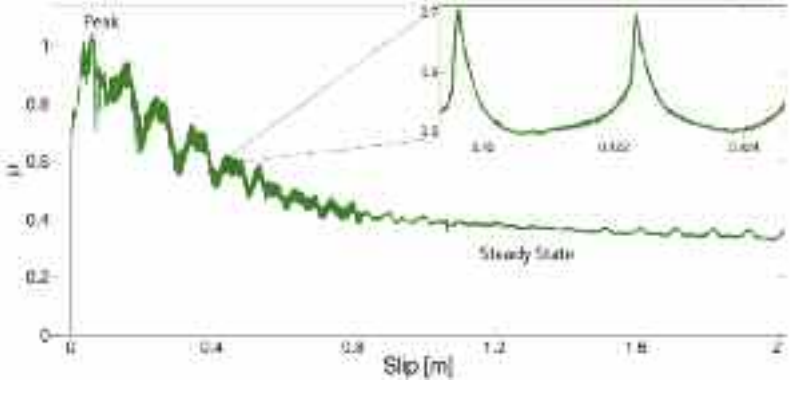

Fig. 1 I Friction coefficient vs slip (s1315) at sliding velocity of 10mm/s. The presence of viscous fluid between two samples of Westerly granite induced stick-slip events.

This complex response of the experimental faults to loading conditions and fluid properties highlights the need for dedicated experiments aimed at uncovering the role of pore fluid physical characteristics on earthquake nucleation and propagation.

Seismic slip on clay nano-foliation

S. Aretusini, O. Plumper, E. Spagnuolo, G. Di Toro

Deformation processes active at seismic slip rates (ca. 1 m/s) on smectite-rich slipping zones are not well understood, although they likely control the mechanical behaviour of: i) subduction zone faults affected by tsunamigenic earthquakes and seismic surface rupturing, and ii) landslide decollements.

Here we present a set of rotary experiments performed on water-dampened 2 mm thick clay-rich (70% wt. smectite and 30% wt. opal) gouge layers sheared at slip rates *V* ranging from 0.01 to 1.5 m/s, for 3 m of displacement under 5 MPa normal stress. Microstructural analyses were conducted on pre- and post-sheared gouges using focused ion beam scanning electron and transmission electron microscopy. Gouges were slip weakening in the first 0.1 m of displacement, with friction coefficient decreasing from 0.4-0.3 to 0.1-0.05. Then, with progressive slip, gouges evolved to slip-strengthening (final friction coefficient of 0.47-0.35) at $V \leq 0.1$ m/s and slip-neutral (final friction of 0.05) at $V=1.5$ m/s. Despite the large difference in the imposed slip rate and frictional behaviour, the slipping zone always consisted of a nano-foliation defined by sub-micrometric smectite crystals wrapping opal grains. The microstructural differences were (1) the thickness of the slipping zone which decreased from 1.5 mm at $V \leq 0.1$ m/s to 0.15 mm at $V=1.5$ m/s, and (2) the structure of the foliated fabric, which was S/C'-type at $V \leq 0.1$ m/s and anastomosing-type at $V=1.5$ m/s. The presence of a similar nano-foliation in all the smectite-rich wet gouges suggests the activation of similar frictional processes, most likely grain boundary and interlayer frictional sliding aided by water films, operating from sub-seismic to seismic strain rates (~$10\text{-}10^4$ s^{-1}). Water films on crystal boundaries and interlayers possibly control the micro- and nano-mechanics of smectite deformation, therefore influencing the bulk frictional behaviour during seismic slip.

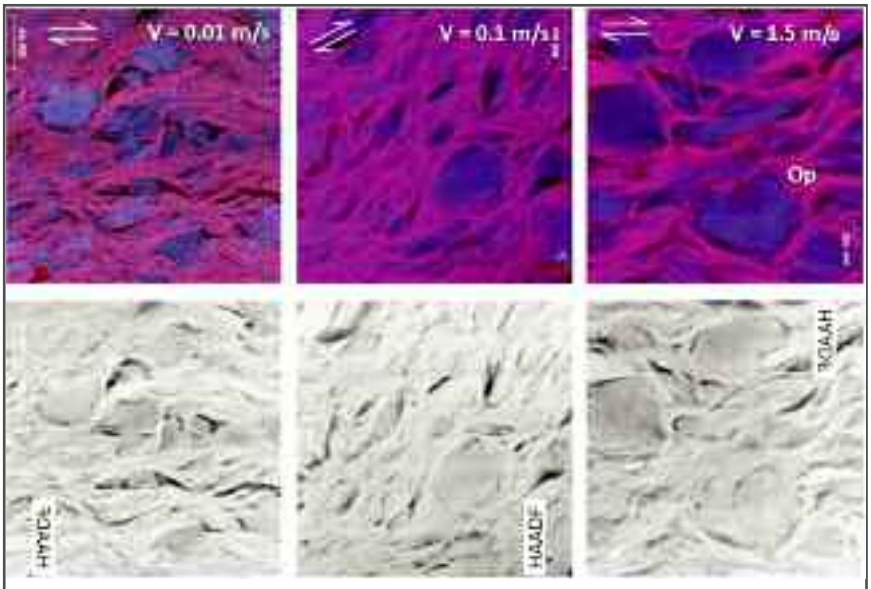

Fig. 1 I Nanofoliation and deformed opals constitute the microfabric of the sheared gouges. The nanofoliation is well-developed at 0.01-0.1 m/s, more irregular at 1.5 m/s.

Transition from aseismic to seismic slip in dolostone-built faults

F. Passelegue, M. Fondriest, A. Nicolas, J. Aubry, A. Schubnel, G. Di Toro

Dolostones are the dominant lithology of the shallow portions of many seismically active regions (e.g., Italian Apennines).Displacement in natural fault zones cutting dolostones and exhumed from < 3-4 km depth is frequently localized on highly reflective (mirror-like) slip surfaces, coated with thin films of nano-granular fault rock. Using saw-cut dolostone samples, we conducted friction experiments under a triaxial configuration simulating natural ambient conditions (confining pressures and temperatures of 30, 60 and 90 MPa at 30, 65 and 100 °C, respectively). Samples were equipped with 14 transducers for acoustic emission recording and localization and wave inversion analysis. At 30 and 65 °C, only slow ruptures (V_r<0.1 m/s) were observed and the experimental faults exhibited ductile behaviour. At 65 °C, a slipstrengthening behaviour was observed after the main slow rupture, leading to a succession of slow ruptures. At T = 100 °C and 30 MPa confining pressure, fault strengthening increased after each rupture, allowing, while the rupture processes remained slow, a sequence of stick-slip events. Instead, at the same ambient temperature but under larger confining pressures (60 and 90 MPa), we observed the transition from slow to fast rupture (V_r>3000 m/s) events, associated to clusters of acoustic activity and dynamic stress drop occurring in few tens of microseconds. In all experiments, mirror-like surfaces and nanoparticles were observed under the scanning electron microscope as a result of slow and fast ruptures. Clearly, mirror-like surfaces and nano powders are not representative of seismic slip events in cohesive dolostones. Instead, the transition from slow to fast ruptures (and generation of acoustic emissions) was related to a flash weakening processes, enhanced at 100° C, which allowed the experimental fault to weaken with slip faster than the rate at which the elastic strain was released from the surrounding medium.

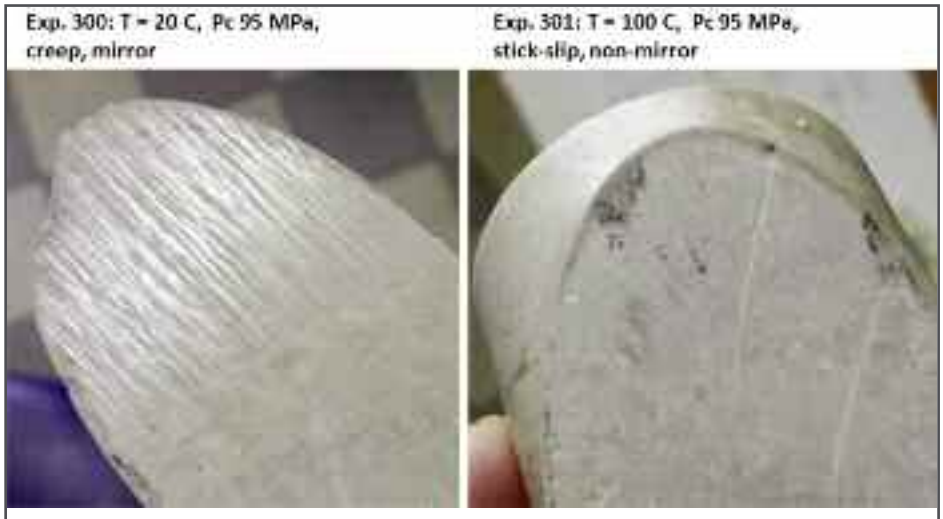

Fig. 1 I In the experiments performed on cohesive dolostones, mirror-like surfaces were produced in the creep events (fault surface to the left). Instead, stick-slip events resulted in the development of more rough surfaces (fault surface to the right).

Crystallographic control on early stages of cataclasis in carbonate fault gouges

M. Demurtas, S.A.F. Smith, M. Fondriest, E. Spagnuolo, G. Di Toro

Carbonates are a recurring lithology in most of active seismic areas worldwide, such as the Apennines (Italy). Here, typical fault products are gouges and cataclasites made of mixtures of carbonate minerals (i.e. calcite and dolomite) that occasionally exhibit a foliation. Natural fault gouges often contain minerals with strong anisotropies, such as cleavage surfaces in phyllosilicates and carbonates. Therefore, the understanding of the role of such anisotropies during shearing is important to develop realistic microphysical models of brittle fragmentation and grain size re-duction. Here we present results of microstructural and coupled EDS-EBSD (Energy Dispersive Spectroscopy – Electron Backscattered Diffraction) analysis on mixtures (50/50wt%) of calcite-dolomite gouges deformed experimentally in a rotary shear apparatus (SHIVA, INGV-Rome) at room temperature under constant normal stress of 17.5 MPa and slip rates of 30 µm/s to 1 m/s. The EDS-EBSD analysis was focused on the gouge layer underlying the slip zone, which has been previously demonstrated to accommodate low finite shear strain during deformation. At all investigated slip rates, calcite develops a crystallographic preferred orientation (CPO) on the (0001) plane, with the c-axis inclined sub-parallel to the principal stress and the [-1-120] direction forming a girdle perpendicular to it.

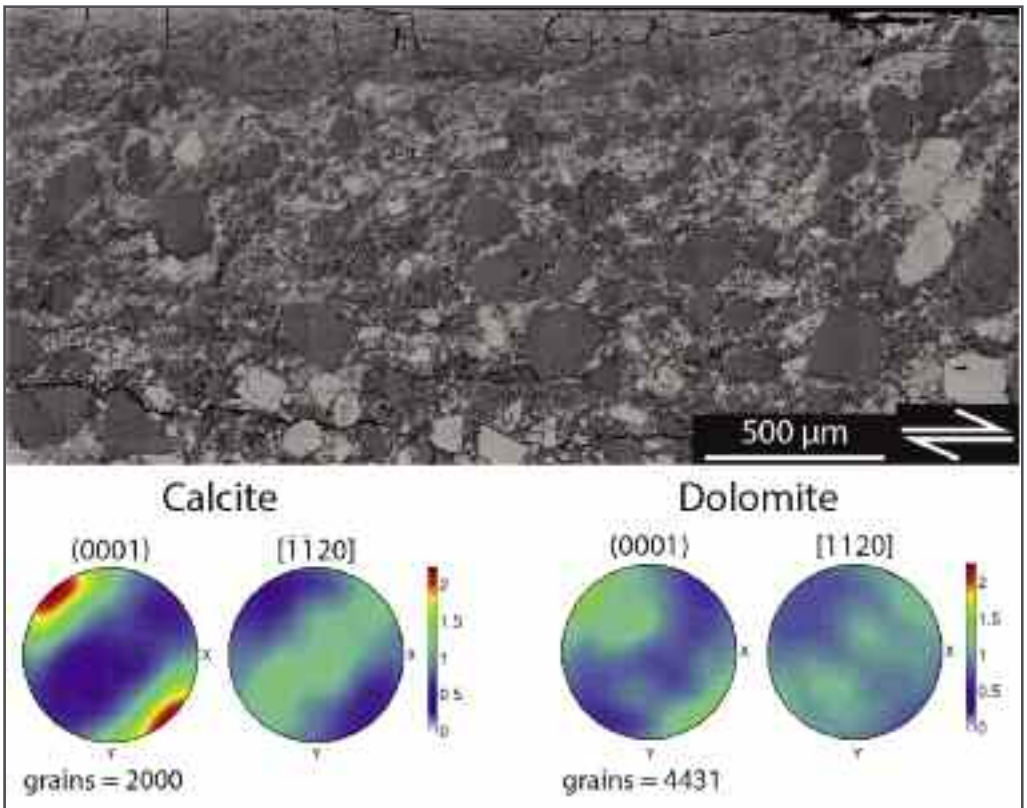

Fig. 1 I Development of a crystallographic preferred orientation (CPO) in the calcite grains during shearing at 1m/s in room humidity conditions, with the CPO is defined by the c-axis perpendicular to it. During this deformation conditions the development of a foliation on gouge is also observed.

Texture strength typically increases with slip rate and appears not to be influenced by the presence of water or foliation development in the gouge during deformation. Misorientation analysis suggests twinning as the principal crystallographic active deformation mechanism. Instead, dolomite grains do not develop a CPO. Microfractures are closely spaced, mainly oriented subparallel to the principal stress and rarely exploit calcite twin planes. The latter typically occur at high angle with respect to fractures, are oriented consistently with the sense of shear and almost orthogonal to the principal stress. Calcite grains commonly exhibit only one twin set. We interpret the development of a CPO in calcite grains in the layer underlying the slip zone as a strain accommodation mechanism of the imposed slip rate (or shear stress) during the early stages of deformation in a granular material (i.e. fault gouge). More intense CPOs at high slip rates (i.e. 1 m/s) may be a consequence of rapid strain localisation on a narrow slip zone, with the fabric in the underlying gouge not experiencing significant changes. Conversely, at low slip rates the gouge volume undergoing protracted deformation is larger and cataclasis progressively weakens the intensity of the texture until the CPO disappears. In conclusion, mineral crystallography plays an important role in the material behaviour during the early deformation stages in carbonate fault gouges. An incorporation of twinning and CPO development as strain accommodation mechanisms with other physico-chemical processes active during the seismic cycle will provide a more complete model of gouge friction and microstructural evolution in carbonate rocks.

Ultra-thin clay layers facilitate seismic slip in carbonate faults

L. Smeraglia, A. Billi, E. Carminati, A. Cavallo, G. Di Toro, E. Spagnuolo, F. Zorzi

Many earthquakes propagate up to the Earth's surface producing surface ruptures. Seismic slip propagation is facilitated by along-fault low dynamic frictional resistance, which is controlled by a number of physico-chemical lubrication mechanisms. In particular, laboratory experiments show that the presence of phyllosilicates within fault gouge is critical for developing dynamic weakening at seismic slip rates. This evidence is crucial for hazard assessment along oceanic subduction zones, where pelagic clays participate to seismic slip propagation. Conversely, the reason why, in continental domains, earthquakes can propagate through high-friction rocks (e.g., limestones or dolostones) up to the Earth's surface is still poorly understood. We propose that, within calcite gouge, ultra-low clay content (≤ 3 wt.%) localized along micrometer-thick layers can facilitate seismic slip propagation during earthquakes in continental domains, possibly enhancing surface displacement. We document the occurrence of micrometer-thick phyllosilicate-bearing layers along a carbonate-hosted seismogenic extensional fault in the central Apennines, Italy. Using friction experiments, we demonstrate that, at seismic slip rates (1 ms $^{-1}$), similar calcite gouges with pre-existing phyllosilicate-bearing (clay content ≤ 3 wt.%) micro-layers weaken faster than calcite gouges or mixed calcite-phyllosilicate gouges.

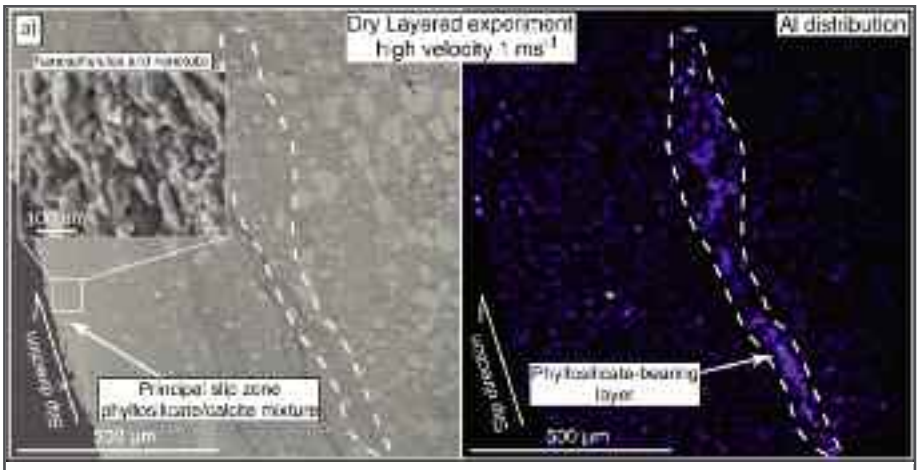

Fig. 1 I Experimental microstructures. Left: FE-SEM image of dry layered gouge experiment sheared at seismic-slip velocity (1 ms^{-1}) showing, toward the principal slip surface, grain size reduction and compaction stronger than wet gouges. Inset shows the nanostructures from the principal slip zone. These structures consist of clumped and chained nanospherules and nanotubes identical to those observed within phyllosilicates along the Tre Monti principal fault. Right: EDS map showing concentration and segregation of phyllosilicates along a micrometer-thick layer.

Preliminary analysis of radon time series before the Ml=6 Amatrice earthquake: possible implications for fluid migration

V. Cannelli, A. Piersanti, E. Spagnuolo, G. Galli

On August 24, 2016, a Ml=6.0 earthquake occurred in Central Apennines, Italy, between the towns of Norcia and Amatrice, causing severe destruction and casualties in a wide area around the epicenter. We present a preliminary analysis of continuous radon concentration data collected from the second half of 2012 to the day after the earthquake by a long term radon monitoring station, installed at Cittareale (Rieti, Italy), about 11 km south-west of the epicenter. We combine the field data analysis with the outcome of dedicated laboratory experiments, aimed to study real time radon emission dynamics from rock samples subject to normal and shear stress loads in absence of fluid transport and migration phenomena. Our results suggest the possibility of a minor role played by phenomena related to fluid migration for the Amatrice seismic event with respect to other recent Apennine earthquakes.

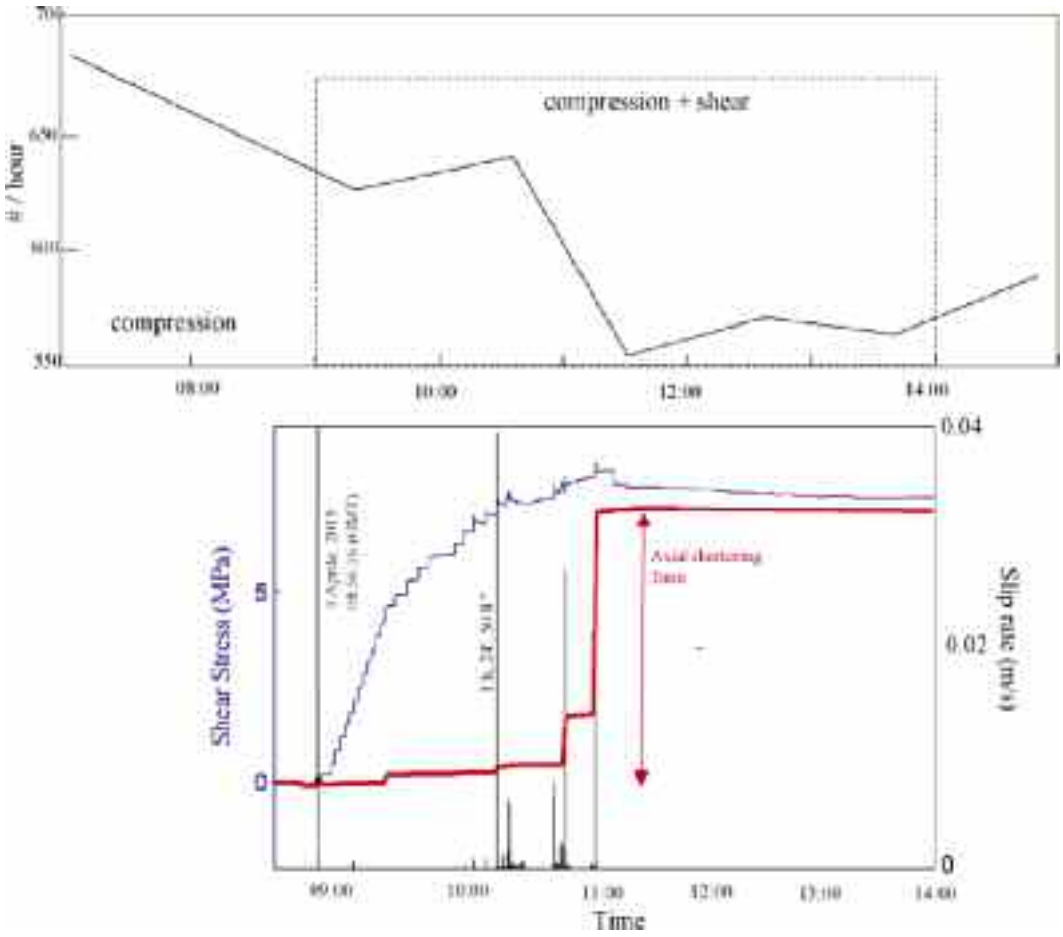

Fig. 1 I Radon variation concentration (top panel) as a function of the shear stress increase (blue solid line, bottom panel) in case of experiment number s1095. The mechanical response of the system made of fault + experimental apparatus is also shown (bottom panel) in terms of slip rate (black solid curve) and axial displacement (shortening, red solid line). The number of radon counts (averaged in counts/hour in top panel) decreases with increasing shear stress at constant normal load (compressive load of 15 MPa) and has a maximum negative slope corresponding to the highest recorded slip pulse with slip-rate of 0.04 m/s. The axial shortening (generally associated to sample grinding and wearing) was of the order of 0.1 mm.

Frictional evolution, acoustic emissions activity, and off-fault damage in simulated faults sheared at seismic slip rates

F. Passelegue, E. Spagnuolo, M. Violay, S. Nielsen, G. Di Toro, A. Schubnel

We present a series of high-velocity friction tests conducted on Westerly granite, using the Slow to HIgh Velocity Apparatus (SHIVA) installed at Istituto Nazionale di Geofisica e Vulcanologia Roma with acoustic emissions (AEs) monitored at high frequency (4 MHz). Both atmospheric humidity and pore fluid (water) pressure conditions were tested, under effective normal stress in the range 5–20 MPa and at target sliding velocities Vs in the range 0.003–3 m/s. Under atmospheric humidity two consecutive friction drops were observed. The first one is related to flash weakening, and the second one to the formation and growth of a continuous layer of melt in the slip zone. In the presence of fluid, a single drop in friction was observed. Average values of fracture energy are independent of effective normal stress and sliding velocity. However, measurements of elastic wave velocities on the sheared samples suggested that larger damage was induced for 0.1 < Vs <0.3 m/s. This observation is supported by AEs recorded during the test, most of which were detected after the initiation of the second friction drop, once the fault surface temperature was high. Some AEs were detected up to a few seconds after the end of the experiments, indicating thermal rather than mechanical cracking. In addition, the presence of pore water delayed the onset of AEs by cooling effects and by reducing of the heat produced, supporting the link between AEs and the production and diffusion of heat during sliding. Using a thermoelastic crack model developed by Fredrich and Wong (1986), we confirm that damage may be induced by heat diffusion. Indeed, our theoretical results predict accurately the amount of shortening and shortening rate, supporting the idea that gouge production and gouge comminution are in fact largely controlled by thermal cracking. Finally, we discuss the contribution of thermal cracking in the seismic energy balance. In fact, while a dichotomy exists in the literature regarding the partitioning between fracture and heat energy, the experimental evidence reported here suggests that both contribute to fault weakening and off-fault damage.

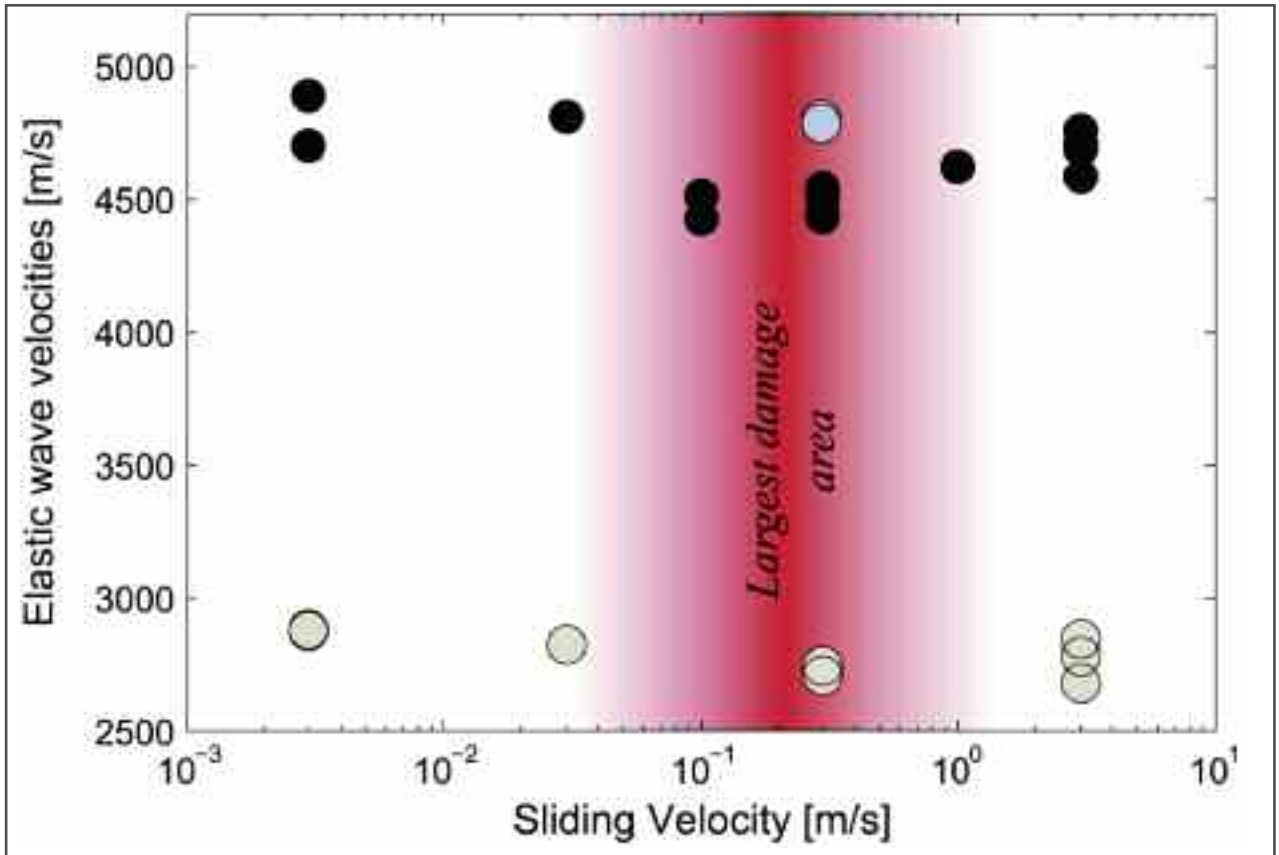

Fig. 1 | Measurements of *P* and *S* wave velocities in postmortem samples as a function of the sliding velocity imposed during each experiment. Black and grey circles correspond, respectively, to *P* and *S* wave velocity measurements. Blue circles correspond to experiments conducted in the presence of water. The red area highlights sliding velocities inducing the highest off-fault damage. The error bars are smaller than the marker's size.

Dislocation Motion and the Microphysics of Flash Heating and Weakening of Faults during Earthquakes

E. Spagnuolo, O. Plümper, M. Violay, A. Cavallo, G. Di Toro

Earthquakes are the result of slip along faults and are due to the decrease of rock frictional strength (dynamic weakening) with increasing slip and slip rate. Friction experiments simulating the abrupt accelerations (>>10 m/s^2), slip rates (~1 m/s), and normal stresses (>>10 MPa) expected at the passage of the earthquake rupture along the front of fault patches, measured large fault dynamic weakening for slip rates larger than a critical velocity of 0.01–0.1 m/s. The dynamic weakening corresponds to a decrease of the friction coefficient (defined as the ratio of shear stress vs. normal stress) up to 40%–50% after few millimetres of slip (flash weakening), almost independently of rock type. The microstructural evolution of the sliding interfaces with slip may yield hints on the microphysical processes responsible for flash weakening. At the microscopic scale, the frictional strength results from the interaction of micro- to nano-scale surface irregularities (asperities) which deform during fault sliding. During flash weakening, the visco-plastic and brittle work on the asperities results in abrupt frictional heating (flash heating) and grain size reduction associated with mechano-chemical reactions (e.g., decarbonation in CO_2-bearing minerals such as calcite and dolomite; dehydration in water-bearing minerals such as clays, serpentine, etc.) and phase transitions (e.g., flash melting in silicate-bearing rocks). However, flash weakening is also associated with grain size reduction down to the nanoscale. Using focused ion beam scanning and transmission electron microscopy, we studied the micro-physical mechanisms associated with flash heating and nanograin formation in carbonate-bearing fault rocks. Experiments were conducted on pre-cut Carrara marble (99.9% calcite) cylinders using a rotary shear apparatus at conditions relevant to seismic rupture propagation. Flash heating and weakening in calcite-bearing rocks is associated with a shock-like stress release due to the migration of fast-moving dislocations and the conversion of their kinetic energy into heat. From a review of the current natural and experimental observations we speculate that this mechanism tested for calcite-bearing rocks, is a general mechanism operating during flash weakening (e.g., also precursory to flash melting in the case of silicate-bearing rocks) for all fault rock types undergoing fast slip acceleration due to the passage of the seismic rupture front.

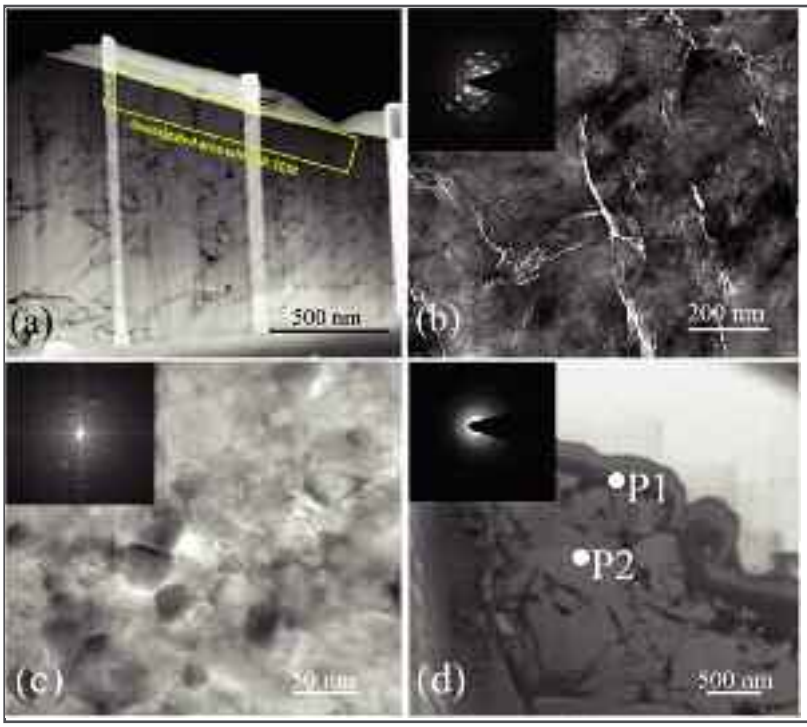

Fig. 1 I Microstructural investigation of deformed cohesive Carrara marble samples. **(a)** Rock volumes immediately below slip surfaces after 1.5 **(a–c)** mm and 5 mm of displacement **(d)**. All images are from FIB-SEM specimens cut perpendicular to the slip surface and perpendicular **(a–c)** and parallel **(d)** to the slip direction. The slip surface is on top, coated with Platinum. **(b)** Inter-cleavage crystal domains exhibit complex TEM diffraction contrast due to a high density of crystal defects, i.e., dislocations. High density of dislocations domains remain either crystallographically coherent or develop a polycrystalline (see SAED pattern) mosaicism nanostructure. **(c)** Numerous nanograins develop within the fracture volumes (bright-field TEM images); **(c)** Deposition of amorphous carbon at 5 mm of slip. P1 is amorphous Carbon from TEM-EDS analyses. P2 is calcite.

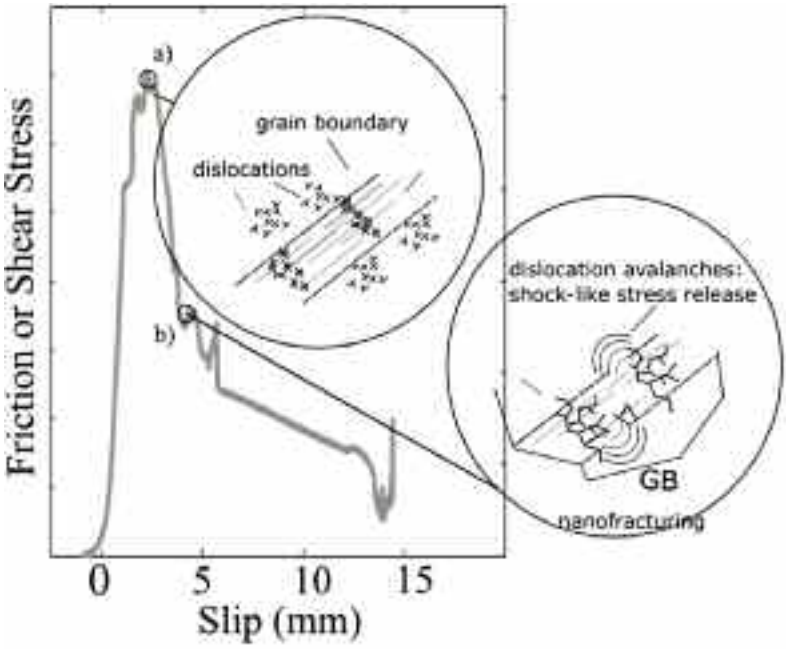

Fig. 2 I Evolution of microstructures and shear stress with slip. At slip initiation (panel **a)**, the asperities are strained: new dislocations are emitted and pile up at microstructural obstacles (e.g., cleavage planes, grain boundaries). With progressive slip (and strain, panel **b)** the stress exerted by the piled-up dislocations overcomes the yield strength of the obstacle and the dislocations are released in "avalanches" causing brittle failure, formation of nano-grains, and temperature increase (flash heating).

Precursory changes in seismic velocity for the spectrum of earthquake failure modes

M.M. Scuderi, C. Marone, E. Tinti, G. Di Stefano, C. Collettini

Temporal changes in seismic velocity during the earthquake cycle have the potential to illuminate physical processes associated with fault weakening and connections between the range of fault slip behaviours including slow earthquakes, tremor and low-frequency earthquakes. Laboratory and theoretical studies predict changes in seismic velocity before earthquake failure; however, tectonic faults fail in a spectrum of modes and little is known about precursors for those modes. Here we show that precursory changes of wave speed occur in laboratory faults for the complete spectrum of failure modes observed for tectonic faults. We systematically altered the stiffness of the loading system to reproduce the transition from slow to fast stick–slip and monitored ultrasonic wave speed during frictional sliding. We find systematic variations of elastic properties during the seismic cycle for both slow and fast earthquakes indicating similar physical mechanisms during rupture nucleation. Our data show that accelerated fault creep causes reduction of seismic velocity and elastic moduli during the preparatory phase preceding failure, which suggests that real-time monitoring of active faults may be a means to detect earthquake precursors (Fig. 1).

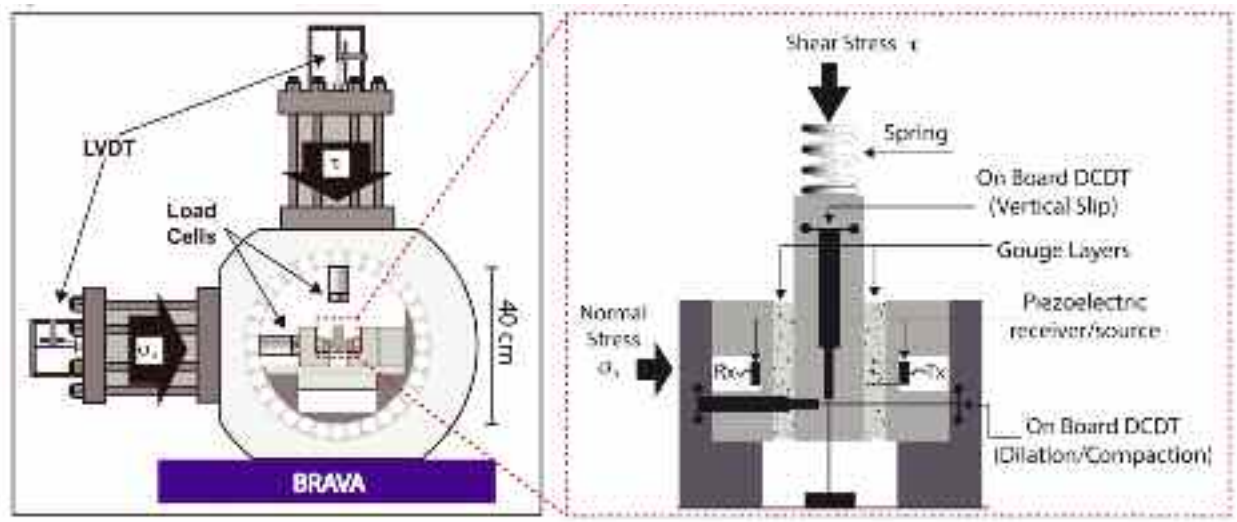

Fig. 1 | In order to develop these types of experiments we have equipped the double direct shear configuration of BRAVA with on-board displacement transducers (direct current displacement transducer) to monitor fault dilation/compaction and true fault slip, PZT_s (T_x and R_x) for elastic wave speed measurements, and a compliant spring positioned in series with the central forcing block of the shear assembly, which is designed to de-stiffen the shear loading system.

The role of fluid pressure in induced vs. triggered seismicity: insights from rock deformation experiments on carbonates

M.M. Scuderi, C. Collettini

Fluid overpressure is one of the primary mechanisms for tectonic fault slip, because fluids lubricate the fault and fluid pressure reduces the effective normal stress that holds the fault in place. However, current models of earthquake nucleation, based on rate- and state- friction laws, imply that stable sliding is favoured by the increase of porefluid pressure. Despite this controversy, currently, there are only a few studies on the role of fluid pressure under controlled, laboratory conditions. Here, we use laboratory experiments, to show that the rate- and state- friction parameters do change with increasing fluid pressure. We tested carbonate gouges from sub hydrostatic to near lithostaticfluid pressure conditions, and show that the friction rate parameter (a – b) evolves from velocity strengtheningto velocity neutral behaviour. Furthermore, the critical slip distance, Dc, decreases from about 90 to 10 μm. Our data suggest that fluid overpressure plays an important role in controlling the mode of fault slip. Since fault rheology and fault stability parameters change withfluid pressure, we suggest that a comprehensive characterization of these parameters is fundamental for better assessing the role of fluid pressure in natural and human induced earthquakes (Fig. 1).

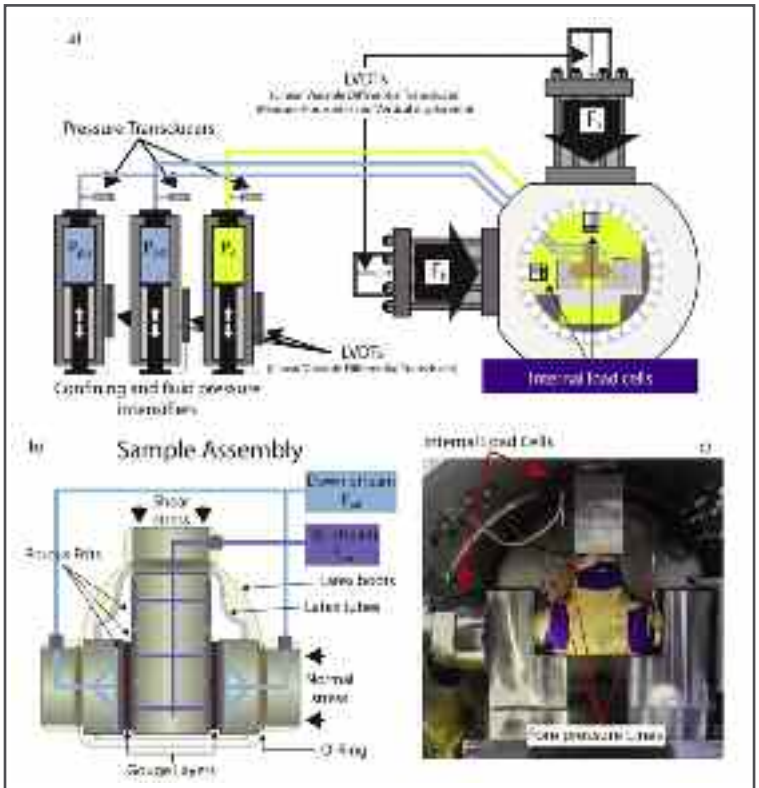

Fig. 1 | To develop this research we have used the double direct shear configuration of BRAVA within the pressure vessel. (a) Two intensifiers are used to pressurize fluid (Ppu, Ppd) and one for confining pressure (Pc). (b) Details of the sample assembly in the double direct shear configuration. (c) Initial set-up showing the jacketed sample assembly with pore fluid pressure tubing and the internal load cells within the pressure vessel.

On the evolution of elastic properties during laboratory stick-slip experiments spanning the transition from slow slip to dynamic rupture

E. Tinti, M.M. Scuderi, L. Scognamiglio, G. Di Stefano, C. Marone, C. Collettini

The physical mechanisms governing slow earthquakes remain unknown, as does the relationship between slow and regular earthquakes. To investigate the mechanism(s) of slow earthquakes and related quasi-dynamic modes of fault slip we performed laboratory experiments on simulated fault gouge in the double direct shear configuration. We reproduced the full spectrum of slip behavior, from slow to fast stick-slip, by altering the elastic stiffness of the loading apparatus (k) to match the critical rheologic stiffness of fault gouge (kc). Our experiments show an evolution from stable sliding, when k>kc, to quasi-dynamic transients when k~kc, to dynamic instabilities when k<kc. To evaluate the micro-physical processes of fault weakening we monitored variations of elastic properties. We find systematic changes in P-wave velocity (Vp) for laboratory seismic cycles. During the coseismic stress drop, seismic velocity drops abruptly, consistent with observations on natural faults. In the preparatory phase preceding failure, we find that accelerated fault creep causes a Vp reduction for the complete spectrum of slip behaviors. Our results suggest that the mechanics of slow and fast ruptures share key features and that they can occur on same faults, depending on frictional properties. In agreement with seismic surveys on tectonic faults our data show that their state of stress can be monitored by Vp changes during the seismic cycle. The observed reduction in Vp during the earthquake preparatory phase suggests that if similar mechanisms are confirmed in nature high resolution monitoring of fault zone properties may be a promising avenue for reliable detection of earthquake precursors.

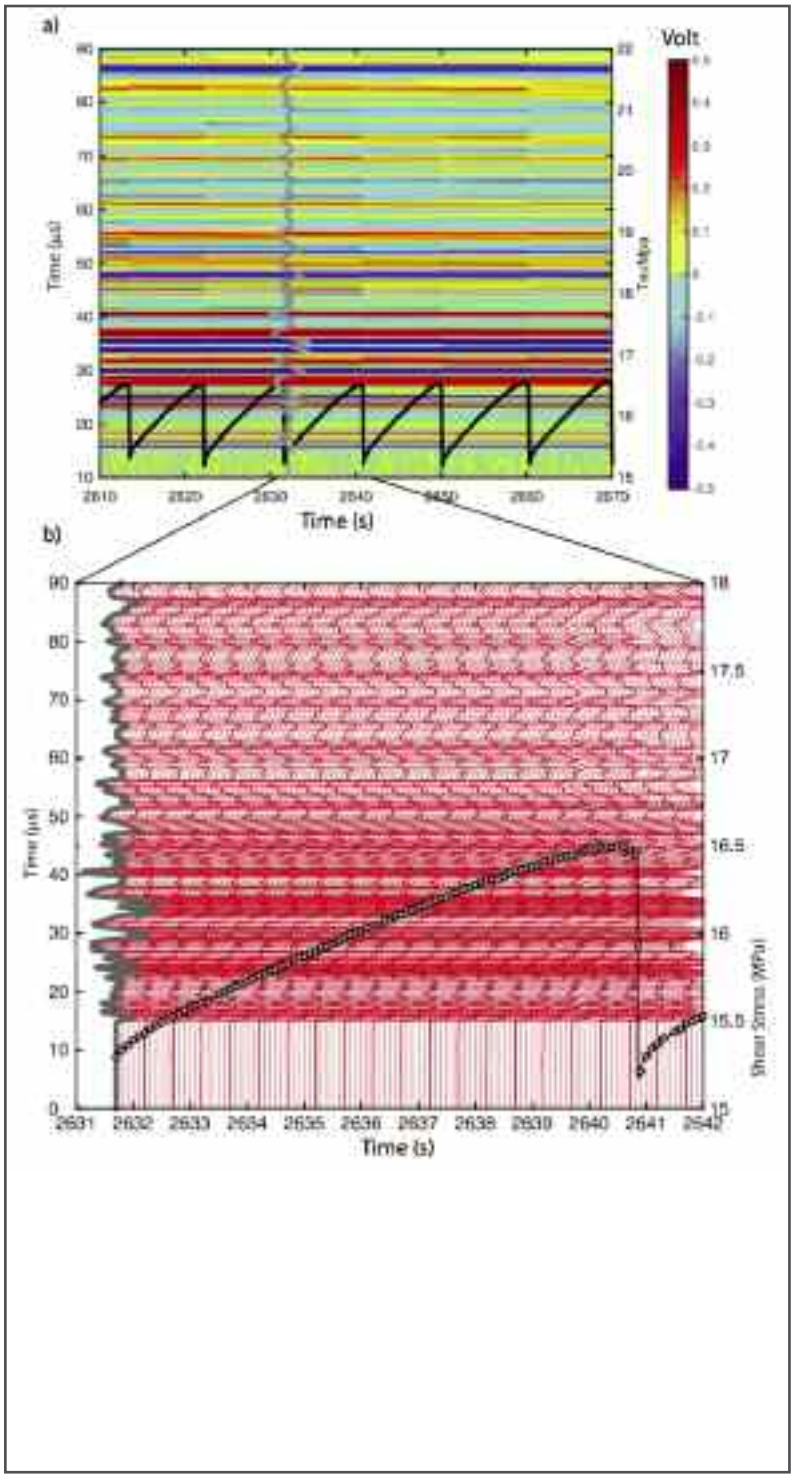

Fig. 1 | **(a)** Black curve shows shear stress for stick-slip cycles in a portion of a representative experiment. Background color represents the acoustic wave amplitude as a function of time (left hand y-axis) from continuous records (with scale in Volts). A typical waveform is shown in gray. **(b)** Zoom on a single stick-slip event showing the master waveform in gray at the beginning of the cycle and all the other seismograms in red. The circles on the shear stress curve represent the point at which a waveform was transmitted. For clarity we plotted only one tenth of the waveforms, which were recorded at 100Hz.

Is fault surface roughness indicative of fault mechanisms? Observations from experimental Limestone faults

A. Sagy, T. Tesei, C. Collettini

Geometrical irregularity of contacting surfaces is a fundamental factor controlling friction and energy dissipation during sliding.

We performed direct shear experiments on 20x20 cm limestone surfaces by applying constant normal load (40-200 kN) and sliding velocity 1-300 µm/s. Before shearing, the surfaces were polished with maximal measured amplitudes of less than 0.1 mm. After shear, elongated islands of shear zones are observed, characterized by grooves ploughed into the limestone surfaces and by layers of fine grain wear. These structures indicate that the contact areas during shear are scattered and occupy a limited portion of the entire surface area.

The surfaces was scanned by a laser profilometer that measures topography using 640 parallel beams in a single run, offer up to ~10 µm accuracy and working ranges of 200 mm. Two distinctive types of topographical end members are defined: rough wavy sections and smooth polished ones. The rough zones display ridges with typical amplitudes of 0.1-1 mm that cross the grooves perpendicular to the slip direction. These features are associated with penetrative brittle damage and with fragmentation. The smoother zones display reflective mirror-like surfaces bordered by topographical sharp steps at heights of 0.3-0.5 mm. These sections are localized inside the wear layer or between the wear layer and the host rock, and are not associated with observed penetrative damage.

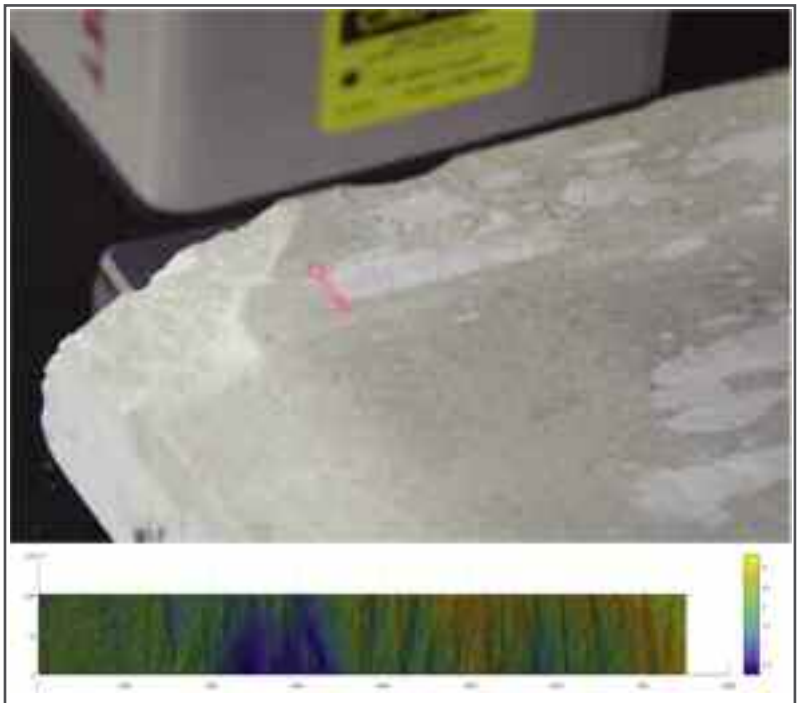

Fig. 1 I Laser scanning and topographic map of an experimental fault groove.

Preliminary statistical analysis suggests that the roughness of the ridges zones can be characterized using a power-low relationship between profile length and mean roughness, with relatively high values of Hurstex ponents (e.g. $H > 0.65$) parallel to the slip direction. The polished zones, on the other hand, corresponded to lower values of Hurstex ponents (e.g. $H \leq 0.6$).

Both structural and roughness measurements indicate that the distinctive topographic variations on the surfaces reflect competing mechanical processes which

occur simultaneously during shear. The wavy ridged zone is the surface expression of penetrative cracking and fragmentation which widen the shear zone, while the smooth zones reflect localized flow and plastic deformation of the wear material. The similarity in topography of shear structures between experimental and natural faults suggests similar mechanical processes.

Weakness of Serpentine minerals revealed by friction experiments under low and high temperature conditions

T. Tesei, C. Harbord, N. De Paola, C. Viti , C. Collettini, P. Scarlato

Serpentines are important constituents of fault rocks and mélanges in a large variety of tectonic settings, including some major plate-boundary structures such as the San Andreas fault. Many of these structures are considered frictionally weak on geological and geophysical basis (i.e. μ<<0.6). However, previous studies report that the strength of serpentines is not low enough to explain such fault weakness, with the possible exception of chrysotileat room T. Instead, the presence of talc, clays and elevated fluid pressures is commonly invoked to solve the "weak fault" conundrum.

Here we report the frictional strength of mineralogically-controlled gouges of serpentine (lizardite, chrysotile/polygonal serpentine and antigorite) under both room and hydrothermal conditions (T up to 170 C°). Experiments were performed in direct shear configuration using a biaxial machine (HP-HT Laboratory, INGV Rome, Italy) and a triaxial apparatus with an external furnace (Rock Mechanics Laboratory, Durham University, UK).

The sliding strength of lizardite and chrisotile/polygonal (the typical association in retrograde serpentinites and in several natural shear zones) is lower than previously reported (μ<0.2) and scarcely affected by temperature changes for T<200° (Fig. 1). Interestingly, these results are in agreement with the fault strength inferred for the central segment of the San Andreas fault where abundant serpentinites are present.

Our observations, together with field evidence from natural shear zones, suggest that serpentine-rich faults may significantly contribute to the weakness of major faults throughout the brittle uppercrust.

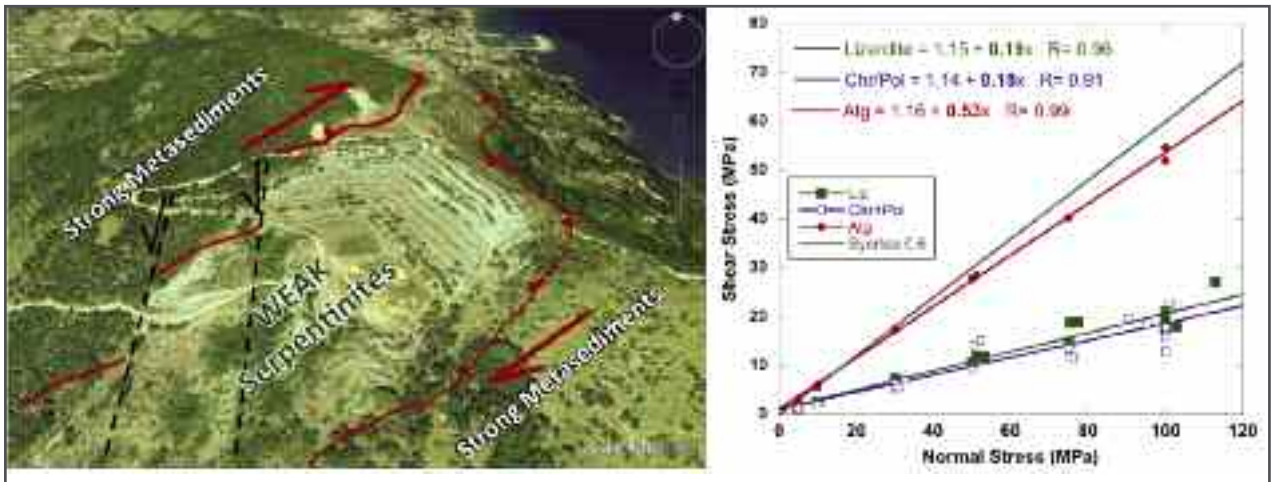

Fig. 1 | **a)** Satellite view of the Monte Fico ophiolitic shear zone. **b)** results of friction experiments showing Chrysotile and Lizardite low friction with respect to Antigorite and other typical crustal rocks (Byerlee friction).

Fault geometry and mechanics of marly carbonate multilayers: an integrated field and laboratory study from the Northern Apennines, Italy

C. Giorgetti, C. Collettini, M.M. Scuderi, M.R. Barchi, T. Tesei

Sealing layers are often represented by sedimentary sequences characterized by alternating strong, e.g. calcite-rich, and weak, clay-rich, lithologies. When involved in faulting processes, these mechanically heterogeneous multilayers develop complex fault geometries. Here we investigate fault initiation and evolution within a mechanical multilayer integrating field observations and rock deformation experiments. Outcropping faults initiate with a staircase trajectory that partially reflects the mechanical properties of the involved lithologies, as suggested by our deformation experiments (Fig. 1). However, some low angles of fault initiation in calcite-rich layers (θi = 5°-20°; Fig. 1a) and high angles in clay-rich layers (θi = 45°-86°; Fig. 1a) indicate the important role played by structural inheritance at the onset of faulting. With increasing displacement, faults develop a well-organized fault core characterized by a marly, foliated matrix embedding fragments of limestone. The angles of fault reactivation, which concentrate between 30° and 60° (Fig. 1a), are consistent with the low friction coefficients measured during our experiments on marls (μ_s = 0.39; Fig. 1c), indicating that clay minerals exert a main control on fault mechanics. Moreover, our integrated analysis suggests that fracturing and faulting are the main mechanisms allowing fluid circulation within the low-permeability multilayer, and that its sealing integrity can be compromised only by the activity of larger faults cutting across its entire thickness.

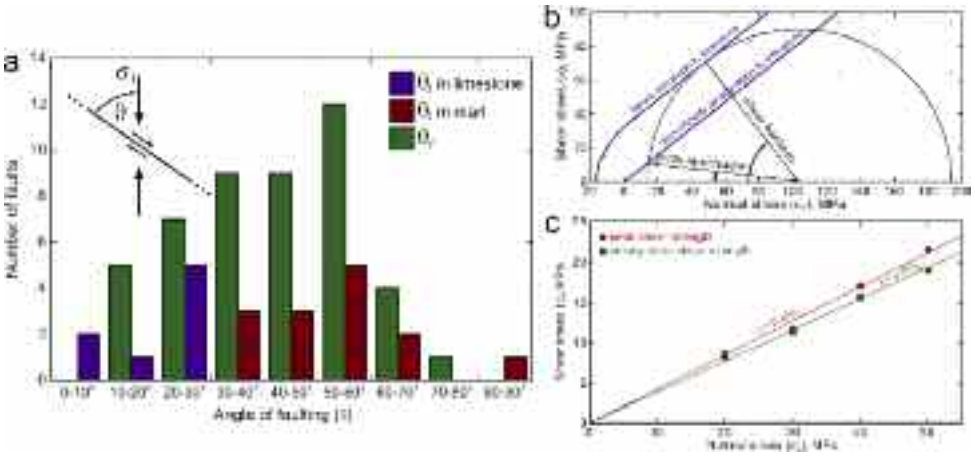

Fig. 1 | **a)** Frequency histograms showing the distribution of θi and θr angles.θi values are small in competent limestone layers, ranging from 5° to 28°, and large in incompetent marly layers, ranging from 32° to 86°. θr values show a bell-shaped distribution with values ranging between θr = 17° and θr = 72°, mostly concentrated between θr = 30° and θr = 60°. **b)** Failure envelope in limestone obtained from triaxial experiments. In competent layers, the initiation of faults with θi of ~26° and the reactivation of pre-existing surfaces with θr between 3° and 48° can simultaneously occur. **c)** Shear stress at peak and steady-state plotted against normal stress. The envelope of peak shear stresses results in friction μi = 0.42, whereas the envelope of steady-state stresses results in lower friction μs = 0.39.

8.3 TECHNOLOGY

Oil temperature control system for conducting long duration experiments with BRAVA

G. Di Stefano, M.M. Scuderi, C. Giorgetti, C. Collettini, T. Tesei

In some rock mechanics test it is required a long experimental time, this is especially during rock deformation test that involve fluid saturation and permeability measurements. It is known that low porosity fault rocks, with permeability below $10^{-18}m^2$, require long time to saturate and to measure the resulting permeability after sheared. However, it is important to understand the hydrological properties of such rocks because they are commonly found along seismogenic fault zone and in many cases they can potentially influence fault slip behaviour. In order to perform experiments capable to: 1) saturate low permeability porous fault rock and measure the permeability of samples that have this parameter very low, and 2) perform experiments at a very slow deformation rate (< 0.1 µm/s), with maximum displacement about 20mm, we have equipped the BRAVA with a safety switch to avoid the breakage of the apparatus due to high oil temperature.

The figure 1 summarizes the BRAVA hydraulic circuit. Two axial pistons pumps connected to different forward pipelines power the apparatus. The main pump provides oil pressurized (220bar) to move two piston cylinder (not showed)

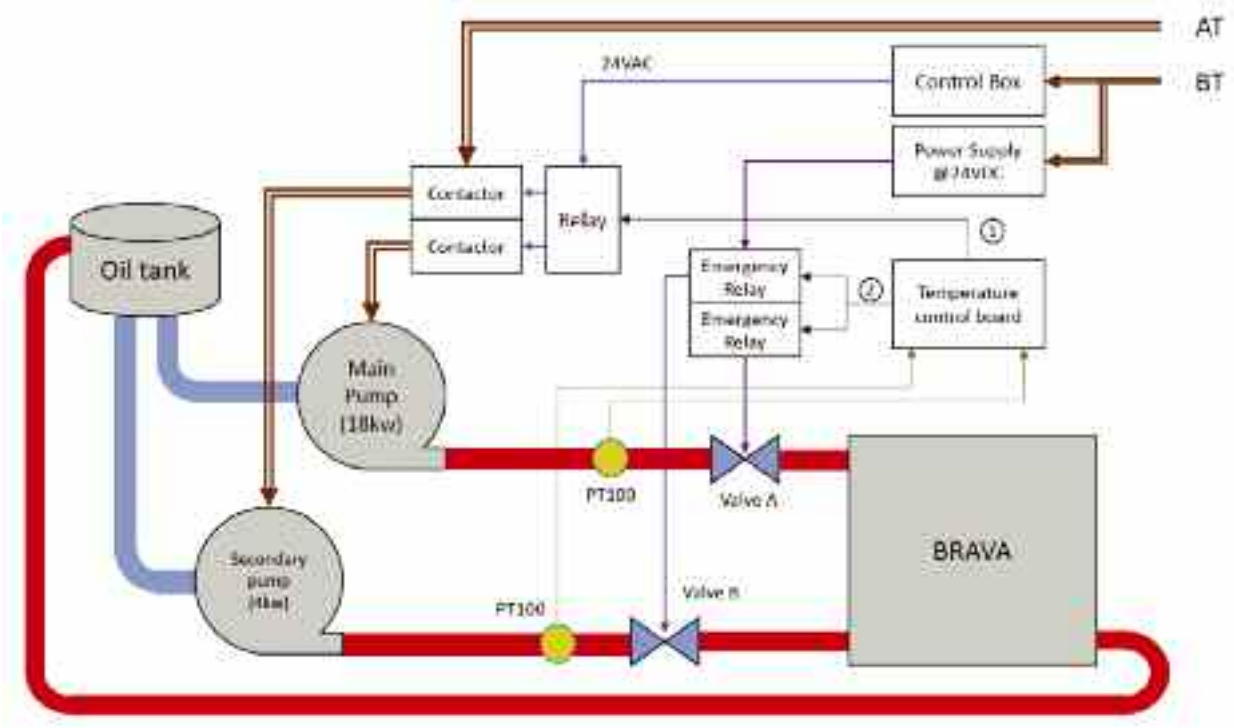

Fig. 1 I Sketch of the hydraulic circuit of the BRAVA and the temperature controlling system. Two PT100 sensors measure the temperatures of the pressurized oil into the forward pipelines. When an alarm happens, the system switch off the relay before and then disables the emergency relays of the valves avoiding the pressure jump.

positioned orthogonally, which operate in biaxial configuration to generate normal and shear stress on a 50x50mm simulated fault gauge. At the same time, the secondary pump provide soil pressurized (160bar) to drive three pistons used to apply confining pressure and up- and down- pore fluid pressure and fluid flow to the sample.

A chiller installed near the pumps keeps the oil temperature inside the tank below the operating value, in order to guarantee the normal compressibility module and viscosity of the pressurized mineral oil and therefore the proper functioning of some hydraulic components. For long experiments (more than one day), especially during the summer, it is very important to keep the chiller continually operative to guarantee that this temperature not exceed the nominal values. However, this does not safe as it has done in few times.

The temperature control system, here presented, checks the temperature of the pressurized oil and stops the pumps, and the experiments, if anomalies occurs in the cooling system. The temperature control system consists of a micro-controller (PIC16F877), two 4-20mA output traducer with PT100 temperature sensors and two actuators (one relay and one opt-isolated switch) to cut electricity supply to the pumps and valves. During an experiment, the micro-controller read the temperatures of the oil pressurized in both forward pipelines that supply the pistons cylinders. When one or both temperatures cross the first threshold value for N times (N is a configurable parameter), the control system goes in pre-alarmed status (green led on). If the temperature keep increasing, a “trend” counter increases its value, otherwise if the temperature goes down, it decreases it value. If the temperature exceeds the second threshold, the micro-controller enable the alarm status (red led on), then disables the relay, for three times, cutting the current to the contactors coil of the pumps. After a short relaxation phase of the pistons cylinders (about one minute late), the controller switches off the valves A and B avoiding pressure jump.

FTIR spectrometer for continuous monitoring of the gas emission from the ETNA craters

A. La Spina, R. Maugeri, G. Di Stefano, G. Salerno, M. Mari, G. Riccobono

This activity represents a framework of "Vulcamed" project. The goal of this work is to development a remote controlled system with FTIR open-path spectrometer, and the installation inside the shelter in the Montagnola site (ETNA volcano). Using a FTIR methodology is possible to detect the main gases components (H_2O, CO_2, SO_2, HCl, HF, CO e OCS) released during degassing activity of the craters. By a spectral analysis is possible to characterize the volatile gaseous components emitted during an eruption. The analysis is been conducted using a simulated absorbing spectrum model of the gases and considering the atmospheric and volcanic parameters.

The system (Fig. 1) consists of a FTIR open-path spectrometer (EM27 Bruker) (1), a tracking mirror (2) and a small camera (3). Through a thermally controlled porthole (4) realized on the north side of the shelter, the spectrometer looks the summit craters of the volcano. The moving mirror remotely controlled can change the path of the spectrometer for performing the scanning of the upper craters. The mirror is on a mobile platform, motorized in azimuth and elevation by two step-motors. Before of the spectrum measurement process, the removable small camera is in front of the FTIR aperture. The camera allows: 1) to transfer a vision of the eruptive scenarios and typology of the eruptive activity; 2) to have a correct alignment of the FOV of the spectrometer on a particular target of the place of eruption in order to guarantee that maximum incident radiation maximizes the signal-noise ratio of the spectrometer. An Arduino board controls the thermalization process of the porthole, the movements of azimuth and elevation of the mirror and the camera positioning through a RC servomotor. At the same times, the Arduino board receives commands from a main PC through a serial bus RS232, installed inside the shelter, which is continually linked to the INGV Etna Observatory. A Raspberry board acquires the camera image and video. It is based on an OmniVision OV5647 sensor of 5Mpixel, can generate video up to 30 frame/s, and pictures 2592 x 1944 pixel.

Fig. 1 | **Left side:** The complete system installed inside facility shelter on the Montagnola site. **1)** The spectrometer FTIR EM27; **2)** tracking mirror; **3)** camera; **4)** thermos-controlled porthole. **Right side**: View of the upper craters from the window.

The development of the system is been conducted by a collaboration of three INGV laboratory. The electronic parts and the software for the remote controlling of the system is been developed at the INGV of Catania. The mechanical design, the realization of the tracking system with assembling of some electronic components to control the mirror movement are been made in the NTS laboratory. The main chassis of the system and the flange of the porthole are been realized at the mechanic workshop of INGV (Palermo).

A preliminary attitude and control system for stratospheric payloads

G. Romeo, A. Iarocci

LNTS is involved, along with the Physics Department of La Sapienza University, in the PNRA project Winter long duration stratospheric balloons from Polar regions. A new opportunity for astronomy, cosmology, physics and atmospheric observations is the possibility to fly stratospheric payloads at 30 – 40 km of altitude during the polar night. The absence of solar irradiation for long periods, and the extremely low temperature and stable environment of the winter stratosphere represent ideal environmental conditions for astronomical measurements.

At this preliminary stage of the project LNTS provides the Flight Controller board of the payload, the CRIUS All In One PRO unit, based on Arduino platform. In particular LNTS is involved in the development and design of the software that must be uploaded in the CRIUS unit. This is necessary to obtain flight data acquisition coming from the sensors present on the board:

- Inertial Measurement Unit (accelerometers, gyroscopes);
- Magnetometer;
- Altimeter sensor;
- Temperature sensors (internal and external).

The system performs the data log on external SD memory. Then sends it by a serial communication link to the Iridium SBD board, that in turn sends data to the ground station via the Iridium satellite network.

A first test launch is scheduled for early January 2017 from Svalbard Islands, Arctic Circle.

In a following step LNTS will equip the payload of a complete attitude control system, capable of varying the rotation speed of the payload.

Fig. 1 I Integration and assembly of the payload.

Fig. 2 I The CRIUS unit with the SD card.

LiPo battery tester

G. Romeo, G. Spinelli

With a specific energy of more than 200 Wh/kg LiPo batteries represent the usual way to power drones. Unlike ordinary fuel, you cannot establish the amount of energy available just weighting or looking. The common relationship between voltage and energy works only for battery packs in pretty good shape, and using a doubtful battery pack may result in crashes and severe equipment damage. The only way to be sure a battery will supply the energy required is to have it recently checked under operative condition. The LuSi Drone (a specially equipped s800) uses a couple of 6s batteries and consumes, just for hovering, 800 W. A significant operative test must be performed by providing a power constant load, while monitoring every cell comportment until the complete discharge. A programmable electronic load has been built on this purpose. It will allow constant power or constant current discharge, measures and records the state of every cell while discharging and will compute the energy supplied by the battery during the discharging cycle. Although the instrument is still under construction, it's already able to perform some tests. Figure. 1 shows the voltage time diagrams obtained by an used battery with a 300 W (constant power) load. On the right the instrument during the assembly.

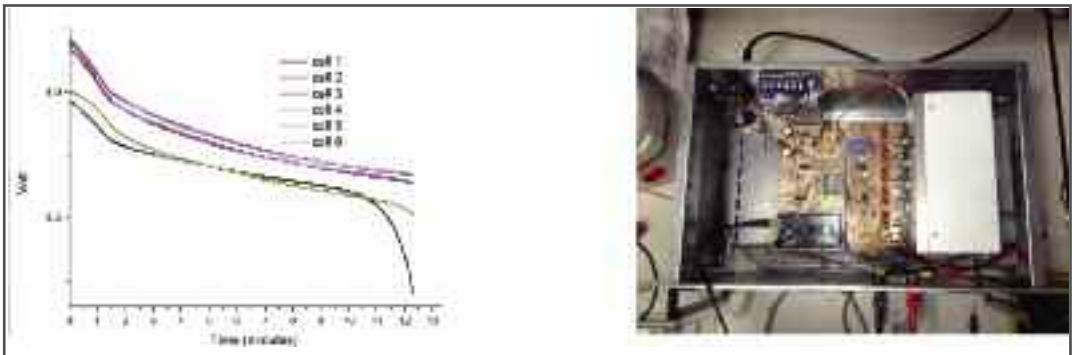

Fig. 1 I Left: the voltage diagram of a 6s 5Ah Li Poly battery charged with a 300 W (constant-power) load. The energy supplied by the battery is limited by the cell 1 that reached the cut off level after 12 minutes. On the right a look of the instrument hardware.

Deep mud sampler

G. Romeo, M. Mari

Designed in the LusiLab frame work this device will allow to sample the mud deep into the LuSi crater. It is mainly made of stainless steel, and can operate until 250°C and 250 bars.

The working principle id shown in fig 1. A hermetic chamber is filled with some inert gas (i.e. nitrogen) and the movable cover is kept in position by the gas pressure. When the external pressure (hydrostatic mud pressure) exceeds the gas pressure, the cover opens, allowing the mud to enter and the gas (lower density) to exit. The force of the spring is negligible, respect to the forces operating in the device, but is enough to close the movable cover after the reaching of the equilibrium.

The use of the gas allows to simply tuning the operating pressure, just regulating the gas pressure. The pressure of commercially available nitrogen cylinders is about 200 atm, corresponding to (assuming a mud density of 5kg/dm**3) 400 meters deepness. Fig 1 shows the working principle (left) and the prototype under construction (right).

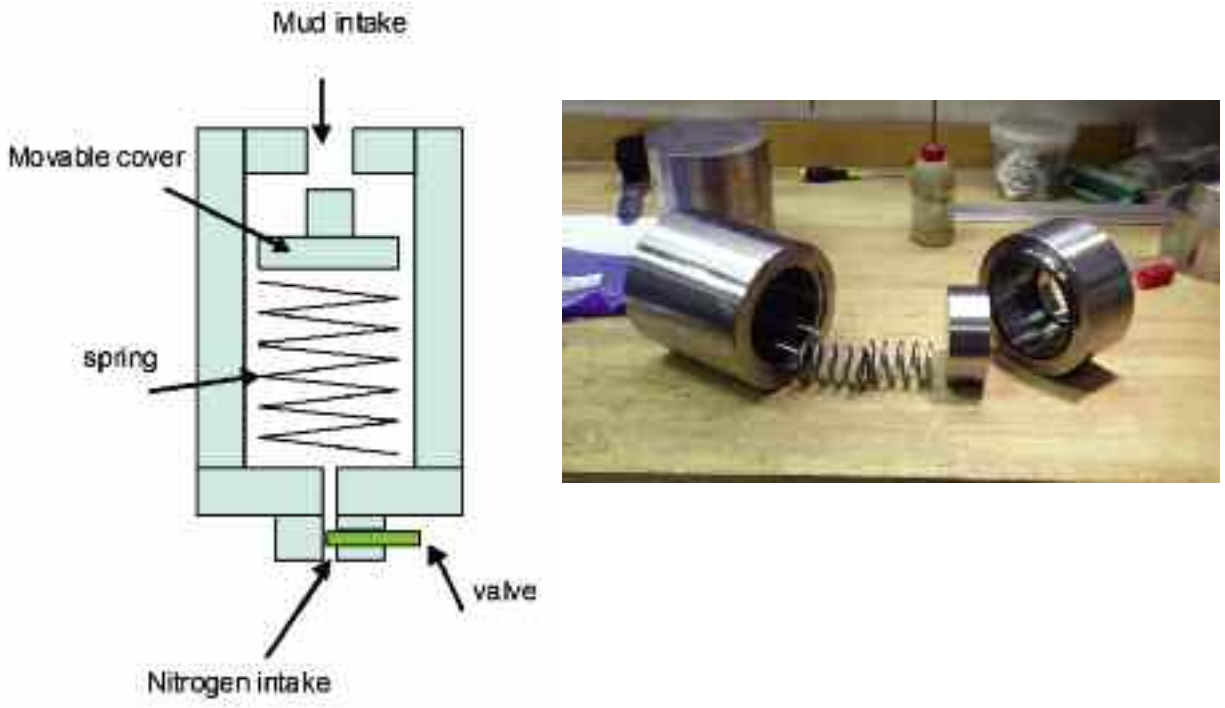

Fig. 1 I **Left**, the deep mud sampler principle (see text). **Right**, the sampler under construction.

Dronable mud sampler

G. Romeo, M. Mari, G. Di Stefano

Developed in the LusiLab frame work this simple mechanical device, suitable for drone use, can collect samples of soil (in particular viscous mud) even in harsh environment. The device is designed to be suspended by a wire that can be connected directly to the drone or to de drone winch (see 2015 annual report). As the device touches the ground a spring is freed and causes the sampler jaw to close (Fig. 1)

The sampler was constructed from Teflon, aluminium and stainless steel, and can be used up to 250 °C. Figure 2 shows its physical aspect (left), and after a drone flight (right).

Fig. 1 I The mud sampler closing sequence: **1)** shows the sampler armed and ready. When the feeler touches the soil surface **2)** the jaw clamp releases the jaw operating the sampling **(3 and 4)**.

Fig. 2 I **left**: the sampler on the worktable, and **right:** after operating it with a drone flight.

A payload for temperature measurements in harsh environments

A. Iarocci, G. Romeo

Contactless temperature measurements, the easiest way to perform measurements using a drone, are heavily affected by errors induced by water vapour. This is the case of the LuSi surface, where contact measurements are mandatory to have the ground truth to allow correcting IR measurements.

The instrument described, designed to be operated with the drone's winch, records temperature (using a digital thermometer), the position (using a built-in GPS) and stores data locally (using a SD card).

The instrument is designed to carry mud temperature measurements close to the crater, where temperatures can reach up to 100 ° C. The measurements that will be obtained will be crucial for studying the mud emissivity of the volcano.

The system (fig. 1) is composed of:

- microprocessor (Arduino PRO mini);
- GPS receiver ;
- temperature sensor;
- SD memory card.

Future developments will provide that when the payload comes back to the ground station, the operator can directly download data and recharge the batteries through the same connector where is normally plugged the temperature sensor.

In fig. 1 a shot of the prototype realized with the 3D-printer (PLA material). In the final version the payload will be made of Teflon® to withstand high temperatures.

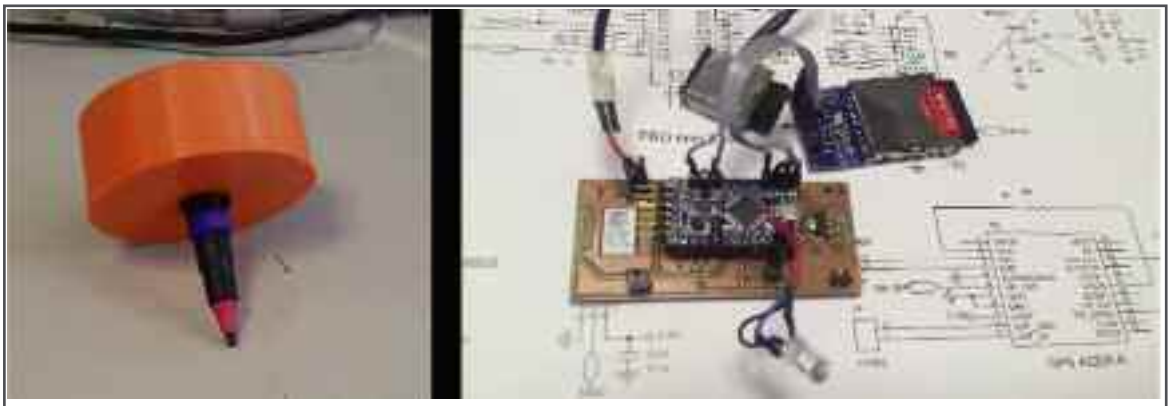

Fig. 1 I On the left a prototype (3D-printed) of the payload. On the right the electronics inside the case.

Machine shop activity

M. Mari

Although it cannot be counted as research work, the machine shop work is essential to the conduct of all experimental investigations. Moreover the machine shop is the reference facility for the whole INGV Rome site, and performs several machining on request. Usually the machining average is of 1000 machining per year (from consumable for physics rocks experiments to more complex dedicated parts). Figures 1 and 2 show some parts (mud sampler and amagnetic pedestal for declination-inclination magnetometers).

Fig. 1 I Mud sampler

Fig. 2 I Amagnetic pedestal for declination-inclination magnetometers.

Test system for comparison of seismic digitizers performance

G. Romeo, F. Pongetti, M. Tozzi

INGV uses many different models of digitizing systems to acquire analog signal seismometers (a / d), for earthquake monitoring and seismic research purposes. Measuring the performance of these devices allows different models to be compared and to choose the best, often with significant cost savings. The performance of seismic digitizers are typically very high (resolution> 24 bit, dynamic range> 140 dB, noise about 1 LSB, sampling 100 to 1000 sps, etc.) and difficult to check with common laboratory instrumentation. We have designed and experimented a custom test system and we have compared the following seismic a/d : Nanometrics (1388503-R01), INGV-Gibilmanna (OBS- BB), Reftek (130-01 / 3 or 01/6), Quanterra (Q330HR), INGV-Roma (GAIA2). The main measured parameters chosen to measure and compare the a/d quality are: linearity, harmonic distortion, noise, temperature stability and others, derivable from these primary measurements.

Fig. 1 I Precision analog ramp-generator and differential driver for seismic digitizers testing.

For linearity evaluation it was designed a high quality analog-ramp signal-generator capable of driving all the a/d under test simultaneously (Fig. 1). To achieve maximum linearity the ramp is generated charging a capacitor by a constant current and compensating the electronic circuit errors. The measurements carried out by this tool show that it must be further improved to obtain precision results in absolute measurements, while it is currently useful for comparative tests (Fig. 2 - A, C). The electronic noise of the a/d was evaluated by measurements taken with short-circuited inputs during long time-intervals in order to assess also thermal drift phenomena (Fig. 2 - B, D). The measure of distortion and dynamic range are carried out by input of frequency tones of high purity. We have designed two high-selectivity analog active filters using low noise electronics to clean a sinusoid waveform. The test set up, and the extraction of digital data from the different digitizer models requires considerable computing steps making the repetition of the tests very long. Currently the system is being finalized.

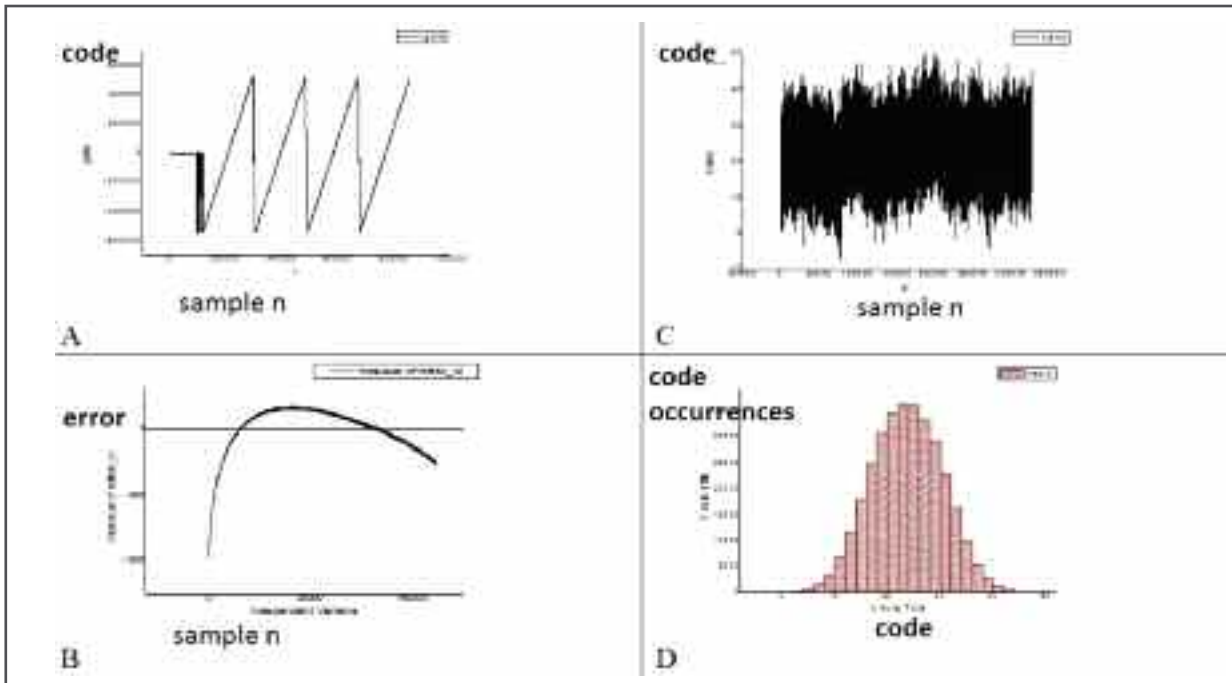

Fig. 2 I Some examples. A series of linear ramps **(A)** are generated by a precision low noise circuit and are input to the seismic a/d digitizers under test. The samples that each digitizer generates are manipulated to generate graphs to quantify error versus linear behaviour **(B)**. The signal acquired when inputs are shorted **(C)** is also used to evaluate noise histograms **(D)** and long-term drift.

9| SEMINARS and TEACHING

Seminars

Di Toro G. | Il motore dei terremoti visto da vicino | Distinguished Lectures della Società Geologica Italiana, Ciclo di seminari 2015-2016 | **Università di Parma** | Parma, Italy | 27 January, 2016

Di Toro G. | Il motore dei terremoti visto da vicino | Distinguished Lectures della Società Geologica Italiana, Ciclo di seminari 2015-2016 | **Università di Chieti** | Pescara, Italy | 28 January 2016

Di Toro G. | A close look at the earthquake engine | **Ecole Normale Superieure, Paris** | Paris, France | 23 February 2016

Di Toro G. | A close look at the earthquake engine | **School of Earth, University of Bristol** | Bristol, UK | 8 March, 2016

Di Toro G. | Fault weakening mechanisms in carbonate-bearing rocks at seismic deformation conditions | **School of Earth, Atmospheric and Environmental Sciences, University of Manchester** | Manchester, UK | 4 May, 2016

Di Toro G. | Fault lubrication in carbonate-built rocks during earthquakes | **Università di RomaTre** | Roma, Italy | 31 May 2016

Di Toro G. | Nascita, vita e morte di un terremoto. Circolo Galileo, Ciclo di seminari Terra! | **Liceo Berto Mogliano** | Treviso, Italy | 24 Ottobre 2016

Di Toro G. | Fault weakening mechanisms in carbonate-bearing rocks at seismic deformation conditions |IsTerre | **University of Grenoble** | Grenoble, France | 17 November, 2016

Training

1. **Fedele M.** | **Master Thesis** | Caratterizzazione di terremoti sperimentali a differenti condizioni al contorno | **Supervisors:** Collettini C., Scuderi M.M. | Sapienza University of Rome
2. **Gambetti V.** | **Stage** | Tracking of volcanic bombs from high-speed video | Università di Roma Tre | **Supervisor:** Taddeucci J. – INGV Roma1
3. **Ledderucci S.** | **Master Thesis** | Parameterization of Strombolian eruption plumes via thermal video analysis: examples from Stromboli (Italy) and Fuego (Guatemala) volcanoes | Università di Roma Tre | **Supervisors:** Palladino D.M. - Sapienza University of Rome | Taddeucci J. – INGV Roma1
4. **Luciani N.** | **Stage + Master Thesis** | Ca rich magmas: Molten carbonate plus solid silicate or Molten silicate plus Solid carbonate? The case study of pleistocene Polino volcanic rocks (central Italy) | **Supervisors:** Lustrino M., Stagno V. – Sapienza University of Rome | Masotta M. – Università di Pisa
5. **Mercuri M.** | **Master Thesis** | Caratterizzazione sperimentale del coefficiente di attrito della calcite | **Supervisors:** Collettini C., Scuderi M.M. | Sapienza University of Rome
6. **Musu A.** | **Stage** | Tracking of volcanic bombs from high-speed video | **Supervisor:** Taddeucci J. - INGV Roma1
7. **Palummo F.** | **Graduate Thesis** | Processi di interazione magma-crosta: caso studio delle fontane di lava etnee | **Supervisors:** Mollo S. – Sapienza University of Rome **|** Nazzari M. - INGV – Roma1
8. **Rossi R.** | **Stage** | Tracking of volcanic bombs from high-speed video | Sapienza University of Rome | **Supervisor:** Taddeucci J. - INGV Roma1
9. **Spagnoli M.** | **Graduate Thesis** | Il ruolo dell'evoluzione magmatica sul controllo della composizione mineralogica: studio microchimico | **Supervisors:** Mollo S. - Sapienza University of Rome **|** Nazzari M. - INGV – Roma1
10. **Stopponi V.** | **Bachelor Thesis** | Experimental viscosity measurements of carbonatitic melts at pressures and temperatures representative for the Earth's upper mantle | **Supervisor:** Stagno V. - Sapienza University of Rome

Thesis

1. **Aretusini S. | PhD |** Frictional processes of clay-rich gouges in megathrust and landslide decollement environments **| Supervisors:** Di Toro G. - University of Manchester, Manchester, UK **|** Spagnuolo E. **-** INGV **-** Roma1.

2. **Caruso M. | PhD |** The Earth's deep volatile cycle over geological time as function of mantle redox state, pressure and temperature **| Supervisors:** Stagno V. – Sapienza University of Rome **|** Scarlato P. – INGV Roma1

3. **Demurtas M. | PhD |**Quantification of the geometrical complexity of seismogenic fault zones **| Supervisors:** Di Toro G. - University of Manchester, Manchester, UK **|** Massironi M. - Università degli Studi di Padova, Padova, Italy **|** Storti F. - Università degli Studi di Parma, Parma, Italy

4. **Forni F. | PhD |** Caldera collapses and evolutionary trends: the case of Phlegraean Fields volcanic system **| Supervisors:** Bachman O. – ETH Zurigo **|** De Astis G. **-** INGV Roma 1

5. **Giorgetti C. | PhD |** Caratterizzazione strutturale e meccanica in faglie in misture di carbonati e fillosilicati **| Supervisors:** Collettini C., Scuderi M.M. **|** Sapienza University of Rome

6. **Mercuri M. | PhD |** Struttura e comportamento meccanico di zone di faglia carbonatiche in presenza di plaghe argillose **| Supervisors:** Collettini C., Carminati E. - Sapienza University of Rome.

7. **Nazzari M. | PhD |** Unravelling the effect of undercooling on (dis)equilibrium textures and compositions of basaltic magmas **| Supervisor:** Mollo S. **|** Sapienza University of Rome

8. **Orellana F. | PhD |** Frictional propertie of Opalinus clay **| Supervisor:** Violay M. École polytechnique fédérale de Lausanne.

9. **Salvatore V. | PhD |** Dinamiche di eruzioni stromboliane attraverso modellazione analogica, video di monitoraggio e immagini ad alta velocità **| Supervisors:** Palladino D.M. - Sapienza University of Rome **|** Taddeucci J. - INGV Roma1

10. **Tecchiato V. | PhD |** Il ruolo dei mush cristallini nei processi di differenziazione dei magmi calcalcalini: caratteri giaciturali, petrografici, geochimici e modellistica sperimentale **| Supervisors:** Gaeta M., Mollo S. **|** Sapienza University of Rome

11. **Tournigand P-Y. | PhD |** Field-based study of volcanic ash via visible and thermal high-speed imaging of explosive eruptions **| Supervisors:** Palladino D.M. - Sapienza University of Rome **|** Taddeucci J. - INGV Roma1

10| VISITING SCIENTISTS

Agliardi F. | Università Milano Bicocca | September

Brenna M. | University of Otago | April

Cigala V. | University of Munich, Germany | July

Cornelio C. | Swiss Institute of Technology Lausanne, Switzerland | October

De Cristofaro S.P. | Università di Torino | June

Fondriest M. | Universitiy of Manchester | March

Kueppers U. | University of Munich, Germany | July

Kuo L.W. | National Central University, Taoyuan City (Taiwan) | May

Passelegue F. | The University of Manchester, Unite Kingdom | December

Polo L. | University of São Paulo | May

Smeraglia L. | Sapienza University of Rome | April

Tisato N. | The University of Texas at Austin, USA | June-July

Violay M. | Swiss Institute of Technology Lausanne, Switzerland | October

11| MEETINGS, WORKSHOP and SYMPOSIA

Tectonic Studies Group Annual Meeting, London (UK), 6-8 January

Aretusini A., Plumper O., Spagnuolo E., Di Toro G.
Seismic slip on clay nanofoliation

Demurtas M., Fondriest M., Clemenzi L., Balsamo F., Storti F., Bistacchi A., Di Toro G.
Structure of a seismogenic normal fault zone in carbonates: Campo Imperatore, Central Apennines (Italy)

Convegno Struttura Ambiente INGV, Roma (Italy), 8-9 March

Ricci T., Sciarra A., Inguaggiato S., Barlow T., Caliro S., Gaudin D., Granieri D., Marieni C., Purser G., Rochelle C., Scarlato P., Papale P.
Geochemical investigations in the Krafla Geothermal Area, NE-Iceland

MED-SUV Final Meeting, Roma (Italy), 6 April

Cannata A., Taddeucci J., Privitera E., Sciotto M., Spina L., Del Bello E., Andronico D., Ricci T., Scarlato P., Kueppers U., Dingwell D. B.
Multi-parametric investigation on the mechanism of multi-vent Strombolian activity

Del Bello E., Taddeucci J., de Michieli Vitturi M., Scarlato P., Andronico D., Scollo S., Kueppers U.
Effect of particle volume fraction on the settling velocity of volcanic ash particles: implications for ash dispersion models

EGU General Assembly, Vienna (Austria), 17-22 April

Bistacchi A., Mittempergher S., Di Toro G., Smith S.A.F., Garofalo P.S., Vho A.
Hydraulic structure of a fault zone at seismogenic depths (Gole Larghe Fault Zone, Italian Southern Alps)

Cannata A., Del Bello E., Kueppers U., Privitera E., Ricci T., Scarlato P., Sciotto M., Spina L., Taddeucci J., Pena Fernandez J., Sesterhenn J.
Multiparametric approach to unravel the mechanism of Strombolian activity at a multivent system: Mt. Etna case study

Laeger K., Petrelli M., Andronico D., Scarlato P., Cimarelli C., Misiti V., Del Bello E., Perugini D.
Unraveling the Eyjafjallajökull 2010 plumbing system and magma chamber, dynamics through high-resolution geochemical investigations

Murphy S., Spagnuolo E., Lorito, S., Di Toro G., Scala A., Festa G., Nielsen S., Piatanesi A., Romano F., Aretusini S.
Incorporation of experimentally derived friction laws in numerical simulations of earthquake generated tsunamis

Passelegue F., Spagnuolo E., Nielsen S., Di Toro G., Schubnel A.
High-Velocity Frictional Properties of Westerly Granite and the Role of Thermal Cracking on Gouge Production

Smith S., Griffiths J., Fondriest M., Di Toro G., Demurtas M.
"Coseismic foliations" in gouge and cataclasite: experimental observations and consequences for interpreting the fault rock record

Spagnuolo E., Nielsen S., Violay M., Di Felice F., Di Toro G.
Frictional behavior of experimental faults during a simulated seismic cycle

Taddeucci J., Alatorre M., Cruz Vázquez O., Del Bello E., Ricci T., Scarlato P., Palladino D.
Bombs, flyin' high. In-flight dynamics of volcanic bombs from Strombolian to Vulcanian eruptions

Tisato N., Goodfellow S.G., Moulas V., Di Toro G., Young P., Grasselli G.
Acoustic emissions in rock deformation experiments under micro-CT

Tournigand P.Y., Taddeucci J., JoséPeña Fernandez J.J., Gaudin D., Sesterhenn J., Scarlato P., Del Bello E.
Retrieving eruptive event conditions from dynamical properties of unsteady volcanic plume using high-speed imagery and numerical simulations

Traforti A., Zampieri D., Massironi M., Viola G., Alvarado P., Di Toro G.
Regional polyphase deformation of the Eastern Sierras Pampeanas (Argentina Andean foreland): strengths and weaknesses of paleostress inversion

The Royal Society KAVLI meeting on Faulting at Chicheley Hall, Buckinghamshire, UK, 25-26 April

Demurtas M., Fondriest, M., Di Toro, G.
Evidence of coseismic sliding in the Campo Imperatore Fault Zone (Central Appenines, Italy)

Di Toro G. INVITED
Seismic slip in carbonate rocks

Fondriest M., Doan M.L, Aben F., Fusseis F., Mitchell T., Di Toro G.
Static versus dynamic fracturing in shallow carbonate fault zones

Kuo L.W., Di Toro G., Di Felice F., Wen C.Y., Spagnuolo E., Song S.R., Suppe J., Li H.
Graphite Raman spectra in fault zones: only geothermometer or a seismic slip indicator?

Passelegue F., Spagnuolo E., Violay M., Nielsen S., Di Toro G., Schubnel A.
Influence of slip rate and normal stress on off-fault damage in high-velocity friction experiments on crustal rocks

Spagnuolo E., Nielsen, S., Violay, M., Di Toro, G
An empirically-based steady-state friction law and implications for fault stability

INGV - Convegno annuale della struttura vulcani, Palermo, Italy, 3-6 May

Del Bello E., Taddeucci J., de Michieli Vitturi M., Scarlato P., Andronico D., Scollo S.
Effetto della concentrazione volumetrica sulla velocità di sedimentazione della cenere vulcanica: implicazioni sui modelli di dispersione

Taddeucci J., Del Bello E., Scarlato P., Ricci T, Cannata A., Privitera E., Andronico D., Kueppers U., Spina L., Sesterhenn J.
Analisi di dati sismo-acustici e video riprese ad alta velocità delle esplosioni stromboliane all'Etna di Luglio 2014: implicazioni per i processi di sorgente

Goldschmidt, Yokohama, Japan, 26 June - 1 July

Di Piazza A., Del Bello E., Mollo S., Alvarado G.E.
Chemical and textural characterization of cannonballs from Cerro Chopo volcano (Costa Rica): a preliminary approach to their origin

Forni F., Bachmann O., Mollo S., De Astis G.
Long-term magmatic evolution at the Campi Flegrei caldera (southern Italy)

Masotta M., Scarlato P., Nazzari M., Mollo S.
Solidification of rhyolitic magmas beneath the Krafla caldera

Scarlato P., Mollo S., Del Bello E., Von Quadt A., Brown R., Gutierrez E., Martinez-Hackert B., Papale P.
The 2013 eruption of Chaparrastique (San Miguel) volcano, El Salvador: Effects of magma storage, mixing, and decompression

Tecchiato V., Gaeta M., Mollo S., Scarlato P.
The coarse-grained, high-Mg basaltic enclaves of Capo Marargiu (Sardinia, Italy): constrains on the differentiation of arc magmas

35 th International Geological Congress, Cape Town, South Africa, 27 August - 4 September

Tecchiato V., Gaeta M., Mollo S., Scarlato P.
Petrological constrains on the coarse-grained, high-Mg basaltic enclaves of Capo Marargiu (Sardinia, Italy)

Gordon Conference in Rock Deformation. Proctor Academy, New Hampshire, USA 21-26, August

Aretusini S., Plümper O., Spagnuolo E., Di Toro G.
Frictional deformation processes in wet Ca-montmorillonite-rich fault gouges

Demurtas M., Smith S., Spagnuolo E., Fondriest M., Di Toro G.
Coseismic origin of foliated cataclasites and preservation potential during the seismic cycle

Passelègue F., Fondriest M., Nicolas A., Aubry J., Schubnel A., Di Toro G.
From slow to fast rupture during laboratory earthquakes in dolostones

Congresso della Società Geologica Italiana, 7-9 September

Di Toro G., Spagnuolo E., Fondriest M., Passelegue F., Aretusini S., Demurtas M., Murphy S., Nielsen S., Plumper O., Kuo L.W.
Shallow earthquakes: are they "brittle" or "ductile"?

Fondriest M., Mitchell T., Di Giulio G., Vassallo M., Balsamo F., Pischiutta M., Di Toro G.
Multiscale velocity structure of a seismogenic normal fault zone

Mittempergher S., Di Toro G., Aretusini S., Gratier J.P.
The evolution of fabric with displacement in natural brittle faults

Southern California Earthquake Center Annual Meeting, Palm Springs, 10-13 September

Rabinowitz H., Savage H.M., Spagnuolo E., Di Toro G.
Biomarker thermal maturity at seismic timescales in high-velocity rotary shear experiments

Cities On Volcanoes, San Francisco (USA), 20-25 November

Del Bello E., Taddeucci J., Merrison J.P., Alois S., Iversen J.J.
Parameterization of volcanic ash remobilization by wind-tunnel erosion experiments

Scarlato P., Mollo S., Del Bello E., Von Quadt A., Brown R., Gutierrez E., Martinez-Hackert B., Papale P.
The 2013 eruption of Chaparrastique (San Miguel) volcano, El Salvador: Effects of magma storage, mixing, and decompression

Weizmann Institute of Science, Rehovot, Israel, 1-3 November

Di Toro G.
Friction in carbonate-built rocks (invited)

AGU Fall Meeting, San Francisco (USA), 12-16 December

Bistacchi A., Mittempergher S., Di Toro G., Smith S.A.F., Paolo S., Garofalo P.S.
The seismogenic Gole Larghe Fault Zone (Italian Southern Alps): quantitative 3D characterization of the fault/fracture network, mapping of evidences of fluid-rock interaction, and modelling of the hydraulic structure through the seismic cycle

Demurtas M., Smith S.A.F., Spagnuolo E., Negrini M., Fondriest M., Di Toro G.
Twinning and fracturing during cataclasis in carbonate fault gouge

Di Toro G., Prando F., Pennacchioni G., Mazzoli C., Nestola F., Zorzi F.
Pseudotachylytes and mirror-like surfaces from extensional faults in Alpine Corsica (France)

Di Toro G., Nielsen S., Passelegue F., Spagnuolo E., Bistacchi A., Fondriest M., Murphy S., Aretusini S., Demurtas M.
What is the earthquake fracture energy?

Fondriest M., Mitchell T. M., Vassallo M., Di Giulio G., Balsamo F., Passelegue F., Pischiutta M., Di Toro G.
Multi-scale velocity structure of an active seismogenic normal fault zone (Central Apennines, Italy)

Hung C.C., Kuo L.W., Dong J.J., Song S.R., Spagnuolo E., Lin W., Di Toro G.
Frictional Properties of Hoping Granitic Gneiss, Northeast Taiwan, and Its Implication

Mints B.G., Houghton B., Orr T., Taddeucci J., Gauding D., Kueppers U., Carey R., Scarlato P., Del Bello E.
Spattering activity at Halema'uma'u in 2015 and the transition between Hawaiian and Strombolian eruptions

Murphy S., Spagnuolo E., Scala A., Di Toro G., Lorito S., Festa G., Nielsen S., Piatanesi A., Romano F., Aretusini S.
Incorporation of friction laws derived from rotary experiments in numerical simulations tsunamigenic earthquakes

Passelegue F., Fondriest M., Nicolas A., Aubry J., Schubnel A., Di Toro G.
From slow to fast rupture during laboratory earthquakes in dolostones

Rempe M., Di Toro G., Mitchell T., Hirose T., Smith S.A.F., Renner J.
The effect of fluids on the frictional behavior of calcite gouge

Scala A., Murphy S., Lorito S., Festa G., Trasatti E., Romano F., Piatanesi A., Di Toro G., Spagnuolo E.
Slip distributions in a suite of dynamic simulations of mega-thrust earthquakes and their comparison with observations

Smeraglia L., Billi A., Carminati E., Cavallo A., Di Toro G., Spagnuolo E., Zorzi F.
Phyllosilicate-rich ultra-thin layers in carbonate fault gouge drive seismic slip propagation

Smith S.A.F., Demurtas M., Spagnuolo E., Fondriest M., Di Toro G.
Coseismic Origin of Foliated Cataclasites and Preservation Potential During the Seismic Cycle

Taddeucci J., Scarlato P., Del Bello E.
Multiparametric Experiments and Multiparametric Setups for Metering Explosive Eruptions (Invited)

Turner N., Houghton B., von der Lieth J., Hort M., Taddeucci J., Kueppers U., Ricci T., Gaudin D.
Mapping the Active Vents of Stromboli Volcano with an Unmanned Aerial Vehicle

12| PUBLICATIONS

1. *Beeler N., Di Toro G., Nielsen S.*
Earthquake source properties from pseudotachylite
Bulletin of the Seismological Society of America | 106, 2764-2776

2. *Cannelli V., Piersanti A., Spagnuolo E., Galli G.*
Preliminary analysis of radon time series before the Ml=6 Amatrice earthquake: possible implications for fluid migration
Annals of Geophysics | 59 (5).

3. *Capponi A., Taddeucci J., Scarlato P., Palladino D.M.*
Recycled ejecta modulating Strombolian explosions
Bulletin of Volcanology | 78, 2-13

4. *Carpenter B.M., Collettini C., Viti C., Cavallo A.*
The influence of normal stress and sliding velocity on the frictional behaviour of calcite at room temperature: Insights from laboratory experiments and microstructural observations
Geophysical Journal International | 205, 548-561

5. *Deegan F.M., Troll V.R., Bédard J.H., Evenchick C.A., Dewing K., Grasby S., Geiger H., Freda C., Misiti V., Mollo S.*
The stiff upper LIP: Investigating the High Arctic Large Igneous Province
Geology Today | 32, 92-98

6. *Della Ventura G., Redhammer G.J., Robert J.L., Sergent J., Iezzi G., Cavallo A.*
Synthesis and crystal-chemistry of amphiboles along the join richterite – ferrorichterite: a combined spectroscopic (FTIR Mössbauer), XRPD and microchemical study
The Canadian Mineralogist | 54, 97-114

7. *Demurtas M., Fondriest M., Balsamo F., Clemenzi L., Storti F., Bistacchi A., Di Toro G.*
Structure of a normal seismogenic fault zone in carbonates: the Vado di Corno Fault, Campo Imperatore, Central Apennines (Italy)
Journal of Structural Geology | 90, 185-206

8. *Forni F., Bachmann O., Mollo S., De Astis G., Gelman S.E., Ellis B.S.*
The origin of a zoned ignimbrite: Insights into the Campanian Ignimbrite magma chamber (Campi Flegrei, Italy)
Earth and Planetary Science Letters | 449, 259–271

9. *Gaudin D., Taddeucci J., Houghton B.F., Orr T.R., Andronico D., Del Bello E., Kueppers U., Ricci T., Scarlato P.*
3-D high-speed imaging of volcanic bomb trajectory in basaltic explosive eruptions
Geochemistry Geophysics Geosystems | 17, 4268-4275

10. *Giorgetti C., Collettini C., Scuderi M.M., Barchi M., Tesei T.*
Fault geometry and mechanics of marly carbonate multilayers: An integrated field and laboratory study from the Northern Apennines, Italy
Journal of Structural Geology | 93, 1-16

11. *Houghton B.F., Taddeucci J., Andronico D., Gonnermann H.M., Pistolesi M., Patrick M.R., Orr T.R., Swanson D.A., Edmonds M., Gaudin D., Carey R.J., Scarlato P.*
Stronger or longer: Discriminating between Hawaiian and Strombolian eruption styles
Geology | 44, 163-166

12. *Iezzi G., Bromiley G.D., Cavallo A., Das P.P., Karavassili F., Margiolaki I., Stewart A.A., Tribaudino M., Wright J.P.*
Solid solution along the synthetic $LiAlSi_2O_6$-$LiFeSi_2O_6$ (spodumene-ferri-spodumene) join: A general picture of solid solutions, bond lengths, lattice strains, steric effects, symmetries, and chemical compositions of Li clinopyroxenes
American Mineralogist | 101, 2498-2513

13. *Marra F., Gaeta M., Giaccio B., Jicha B.R., Palladino D.M., Polcari M., Sottili G., Taddeucci J., Florindo F., Stramondo S.*
Assessing the volcanic hazard for Rome: 40^{39} and In-SAR constraints on the most recent eruptive activity and present-day uplift at Colli Albani Volcanic District
Geophysical Research Letters | 43, 6898-6906

14. *Masotta M., Keppler H., Chaudhari A.*
Fluid-melt partitioning of sulfur in differentiated arc magmas and the sulfur yield of explosive volcanic eruptions
Geochimica et Cosmochimica Acta | 176, 26-43

15. *Masotta M., Mollo S., Gaeta M., Freda C.*
Melt extraction in mush zones: The case of crystal-rich enclaves at the Sabatini Volcanic District (central Italy)
Lithos | 248-251, 288-292

16. *Mitchell M.M., Toy V., Di Toro G., Renner J., Sibson R.*
Fault welding by pseudotachilyte formation
Geology | 44, 1059-1062

17. *Mollo S., Forni F., Bachmann O., Blundy J. D., De Astis G., Scarlato P.*
Trace element partitioning between clinopyroxene and trachy-phonolitic melts: A case study from the Campanian ignimbrite (Campi Flegrei, Italy)
Lithos | 252-253, 160-172

18. *Nielsen B.S., Spagnuolo E., Smith S.A.F., Violay M., Di Toro G., Bistacchi A.*
G: Fracture energy, friction and dissipation earthquakes
Journal of Seismology | 20, 1187-1205

19. *Nielsen B.S., Spagnuolo E., Smith S.A.F., Violay M., Di Toro G., Bistacchi A.*
Scaling in natural and laboratory earthquakes
Geophysical Research Letters | 43, 1504-1510

20. *Passelegue F.X., Spagnuolo E., Violay M., Nielsen S., Di Toro G., Schubnel A.*
Frictional evolution, acoustic activity and off-fault damage in simulated faults sheared at seismic slip rates
Journal of Geophysical Research | 121, 1-24

21. *Perinelli C., Mollo S., Gaeta M., De Cristofaro S.P., Palladino D. M., Armienti P., Scarlato P., Putirka K.D.*
An improved clinopyroxene-based hygrometer for Etnean magmas and implications for eruption triggering mechanisms
American Mineralogist | 101, 2774-2777

22. *Rizzo A.L., Di Piazza A., de Moor J.M., Alvarado G.E., Avard G., Carapezza M.L., Mora M.M.*
Eruptive activity at Turrialba volcano (Costa Rica): Inferences from $^{3}He/^{4}He$ in fumarole gases and chemistry of the products ejected during 2014 and 2015
Geochemistry, Geophysics, Geosystems | 17, 4478-4494

23. *Scarlato P., Mollo S., Del Bello E., von Quadt A., Richard J.B., Gutierrez, E., Martinez-Hackert, B., Papale P.*
The 2013 eruption of Chaparrastique Volcano (El Salvador): Effects of magma storage, mixing, and decompression
Chemical Geology | 448, 110-122

24. *Scuderi M.M., Marone C., Tinti E., Di Stefano G., Collettini C.*
Precursory changes in seismic velocity for the spectrum of earthquake failure modes
Nature Geoscience | 9, 695-700

25. *Scuderi M.M., Collettini C.*
The role of fluid pressure in induced vs. triggered seismicity: Insights from rock deformation experiments on carbonates
Scientific Reports | doi: 10.1038/srep24852

26. *Spagnuolo E., Plümper O., Violay M., Cavallo A., Di Toro G.*
Dislocations motion and the microphysics of flash heating and weakening of faults during earthquakes
Crystals | 6, 1-14

27. *Spagnuolo E., Nielsen S., Violay M., Di Toro G.*
An empirically-based steady-state friction law and implications for fault stability
Geophysical Research Letters | 43, 3263-3271

28. *Tinti E., Scuderi M.M., Scognamiglio L., Di Stefano G., Marone C., Collettini C.*
On the evolution of elastic properties during laboratory stick-slip experiments spanning the transition from slow slip to dynamic rupture
Journal of Geophysical Research - Solid Earth | 121, 8569-8594

29. *Venuti A., Alfonsi L., Cavallo A.*
Anthropogenic pollutants on top soils along a section of the Salaria state road, central Italy
Annals of Geophysics | 59, G0544

In press

1. *Casagli A., Frezzotti M.L., Peccerillo A., Tiepolo M., De Astis G.*
(Garnet)-spinel peridotite xenoliths from Mega (Ethiopia): Evidence for rejuvenation and dynamic thinning of the lithosphere beneath the southern Main Ethiopian Rift
Chemical Geology.

2. *Del Bello E., Taddeucci J., de Michieli Vitturi M., Scarlato P., Andronico D., Kueppers U., Scollo S., Ricci, T.*
Effect of particle volume fraction on the settling velocity of volcanic ash particles: insights from laboratory experiments and numerical simulations
Scientific Reports | 7, 3962

3. *Di Piazza A., Del Bello E., Mollo S., Vona A., Alvarado G., Masotta M.*
Wrecking like a cannonball: origin of dense spherical basaltic bombs
Bulletin of Volcanology

4. *Gaudin D., Taddeucci J., Scarlato P., Harris H., Bombrun M., Del Bello E., Ricci T.*
Characteristics of puffing activity revealed by ground-based, thermal infrared imaging: the example of Stromboli volcano (Italy)
Bulletin of Volcanology

5. *Smith S.A.F., Griffiths J.R., Fondriest M., Di Toro G.*
"Coseismic foliations" in gouge and cataclasite: experimental observations and consequences for interpreting the fault rock record
Geophysical Monograph Series (American Geophysical Union Special Volume, Washington D.C., USA)

6. *Laeger K., Petrelli M., Andronico D., Misiti V., Scarlato P., Cimarelli C., Taddeucci J., Del Bello E., Perugini D.*
High-resolution geochemistry of volcanic ash highlights complex magma dynamics during the Eyjafjallajökull 2010 eruption
American Mineralogist

Patents

1. *Barba S, Caramelli A, Chiappini M, Romeo G.*
Sistema e metodo per la diffusione di allarmi.
Italian Patent application: 102016000076023

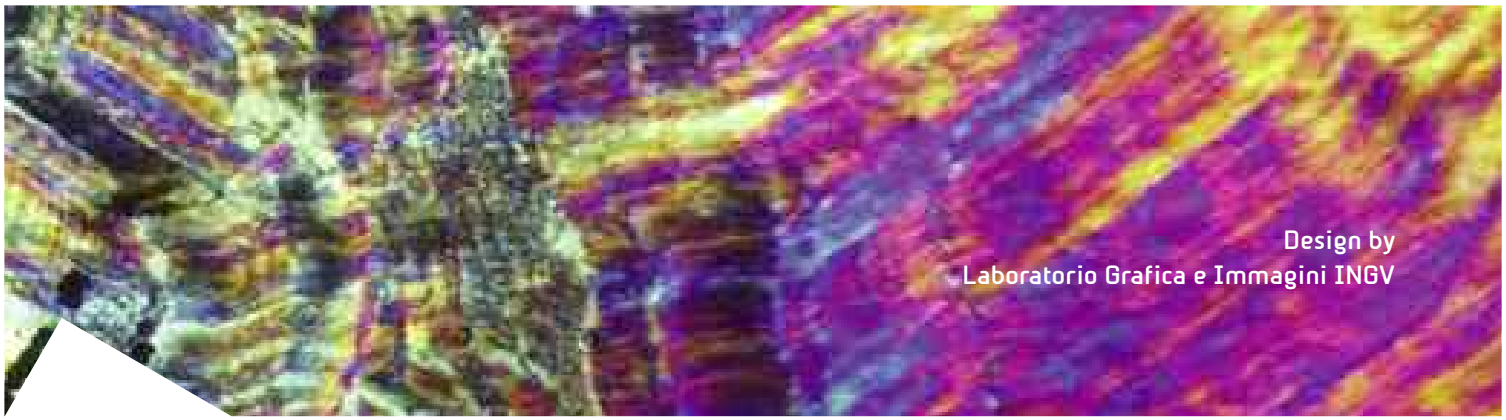

Rome, 09 March 2017

Editing by **Valeria Misiti**